Magnetic excitations

- measured by Triple-Axis Spectroscopy

Part 1: Classical Magnetic Excitations

Localized magnetic moments

Hund's Rules

Magnetic moment: not completely filled electronic shell

3d-shell:

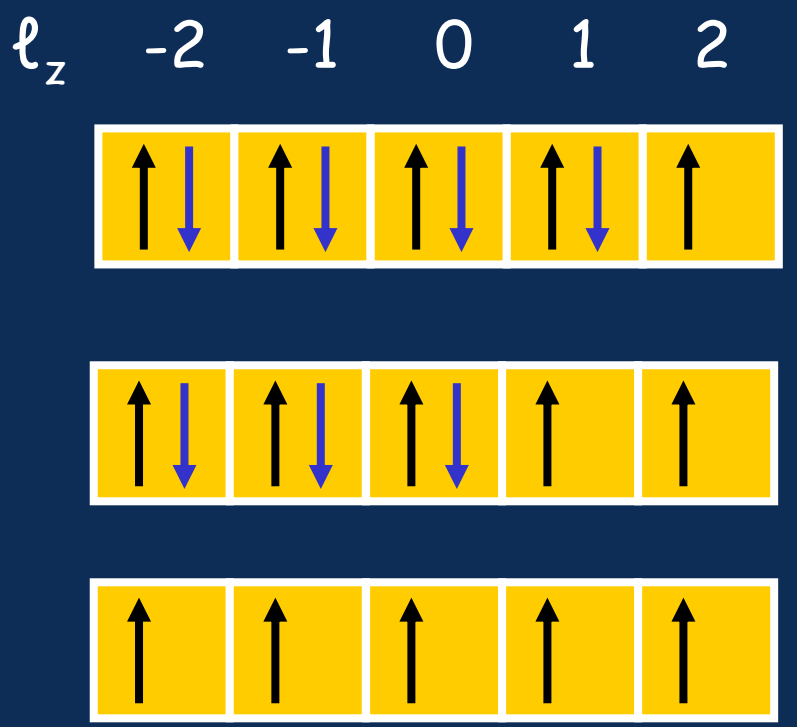

Hund's Rules

Magnetic moment: not completely filled electronic shell

4f-shell:

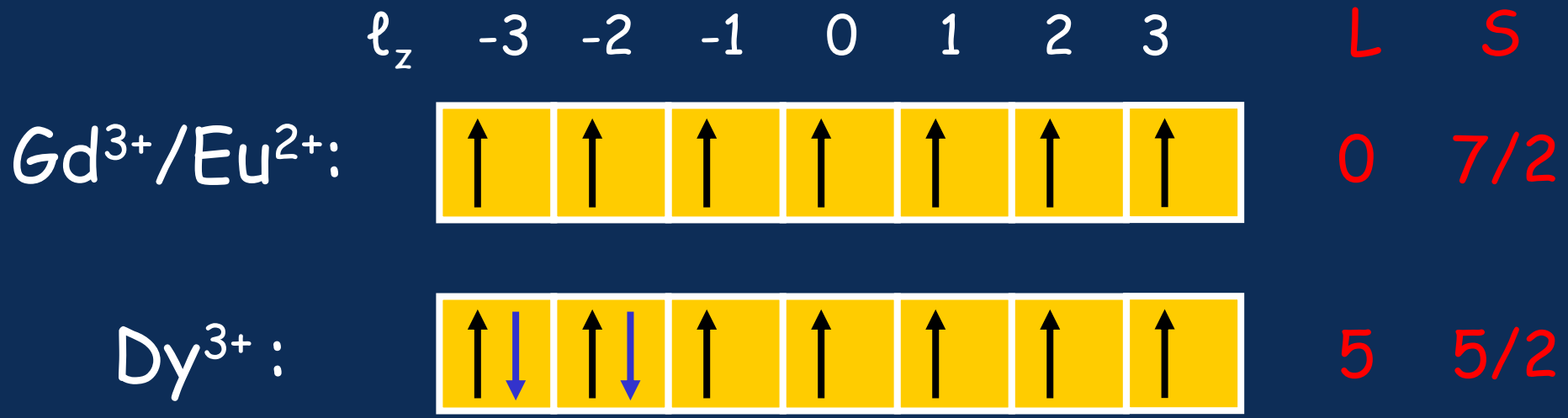

Crystal field and LS-coupling

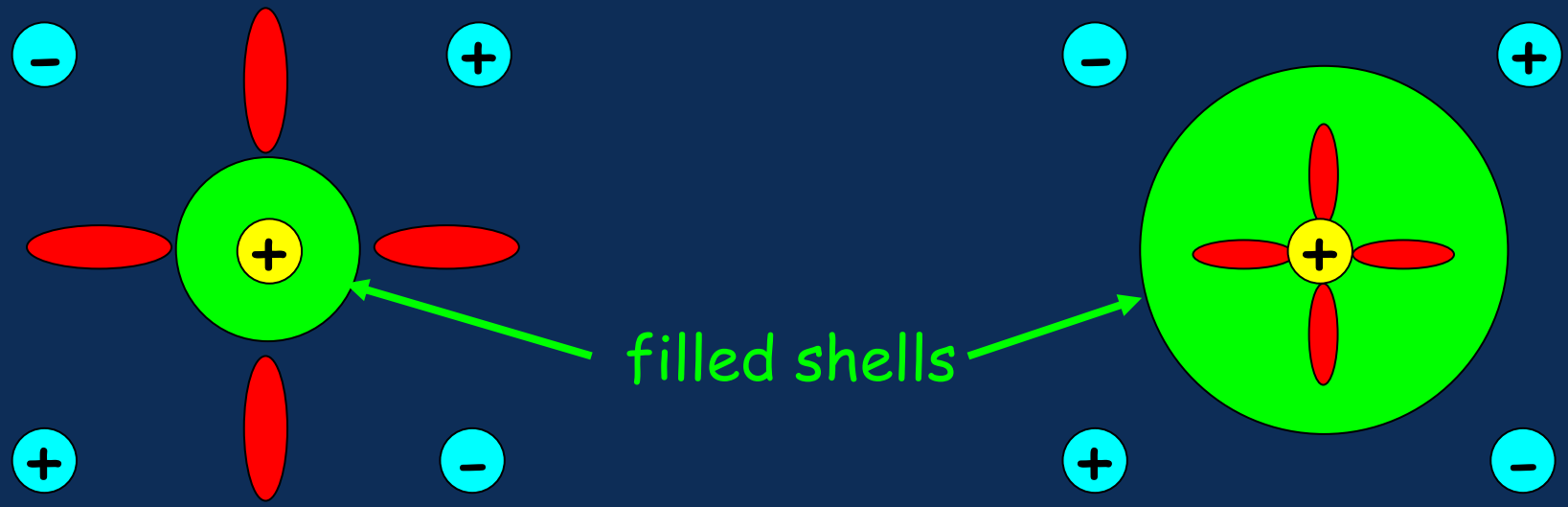

CF influence strong
LS-coupling small

LS-coupling strong
CF influence small

L-multiplet splits into (mostly) singlets
often ground state <L>=0, "pure" S
LS-coupling -> small anisotropies

L+S couple to J
CF splits J-multiplet
large anisotropies

Localised 3d moments

Magnetic moment: not completely filled electronic shell

3d-shell:

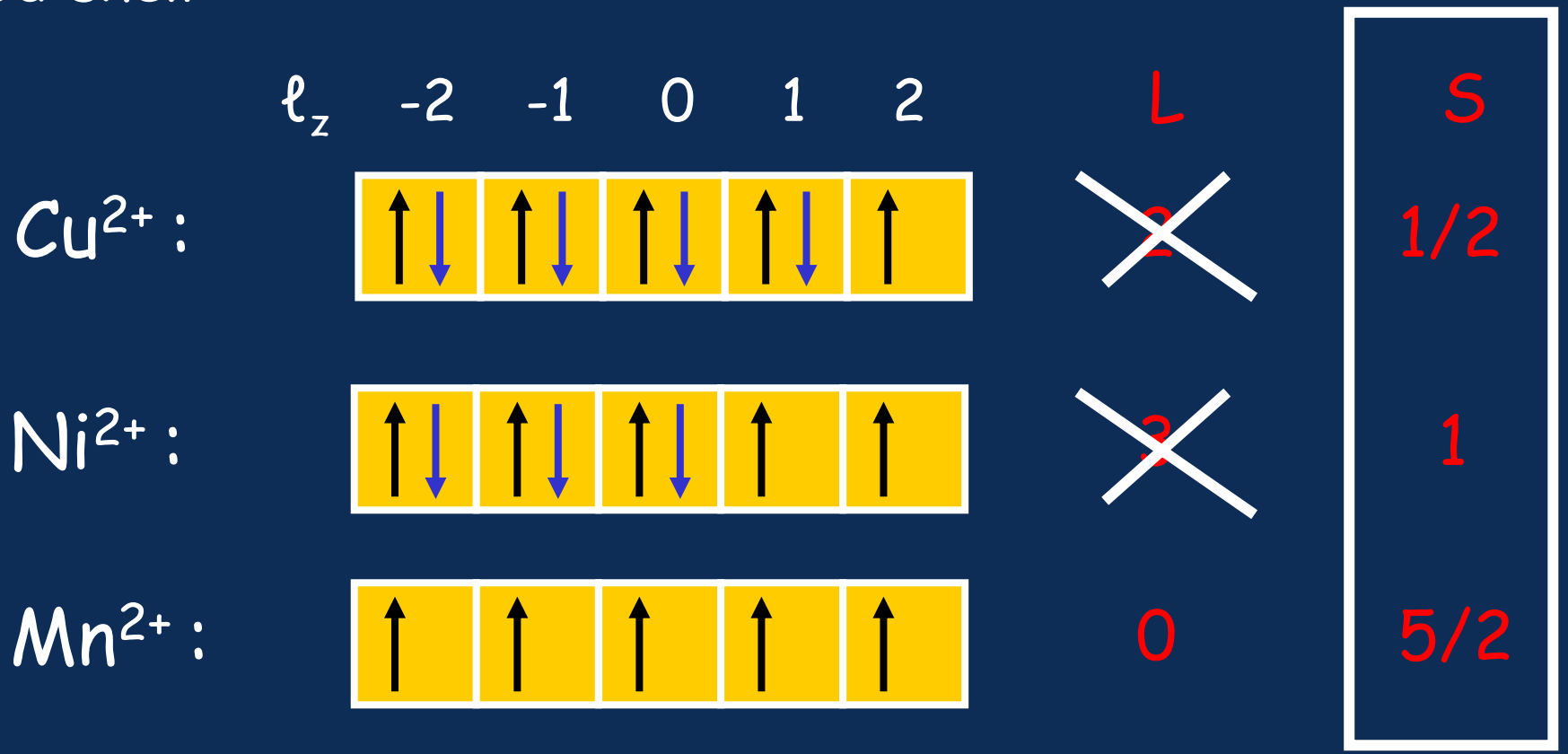

Hund's Rules

Magnetic moment: not completely filled electronic shell

4f-shell:

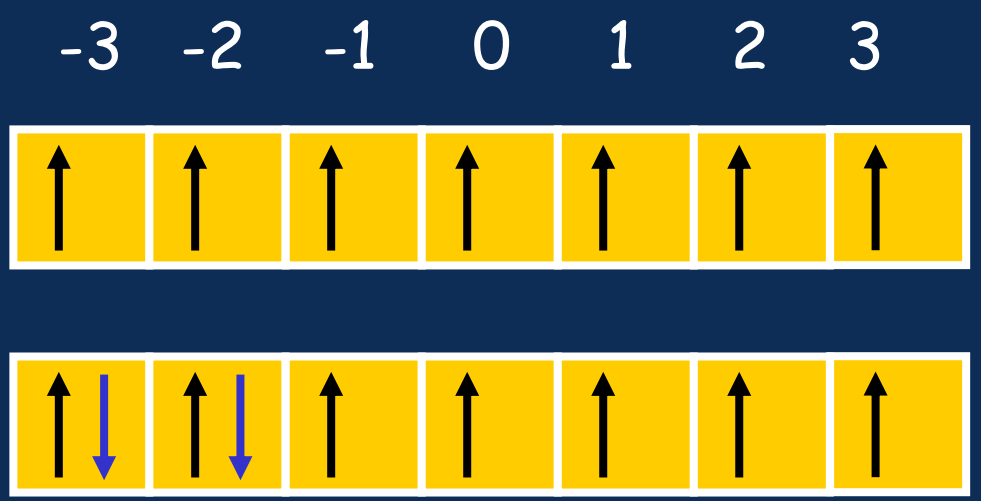

Further Interactions

3d-shell

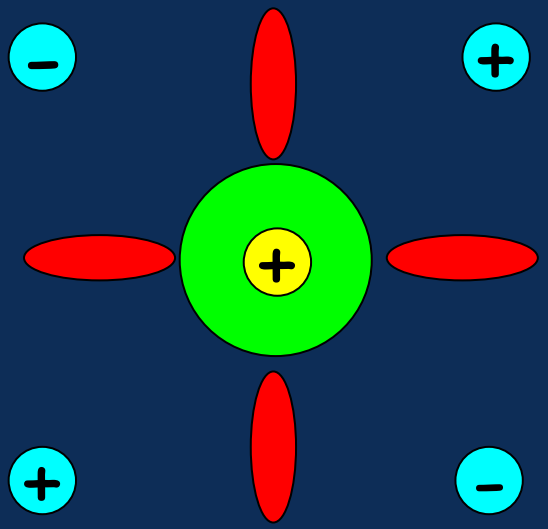

4f-shell

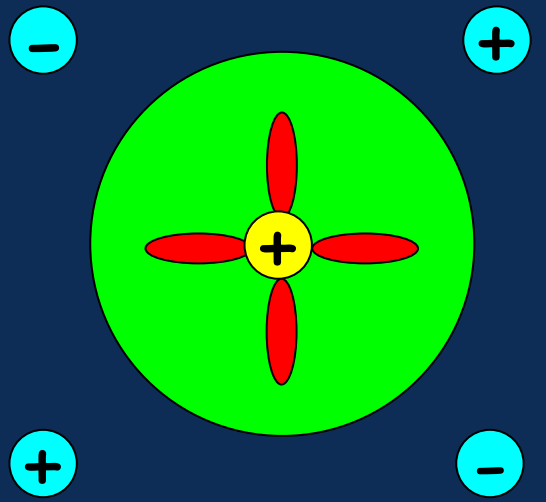

3d-orbitals overlap with neighbours

Direct exchange, Superexchange

S ≤ 5/2 : dipolar interactions small

4f-orbitals well localized

Hybridisation with conduction e^- (RKKY-interaction)

J=L+S large -> dipolar interactions

Superexchange

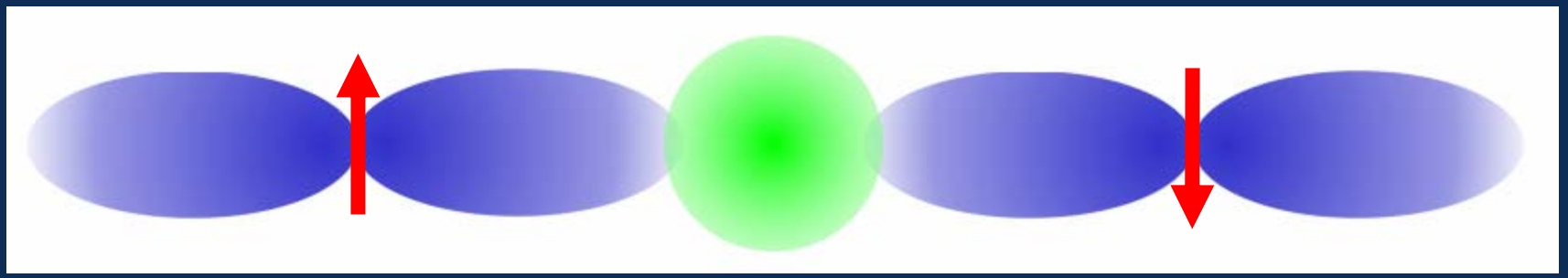

Pauli principle
Coulomb interaction
effectively antiferromagnetic

$$\mathcal{H} = -J \sum \vec{S}_n \vec{S}_{n+1}$$

Interactions responsible for correlated dynamics

3d-shell

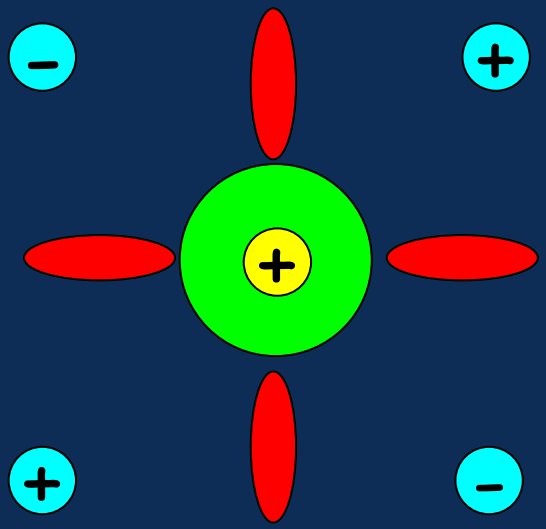

4f-shell

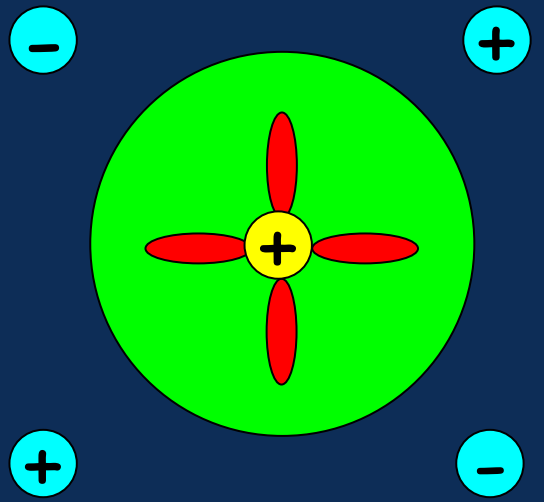

3d-orbitals overlap with neighbours

Direct exchange, Superexchange

S ≤ 5/2 : dipolar interactions small

(CF-split L-levels at very high energies)

4f-orbitals well localized

Hybridisation with conduction e⁻ (RKKY-interaction)

J=L+S large -> dipolar interactions

CF-split J-levels at low energies

1D spin arrays

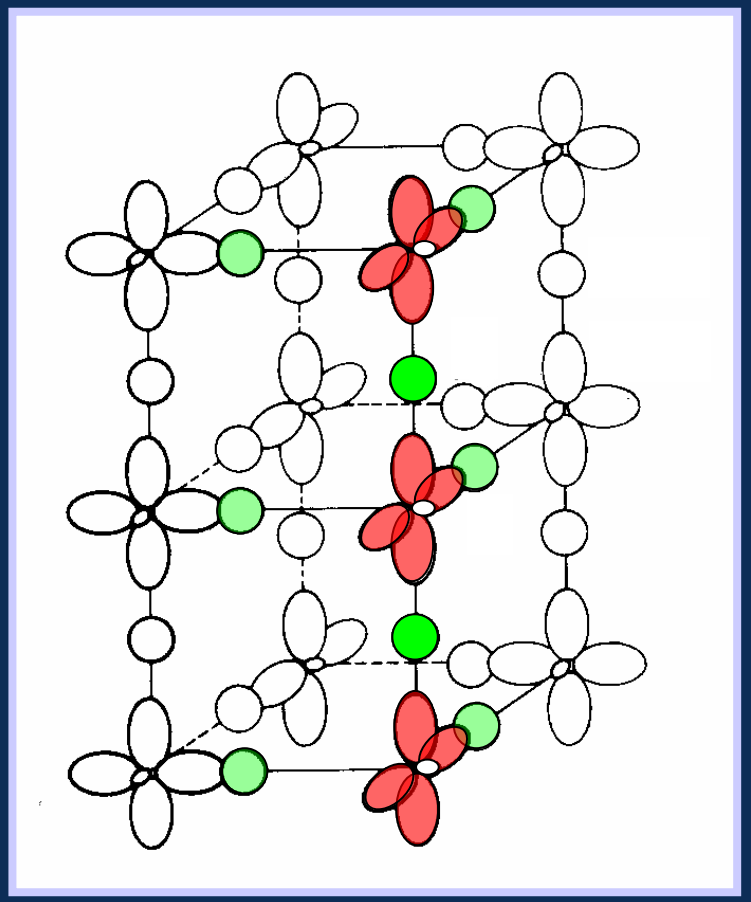

~5Å

$KCuF_3$:

Cu^{2+} $3d^9$ localised

S, L

Stark effect >> spin-orbit

$\langle L^x \rangle$
$\langle L^y \rangle$
$\langle L^z \rangle$
} 0

S=1/2

Ferro- and Antiferromagnets

$$\mathcal{H} = J \sum S_n^z S_{n+1}^z + \frac{1}{2}\left(S_n^+ S_{n+1}^- + S_n^- S_{n+1}^+\right)$$

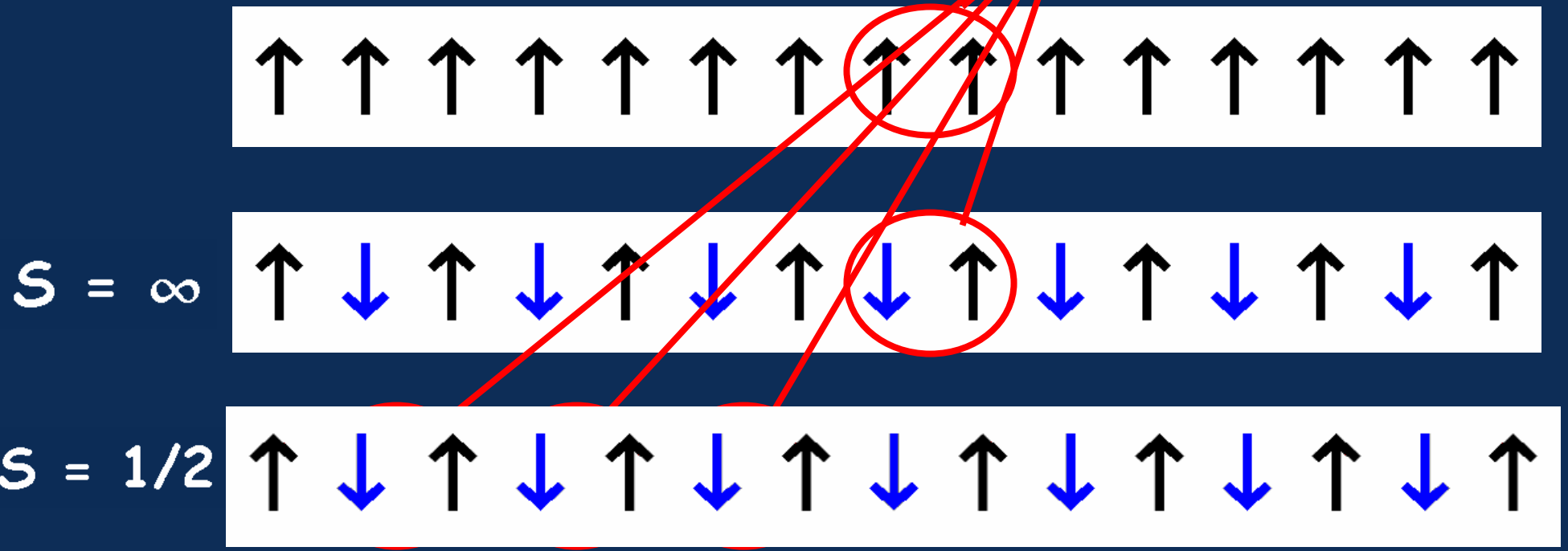

Classical Ferromagnet – Collective excitations

Heisenberg - FM: $\mathcal{H} = -J \sum \vec{S}_n \vec{S}_{n+1}$

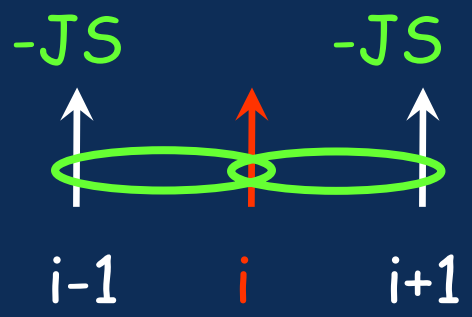

Exchange field $g\mu_B H_{ex}(i) = -J\,(S_{i-1} + S_{i+1})$

Magnetic moment $m_i = -g\mu_B/\hbar\ S_i$

Classical Ferromagnet – Spin waves

Classical: $S \to \infty$, spin = vector

$$\frac{d}{dt}\mathbf{S}_i = \mathbf{m}_i \times \mathbf{H}_{ex}(i)$$

$$= \frac{J}{\hbar}\,\mathbf{S}_i \times (\mathbf{S}_{i-1} + \mathbf{S}_{i+1})$$

QM: small S, spin = operator

$$i\hbar \frac{\partial}{\partial t} S_i^+ = [S_i^+ , \mathcal{H}]$$

$$= \sum_j J\,(S_i^z S_j^+ - S_j^+ S_i^z)$$

non-linear

Linearization $S_i^{x,y} \ll S$ $S_i^z \approx S$

$$\hbar\omega(q) = 4JS\,(1-\cos(qa))$$

Classical spin waves - FM

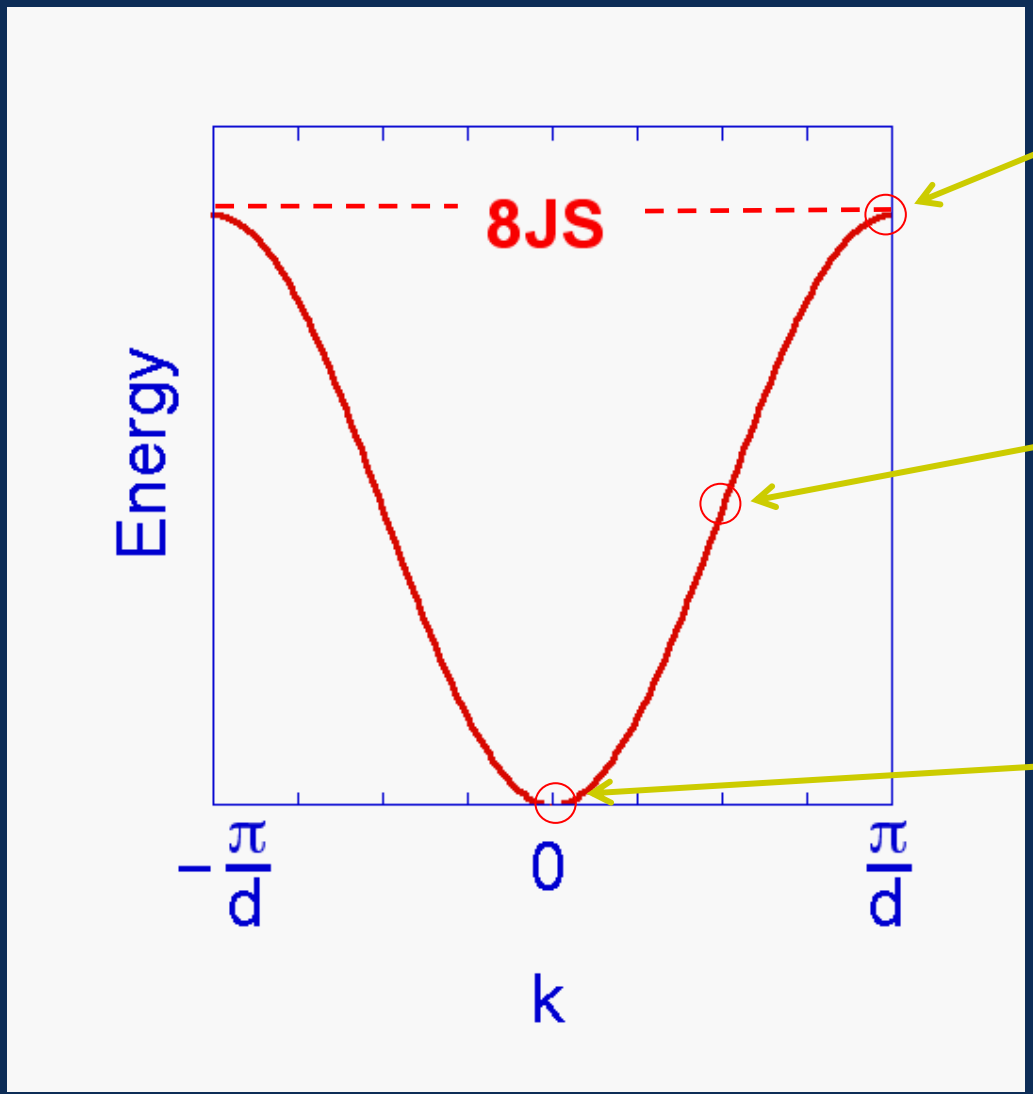

k = π/d

k = π/2d

k = 0

Classical spin waves – a little bit more general

$$H = -\sum_{nm} J(\mathbf{R}_{nm})\, \mathbf{S}_n \mathbf{S}_m$$

$$= -\sum_{q} J(\mathbf{q})\, \mathbf{S}_q \mathbf{S}_{-q}$$

where

$$J(\mathbf{q}) = \sum_n J(\mathbf{R}_n) \exp(-i\mathbf{q}\mathbf{R}_n)$$

$$\mathbf{S}(\mathbf{q}) = \sum_n \mathbf{S}(\mathbf{R}_n) \exp(-i\mathbf{q}\mathbf{R}_n)$$

- 1 magnetic atom per unit cell, 1 ordering vector **Q**

Ground state : $E_{min} = -N S^2 J(\mathbf{Q})$ **Q** maximizes $J(\mathbf{q})$

Linearized Excitations (classical spin waves) :

$$\hbar\omega(\mathbf{q}) = 2S\{ [J(\mathbf{Q}) - \tfrac{1}{2}J(\mathbf{Q}+\mathbf{q}) - \tfrac{1}{2} J(\mathbf{Q}-\mathbf{q})] [J(\mathbf{Q}) - J(\mathbf{q})] \}^{\frac{1}{2}}$$

Classical Magnet – Spin waves

$$\frac{d}{dt}\mathbf{S}_i = \mathbf{m}_i \times \mathbf{H}_{ex}(i) = \frac{J}{\hbar}\,\mathbf{S}_i \times (\mathbf{S}_{i-1} + \mathbf{S}_{i+1})$$

Linearization $S_i^{x,y} \ll S$ $S_i^{z} \approx S$

- x,y,z local coordinate system with z || $\mathbf{m}_i$
- $\mathbf{S}_{i-1}$, $\mathbf{S}_{i+1}$ need to be rotated into the local coordinate system of $\mathbf{S}_i$
- Rotation angle given by **QR**

Linearized Excitations (classical spin waves) :

$$\hbar\omega(\mathbf{q}) = 2S\{ [J(\mathbf{Q}) - \tfrac{1}{2}J(\mathbf{Q}+\mathbf{q}) - \tfrac{1}{2}J(\mathbf{Q}-\mathbf{q})]\,[J(\mathbf{Q}) - J(\mathbf{q})] \}^{\frac{1}{2}}$$

Classical spin waves – Ferromagnetic chain

$$J(q) = \sum_n J(R_n) \exp(-iqR_n)$$

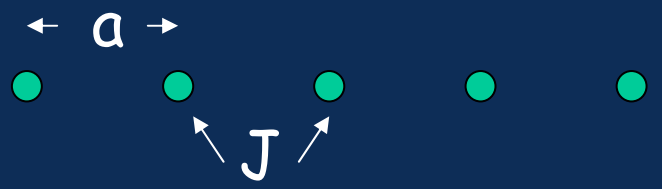

$J(q) = J \exp(-iqa) + J \exp(iqa)$
$= 2 J \cos(qa)$

$J > 0$ (FM)

Ground state : maximize $J(q)$ -> $Q=0$, $J(Q)=2J$

Excitations (classical spin waves) :

$$\hbar\omega(q) = 2S\{ [J(Q)-\tfrac{1}{2}J(Q+q)-\tfrac{1}{2} J(Q-q)] [J(Q)-J(q)] \}^{\frac{1}{2}}$$

$\hbar\omega(q) = 2S\{ [2J-\frac{1}{2}2J\cos(qa)-\frac{1}{2}2J\cos(-qa)] [2J-2J\cos(qa)] \}^{\frac{1}{2}}$
$= 2S\ 2J\ [\ 1-\cos(qa)\ ]$
$= 4SJ\ [1-\cos(qa)]$

Classical spin waves – Antiferromag. chain

$$J(q) = \sum_n J(R_n) \exp(-iqR_n)$$

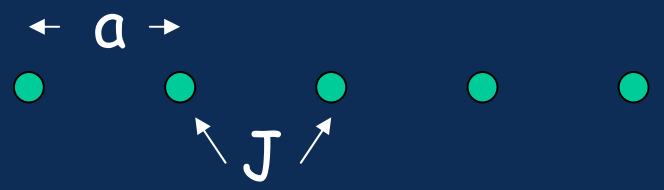

$$J(q) = J \exp(-iqa) + J \exp(iqa) = 2J \cos(qa)$$

$J < 0$ (AF)

Ground state : maximize $J(q)$ -> $Q = \pi/a$, $J(Q) = -2J > 0$

Excitations (classical spin waves) :

$$\hbar\omega(q) = 2S\{ [J(Q)-\tfrac{1}{2}J(Q+q)-\tfrac{1}{2} J(Q-q)] [J(Q)-J(q)] \}^{\frac{1}{2}}$$

$$\begin{aligned}\hbar\omega(q) &= 2S \{ [-2J-J\cos(\pi+qa) -J\cos(\pi-qa)] [-2J-2J\cos(qa)] \}^{\frac{1}{2}} \\ &= 2S \{ -2J [-2J +J\cos(qa) +J\cos(qa)] [1+\cos(qa)] \}^{\frac{1}{2}} \\ &= 4S|J| [1-\cos^2(qa)]^{\frac{1}{2}} \\ &= 4S|J||\sin(qa)|\end{aligned}$$

Classical spin waves - AF

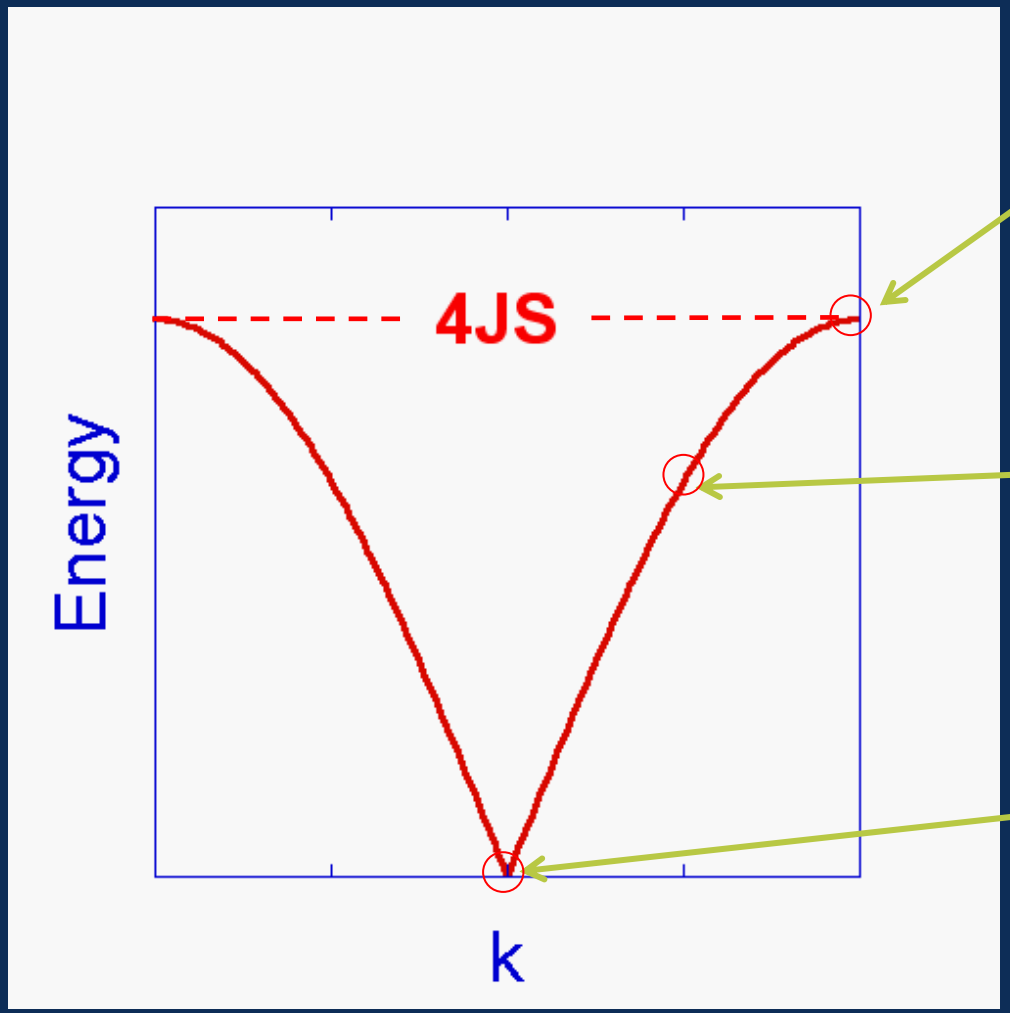

k = π/2d

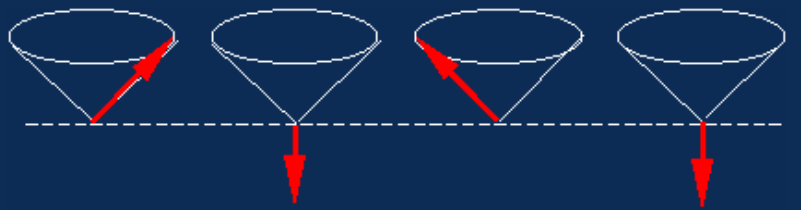

k = 3π/4d

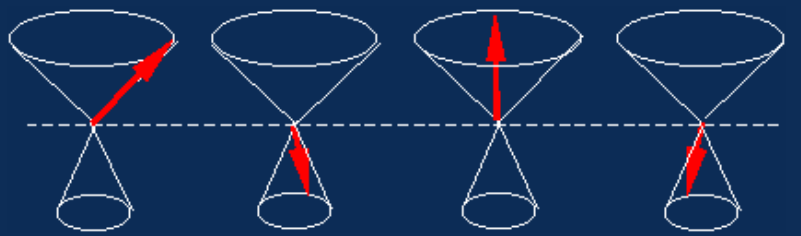

k = π/d

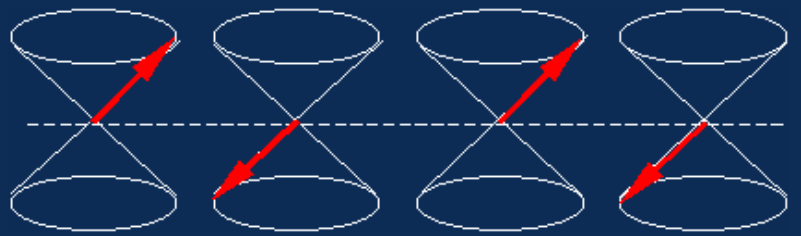

Examples

$LiCuVO_4$

~90mm^3 single crystal: A.V. Prokofiev, W. Assmus, Frankfurt

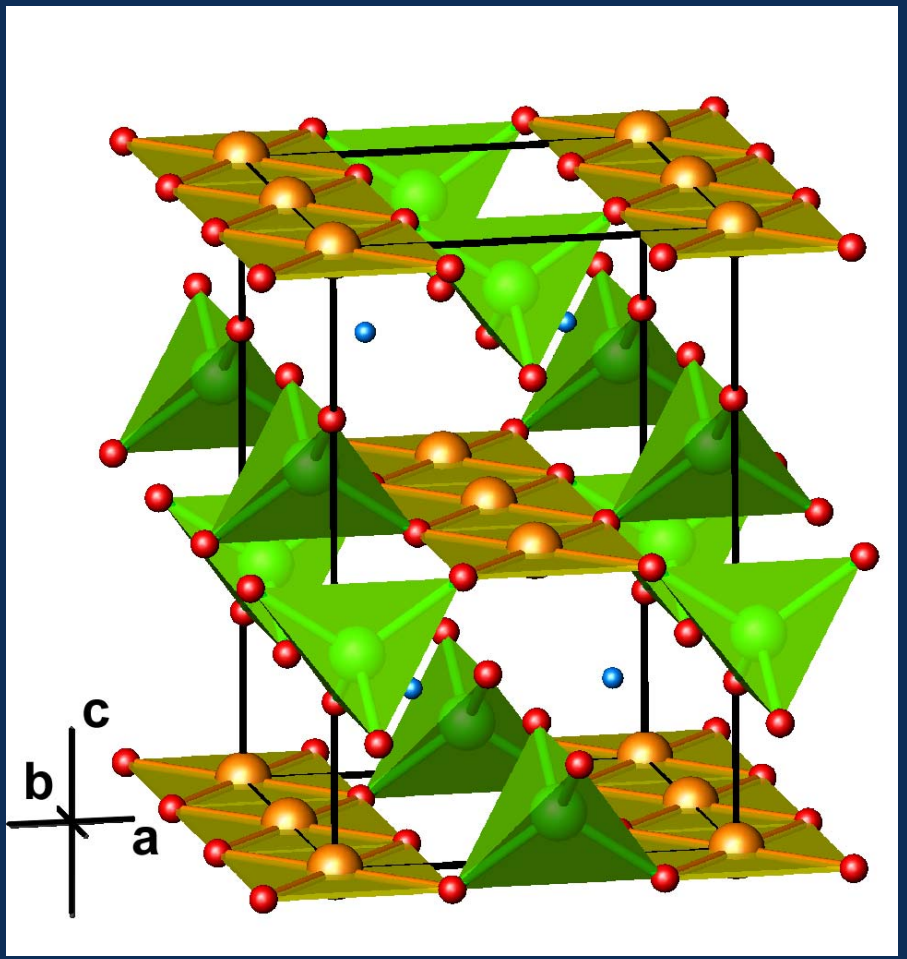

1D nn/nnn Heisenberg AF (Classical)

$$H = J_1 \Sigma S_n S_{n+1} + J_2 \Sigma S_n S_{n+2}$$

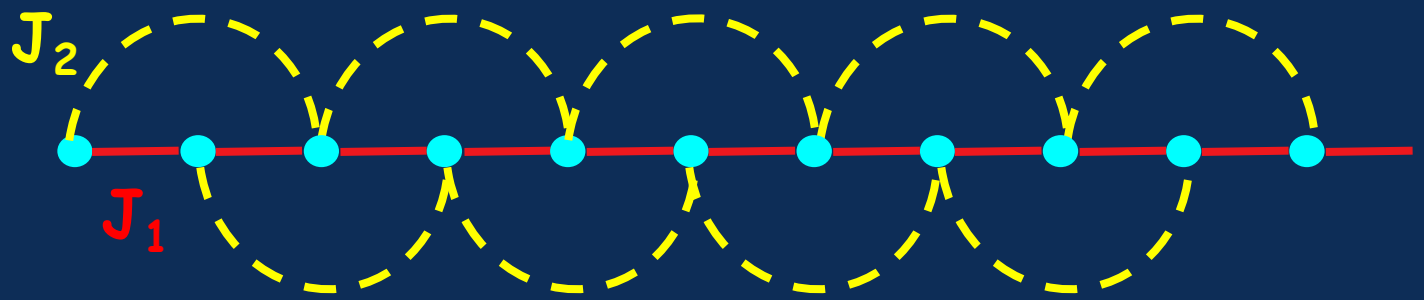

$$J(q) = 2J_1\cos(qa) + 2J_2\cos(2qa)$$
$$= 2J_1\cos(qa) + 2J_2[2\cos^2(qa)-1]$$

$J_2>0$ (AF)

Maximize J(q) -> $\cos(Qa) = -J_1/4J_2$ - helical structure !

Dispersion – $LiCuVO_4$

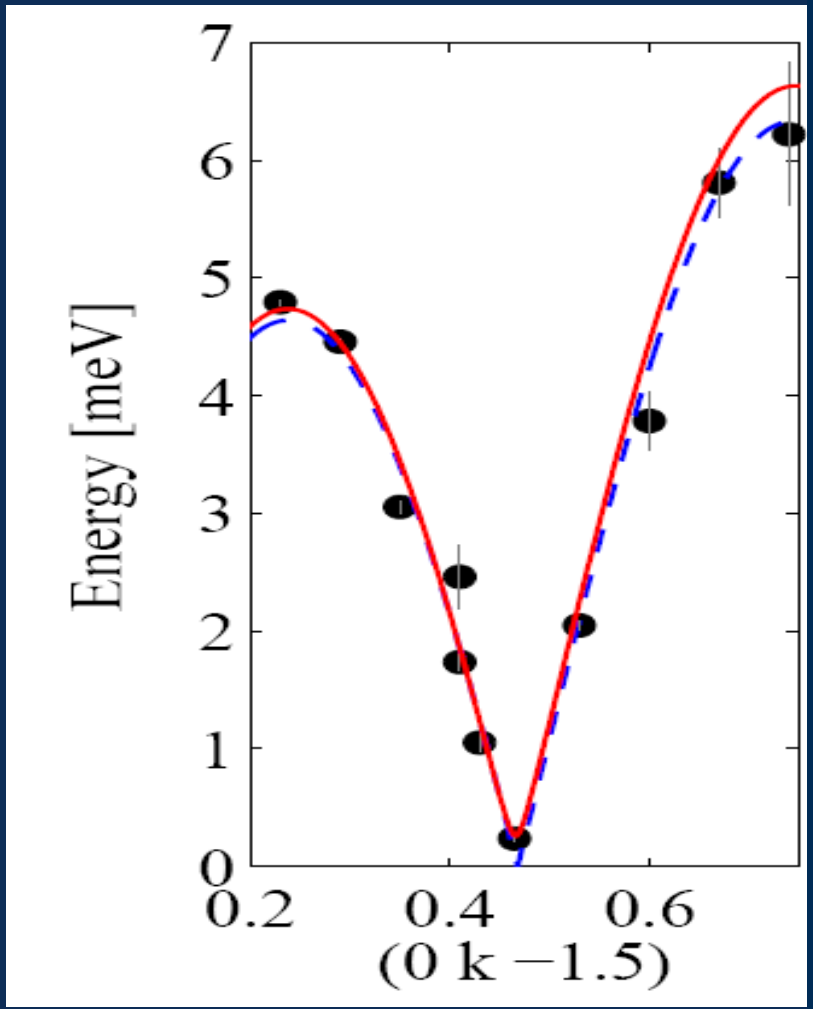

M. E. et al., EPL 2005

Magnetic excitations

- measured by Triple-Axis Spectroscopy

Part 2: Triple-Axis Spectrometer

EXPERIMENTAL FACILITIES AT ILL 2005

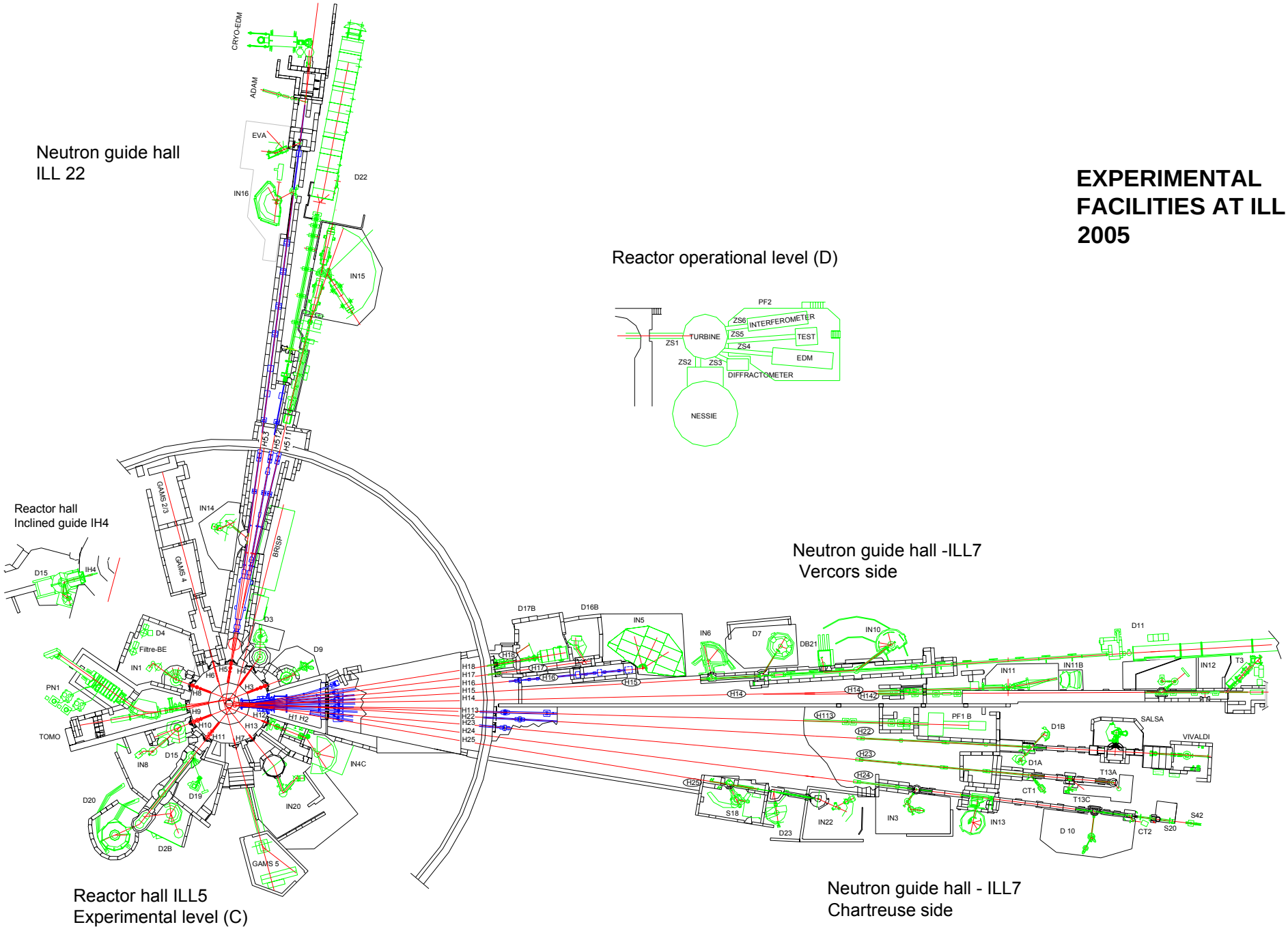

ILL DPT/SMAE
Mars 2006
Amp/Projets instrum

Beam tubes of ILL present state

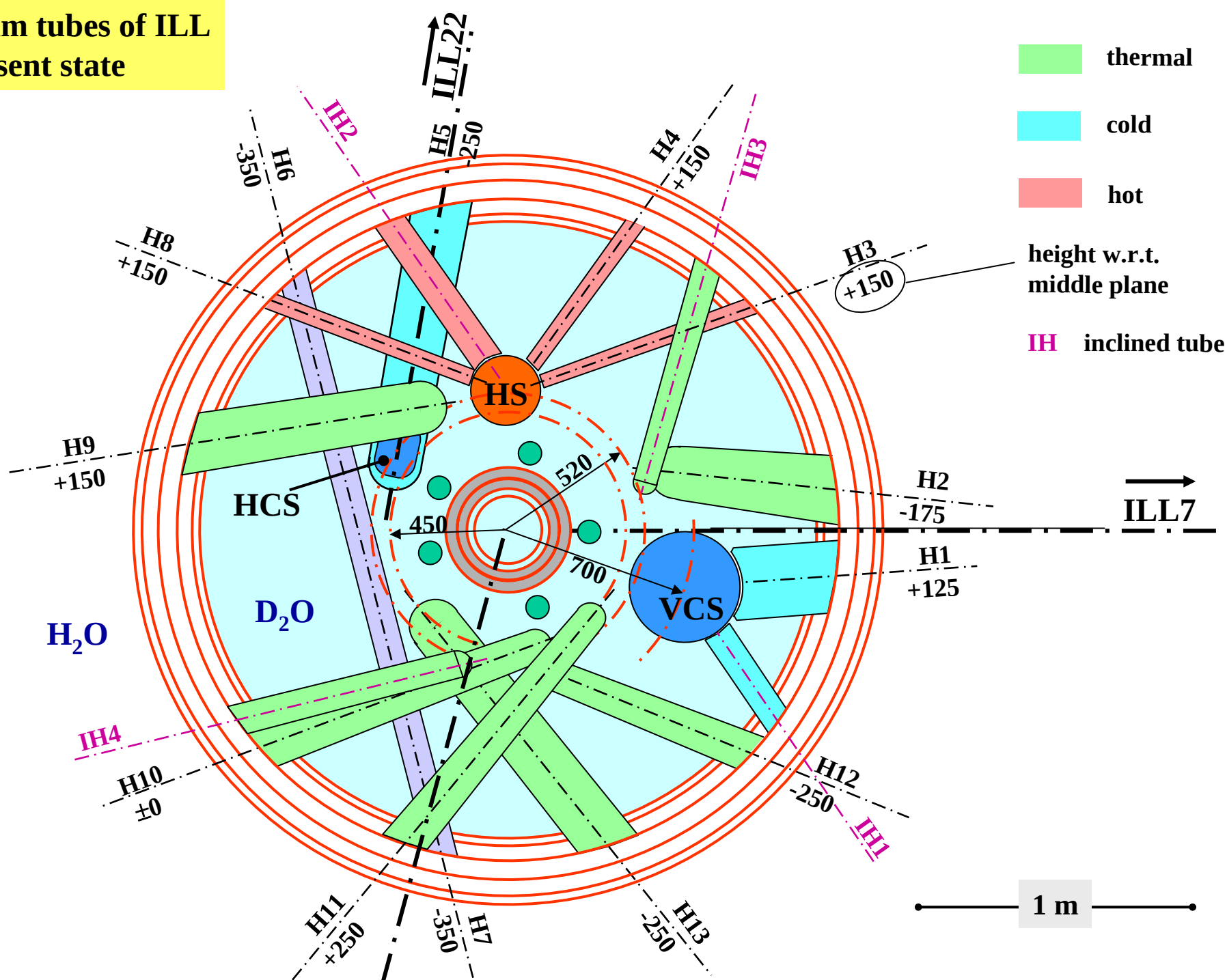

Flux distributions

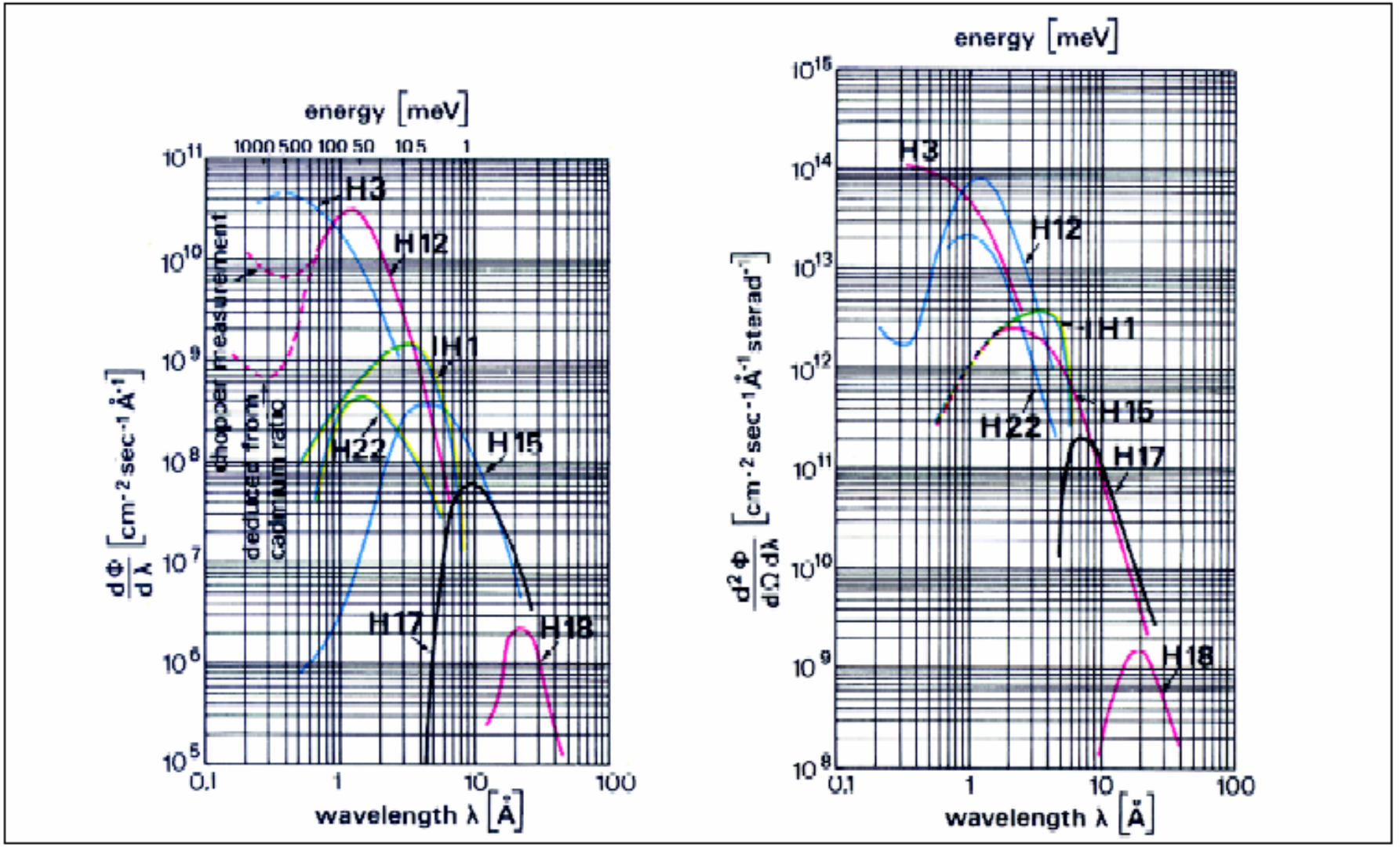

Triple-Axis -Spectrometer

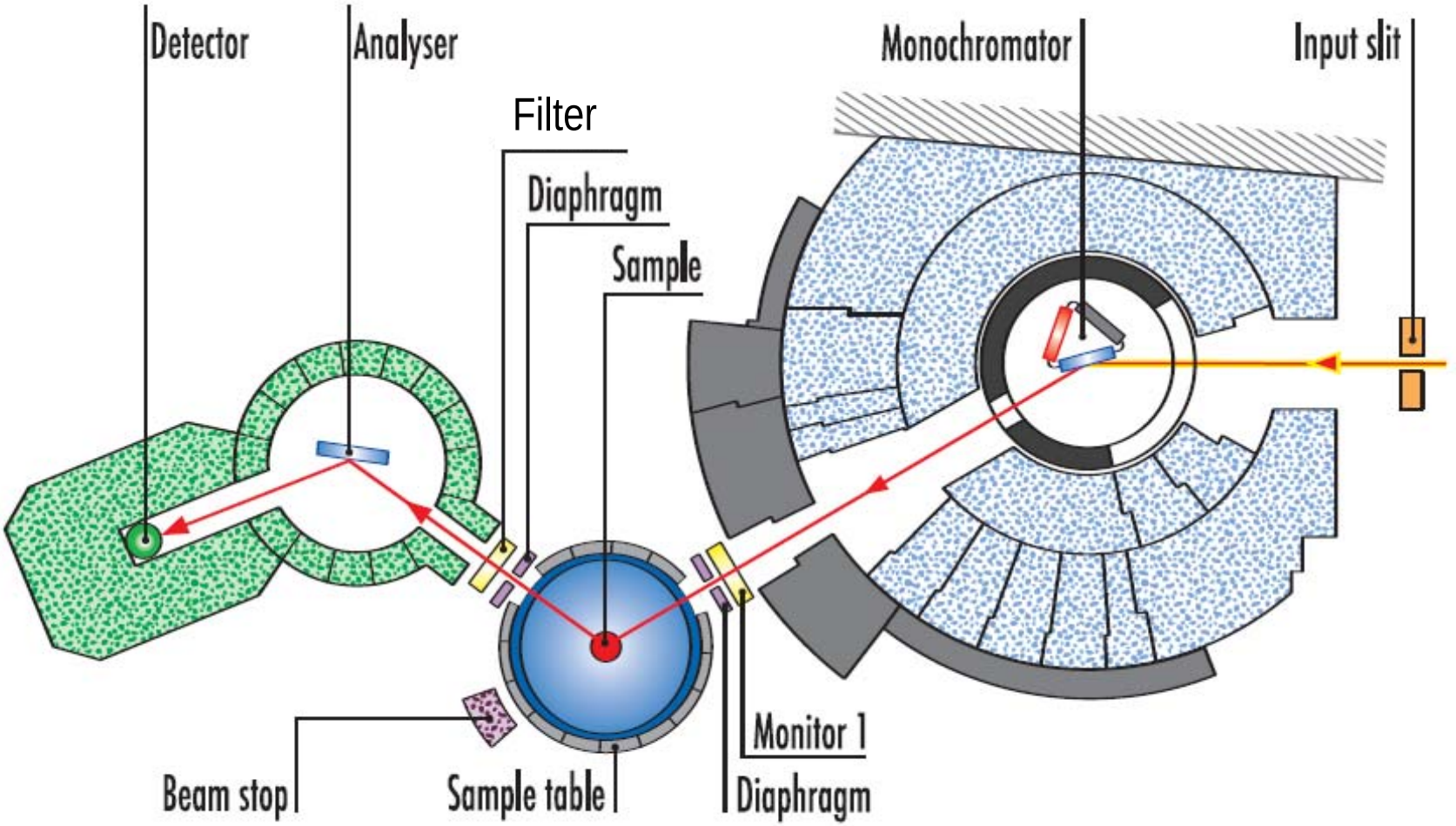

Thermal white incoming beam (IN20)

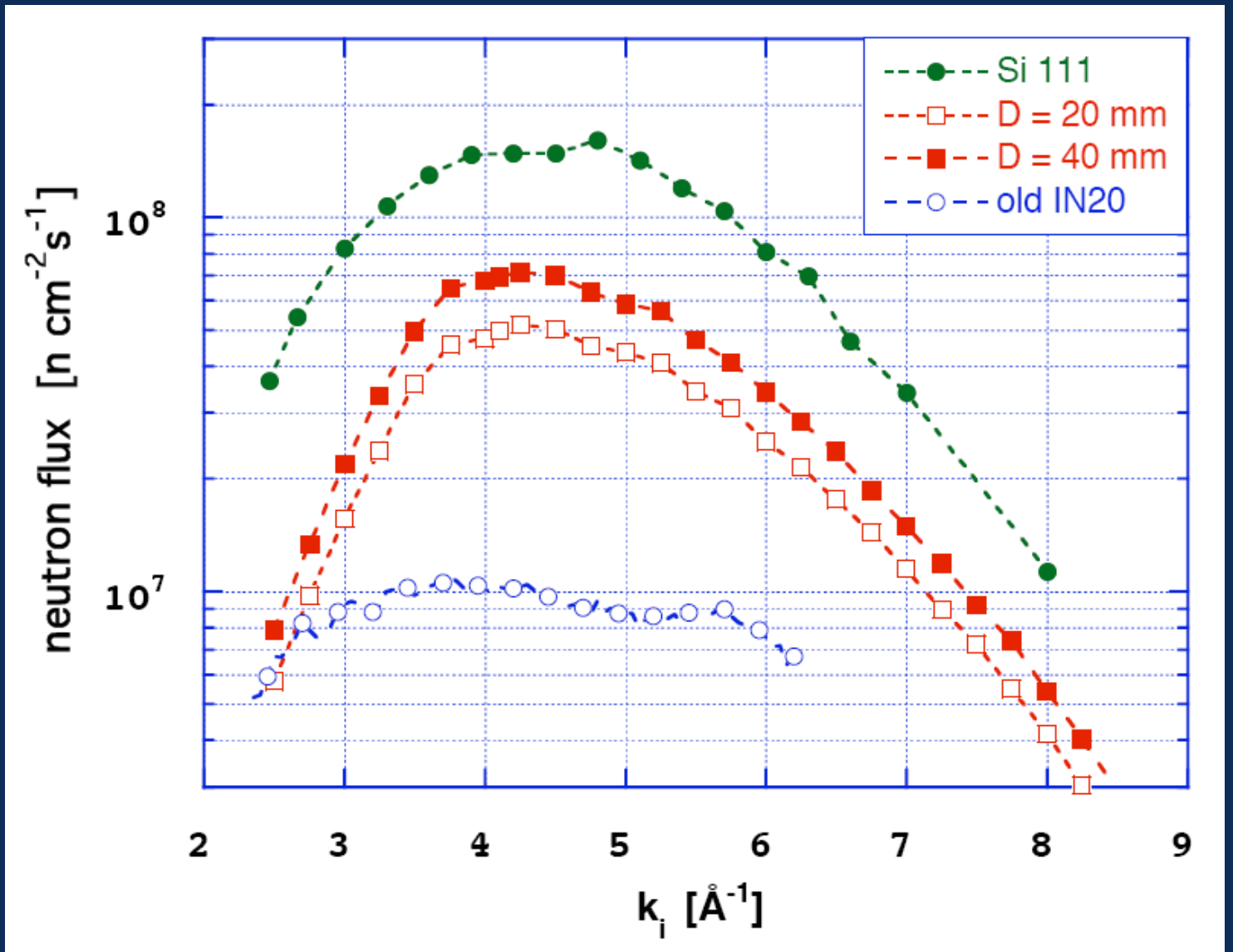

Monochromator/Analyser

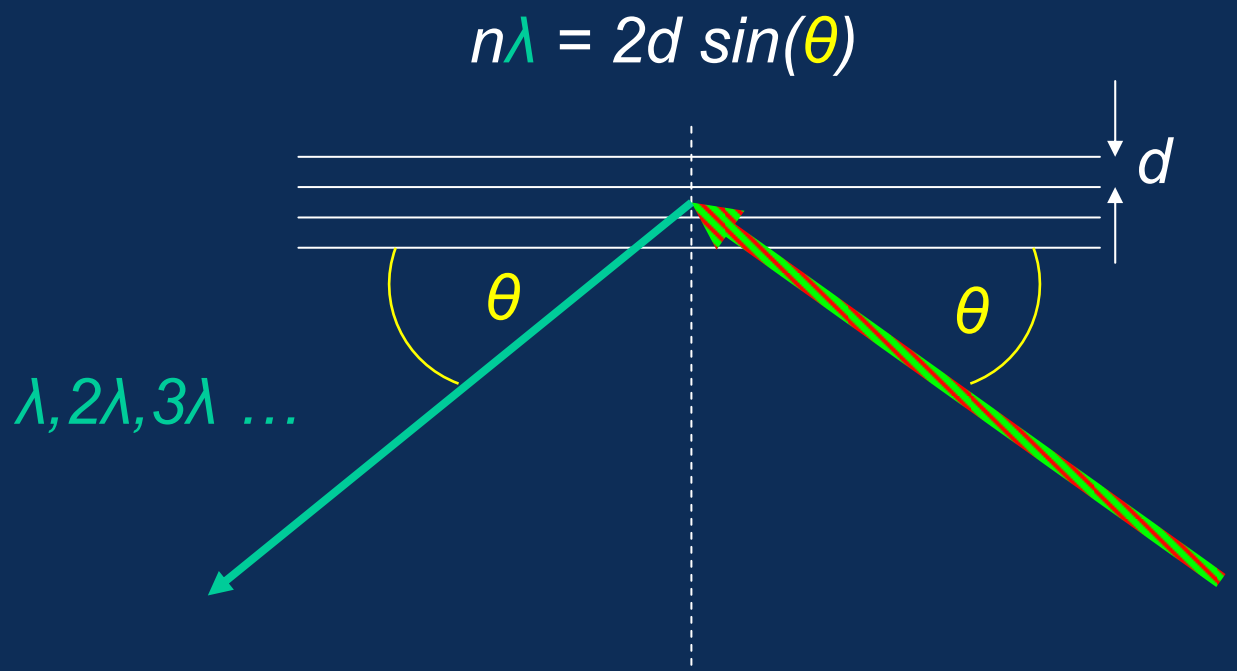

- Mosaicity
- Reflectivity
- Focusing Arrays

Monochromator/Analyser

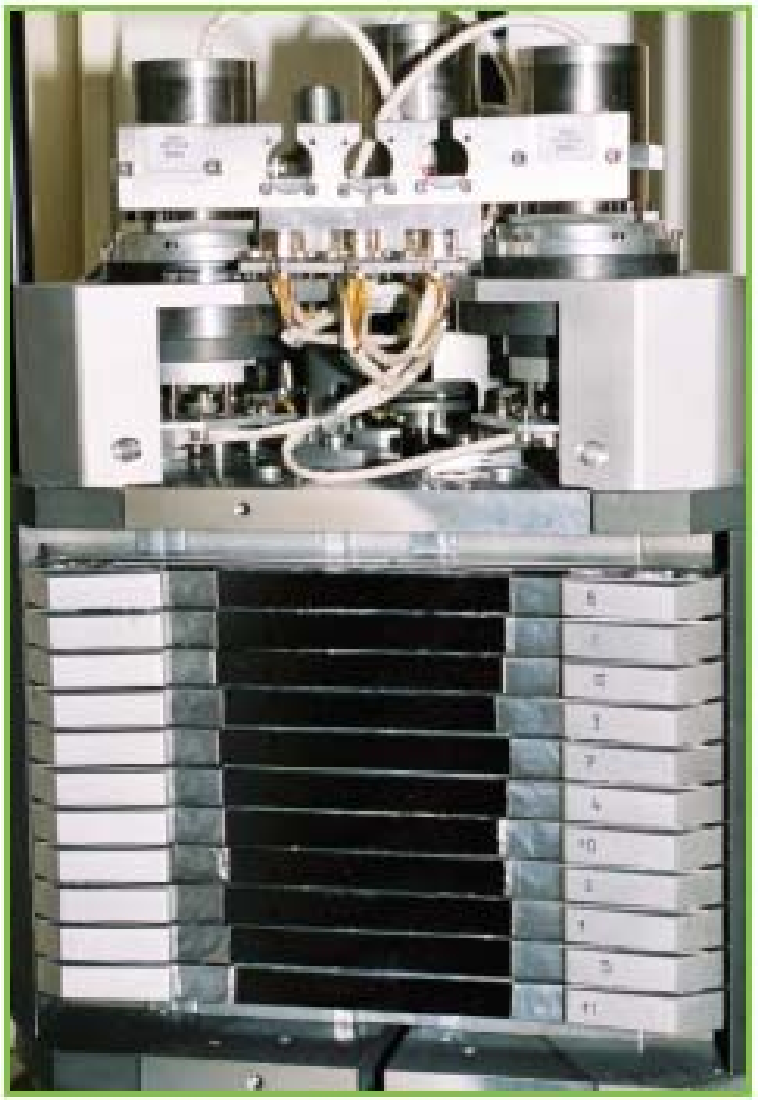

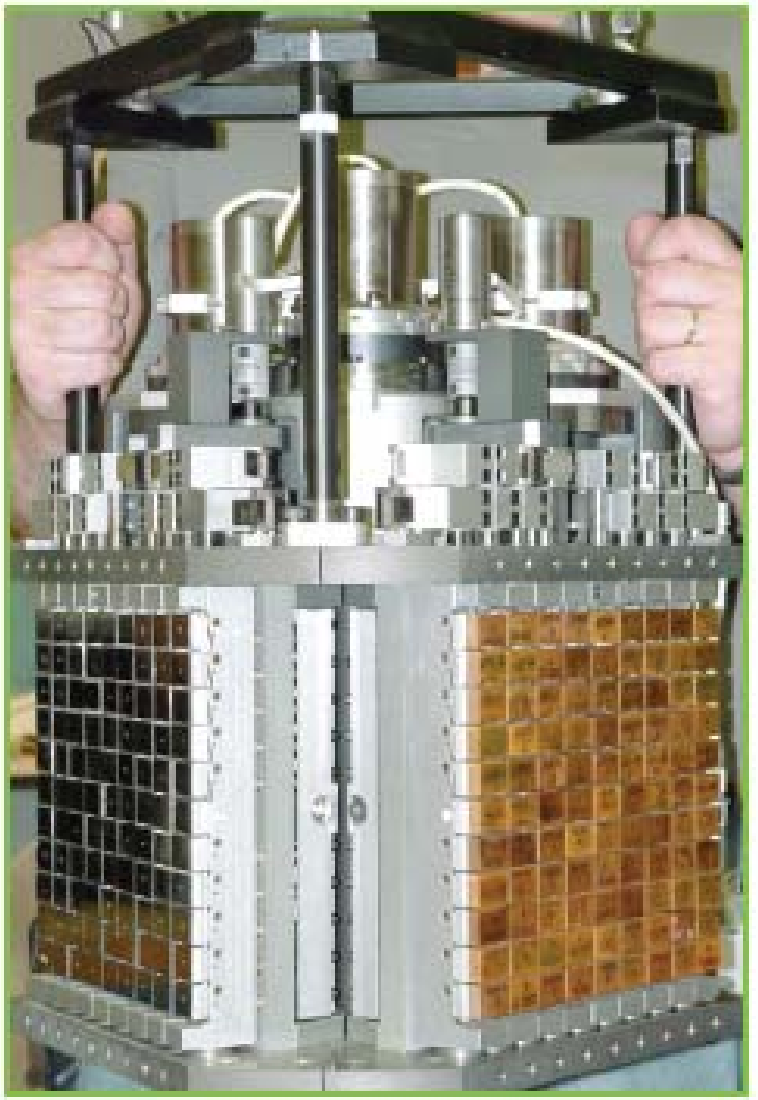

Monochromator/Analyser

- Focusing Arrays

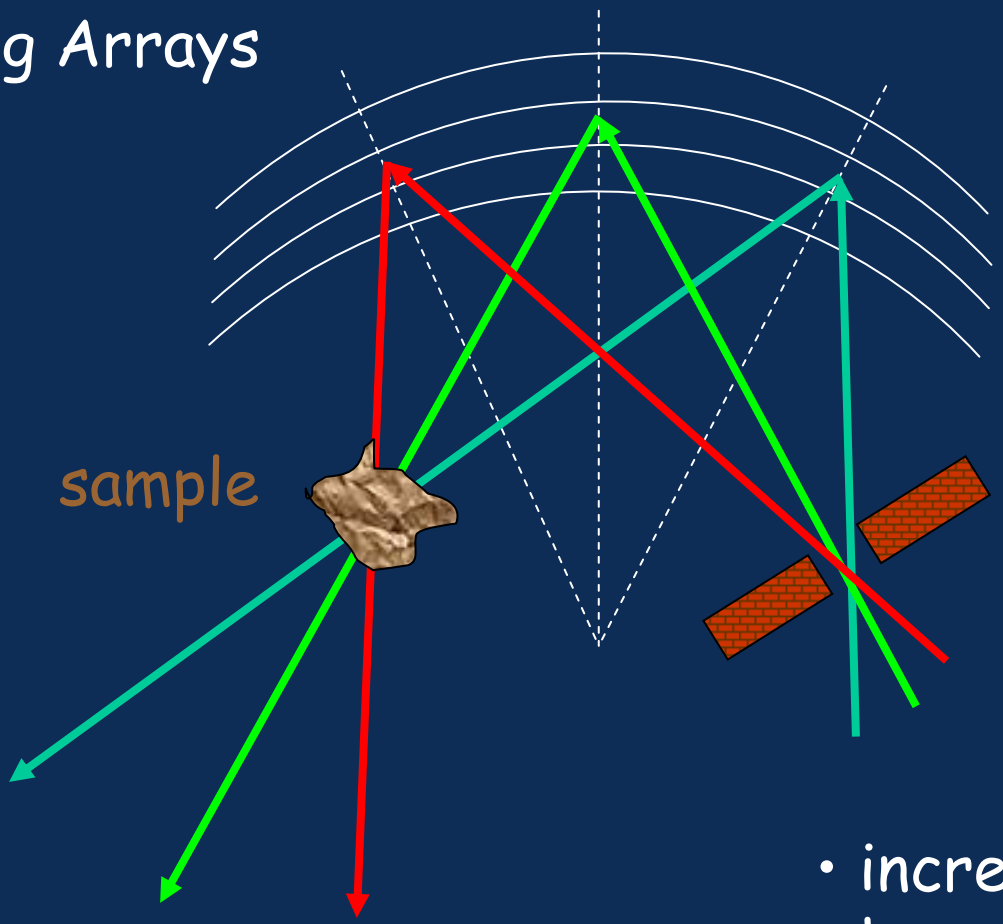

- increase beam divergence
- keep monochromaticity
- reduce background

Sample and sample table

Filters

- Pyrolytic Graphite Filter (high transmission for k = 2.662 $Å^{-1}$
  10^{-3} – 10^{-4} for 2k, 3k

  k = 4.1 $Å^{-1}$
  10^{-2} 2k)
- 77K Be-filter (cuts above 1.55 $Å^{-1}$)
- Velocity Selector (works up to approximately 5 $Å^{-1}$)

Puma/FRMII

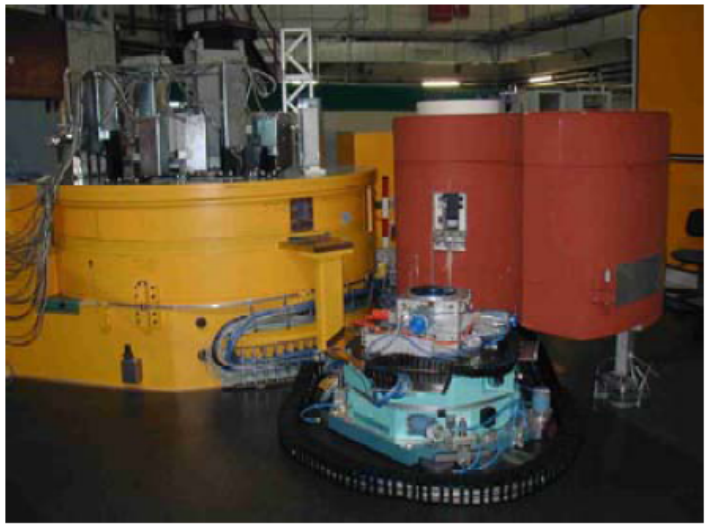

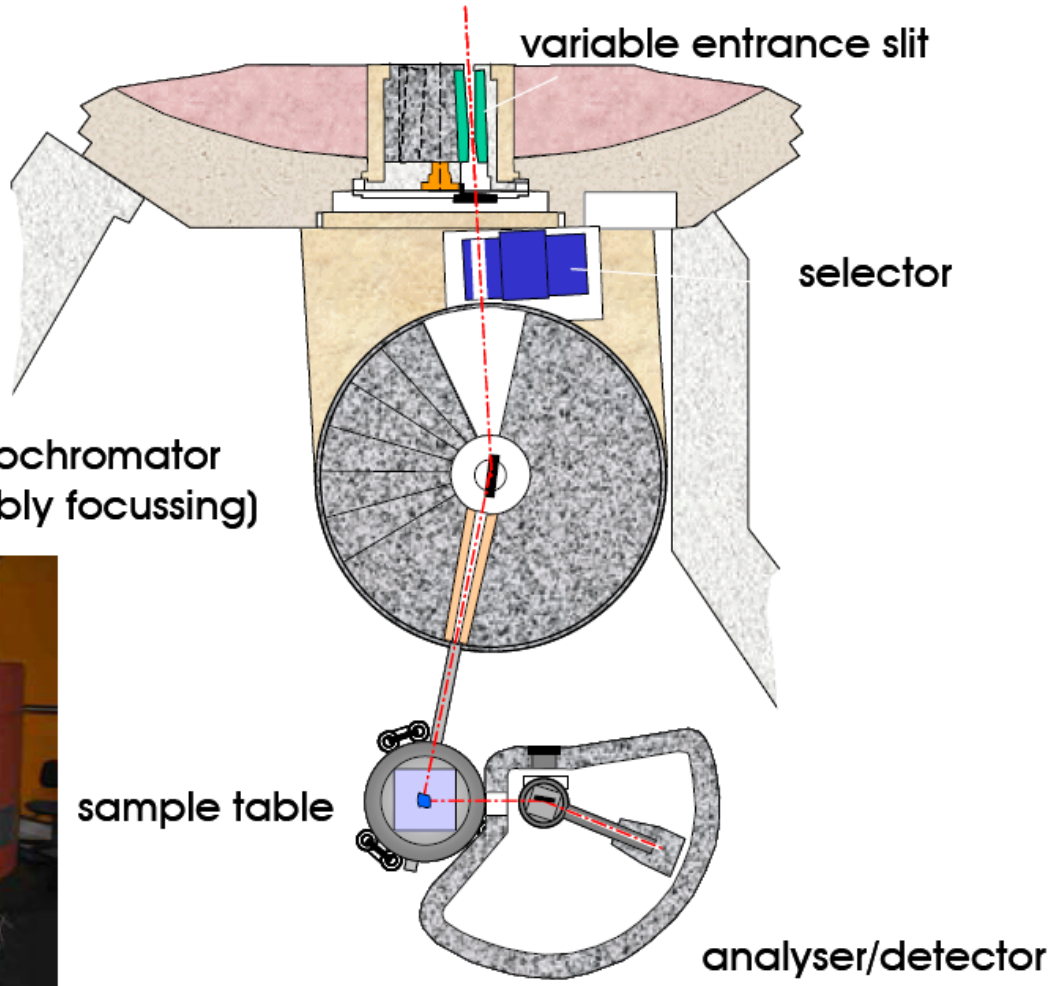

G. Eckold, P.Link, C. Hradil

Detector

$^3He + n \rightarrow {}^4He$ (metastable) $\rightarrow T^+ + p^+ + kin.E$

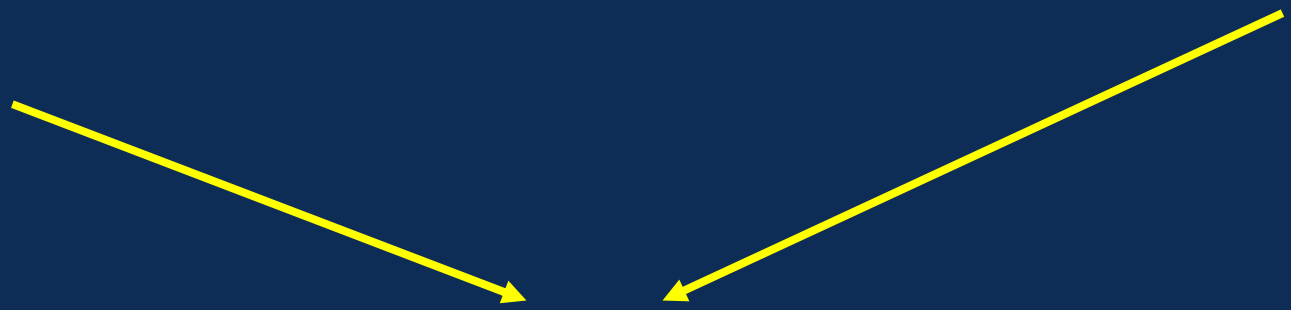

^3He gas discharge (avalanche)

Proportional counter

Triple-Axis -Spectrometer

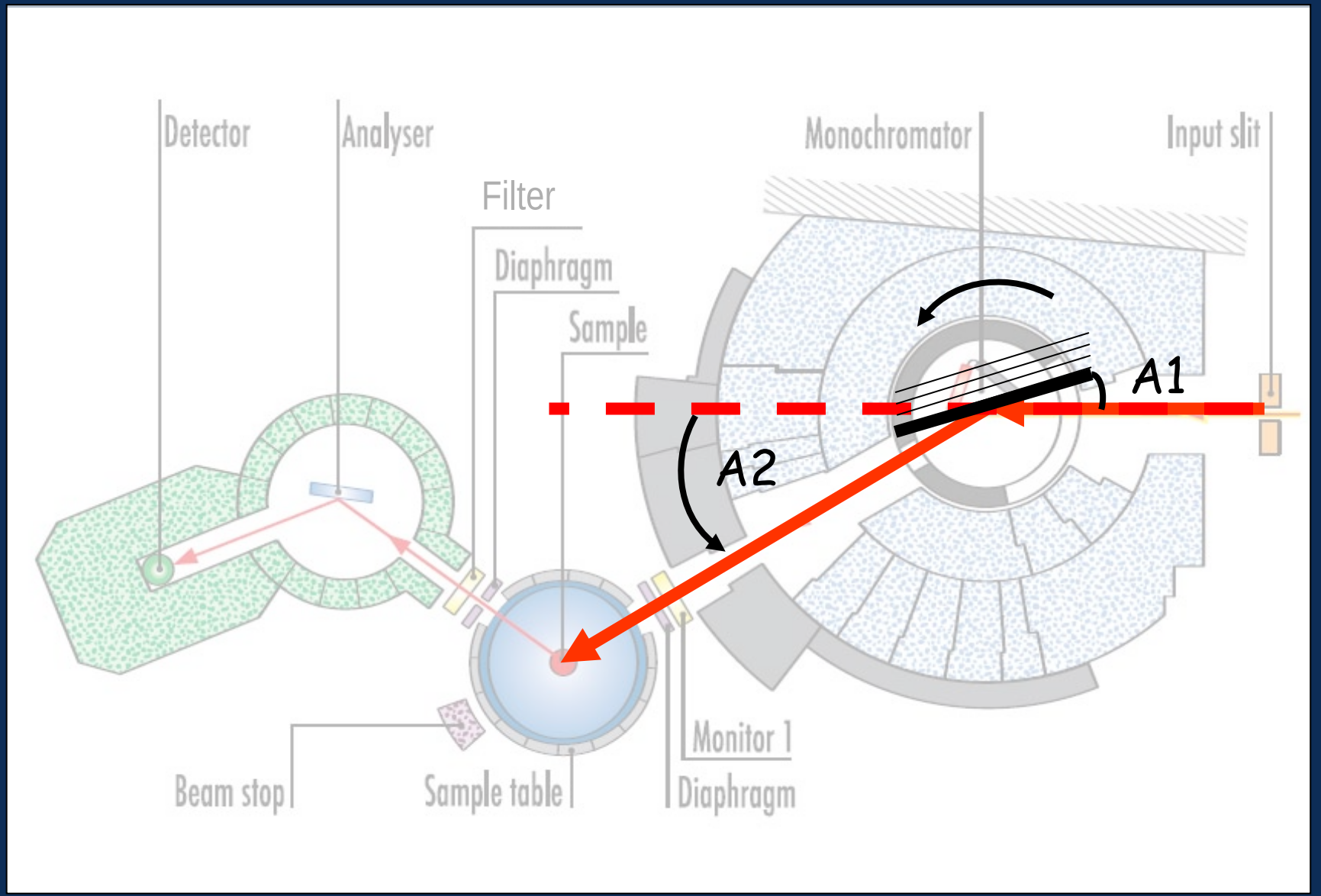

Triple-Axis -Spectrometer

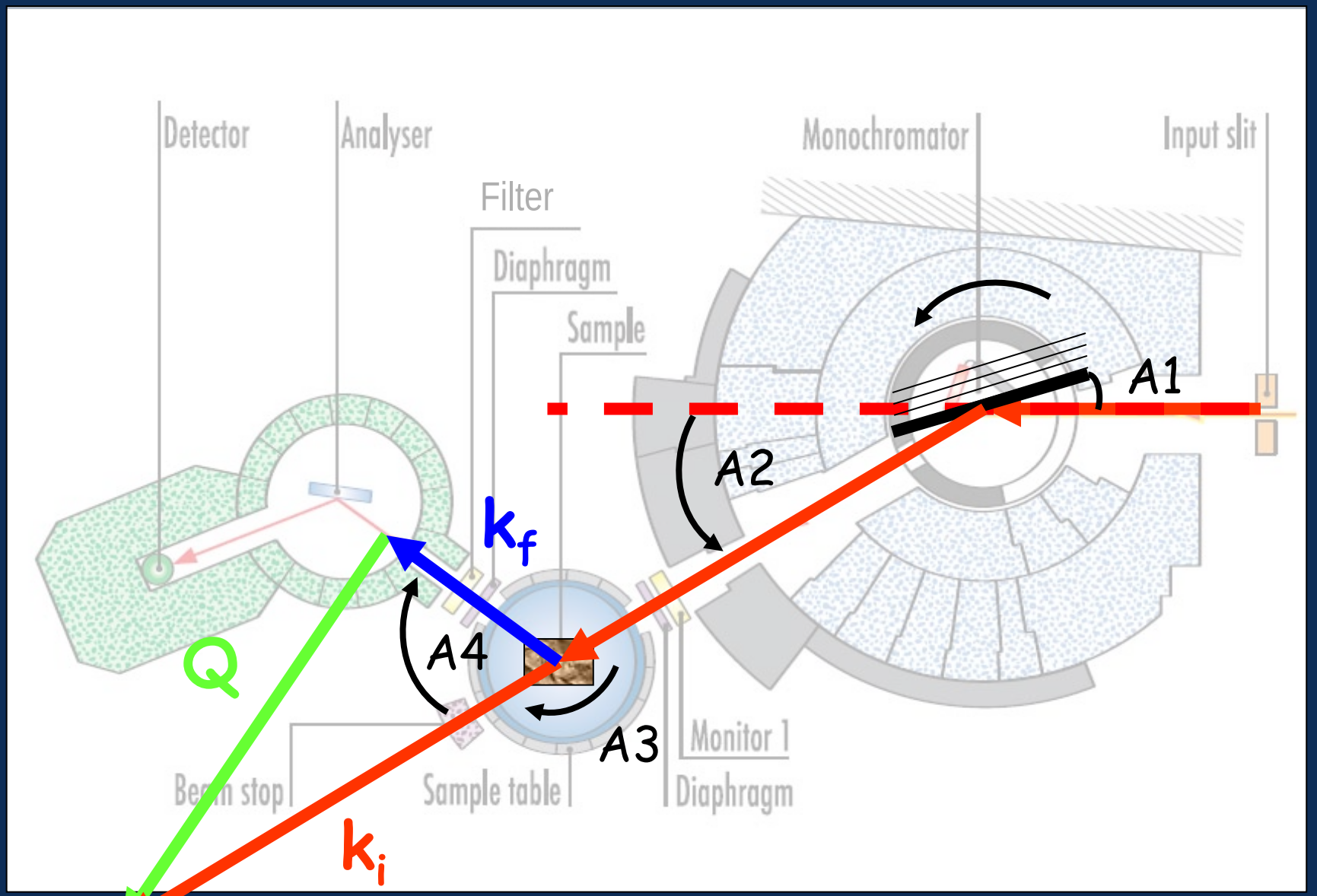

Triple-Axis -Spectrometer

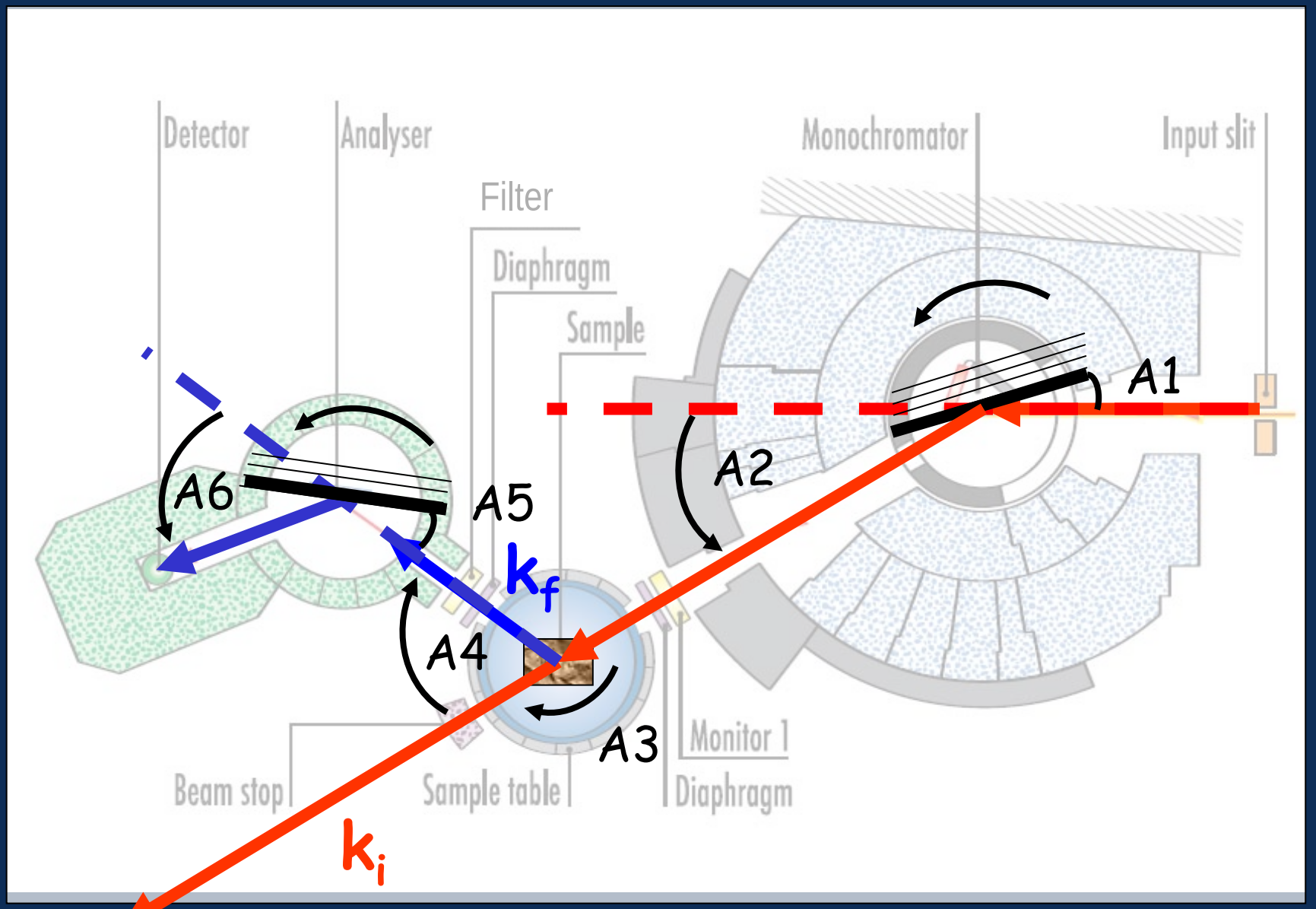

Dispersion – $LiCuVO_4$

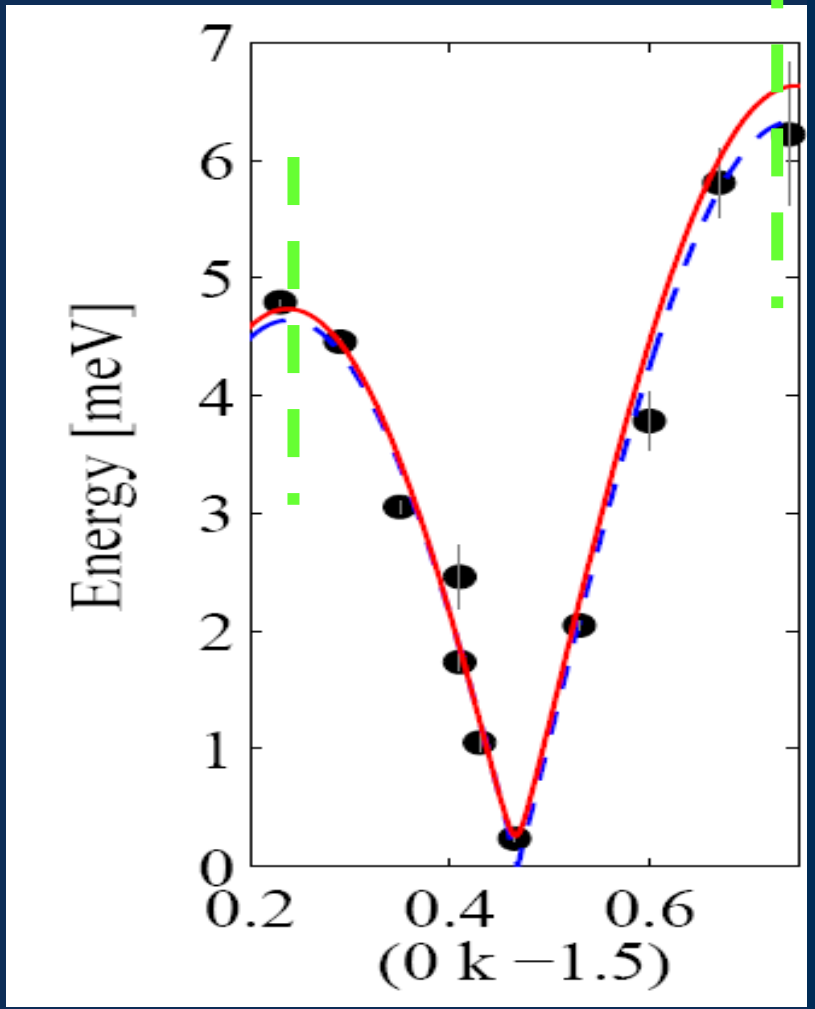

M. E. et al., EPL 2005

Triple-Axis -Spectrometer

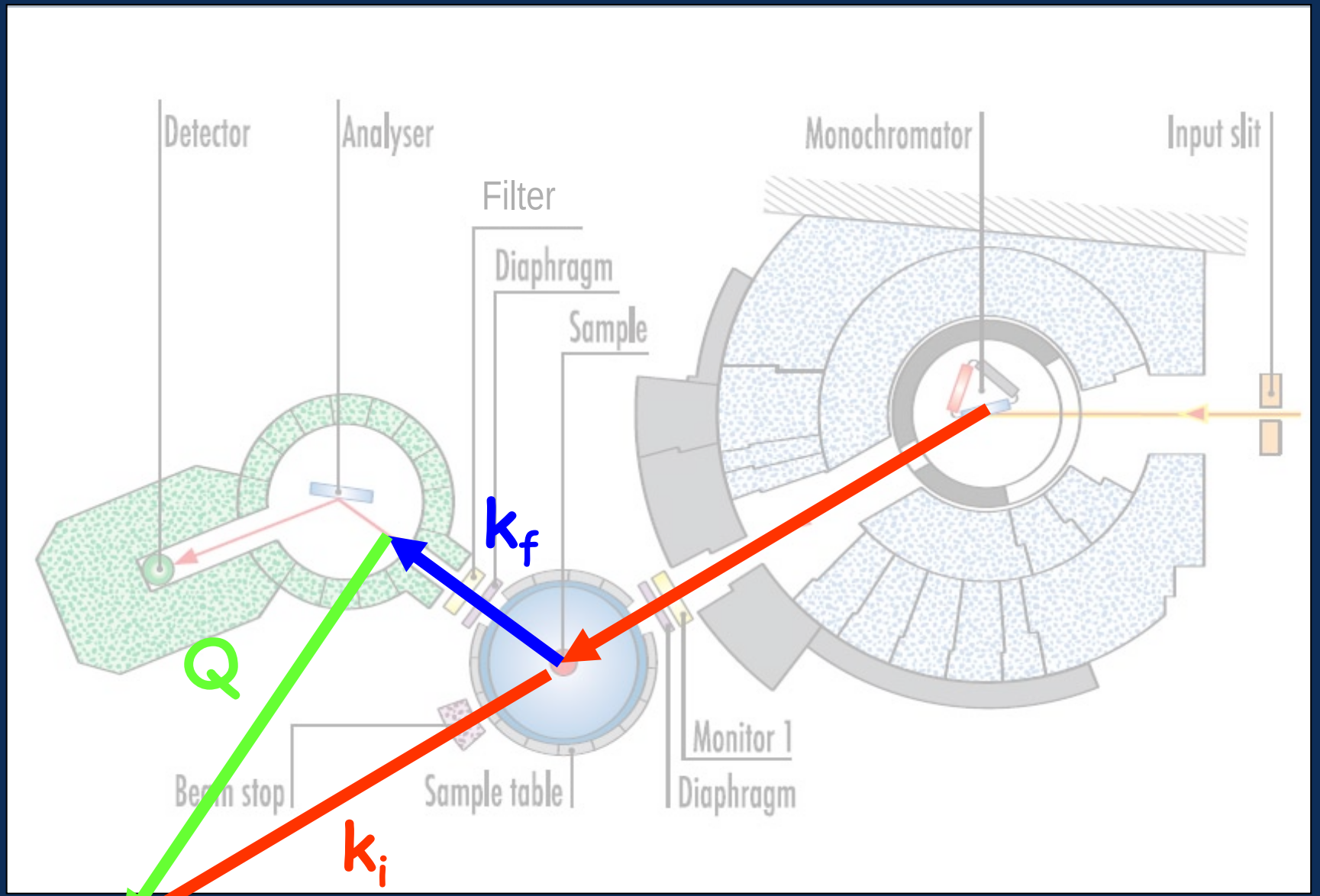

Triple-axis spectrometer (single detector)

Constant k_f mode
Scan E at constant Q

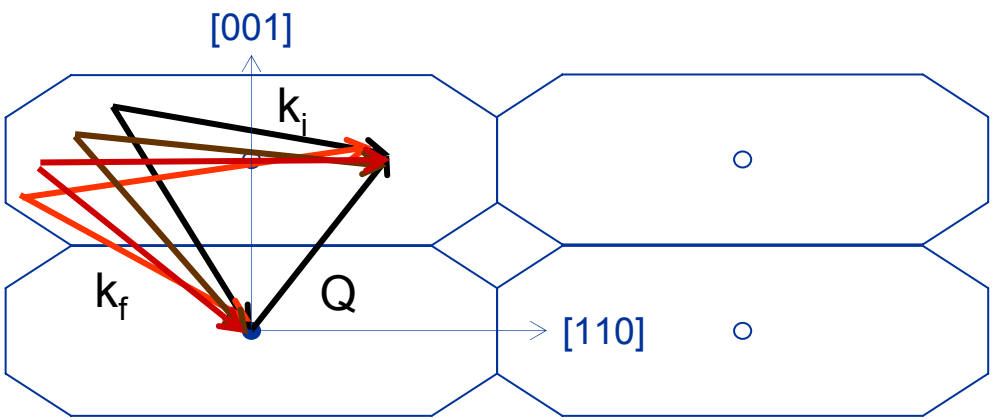

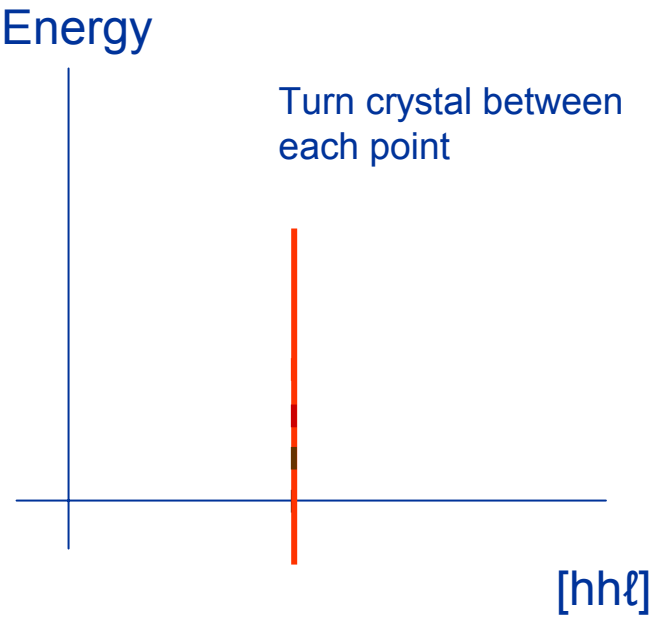

Scan E at constant Q involves rotation of crystal wrt. ki

Inelastic neutron scattering – $LiCuVO_4$

IN20

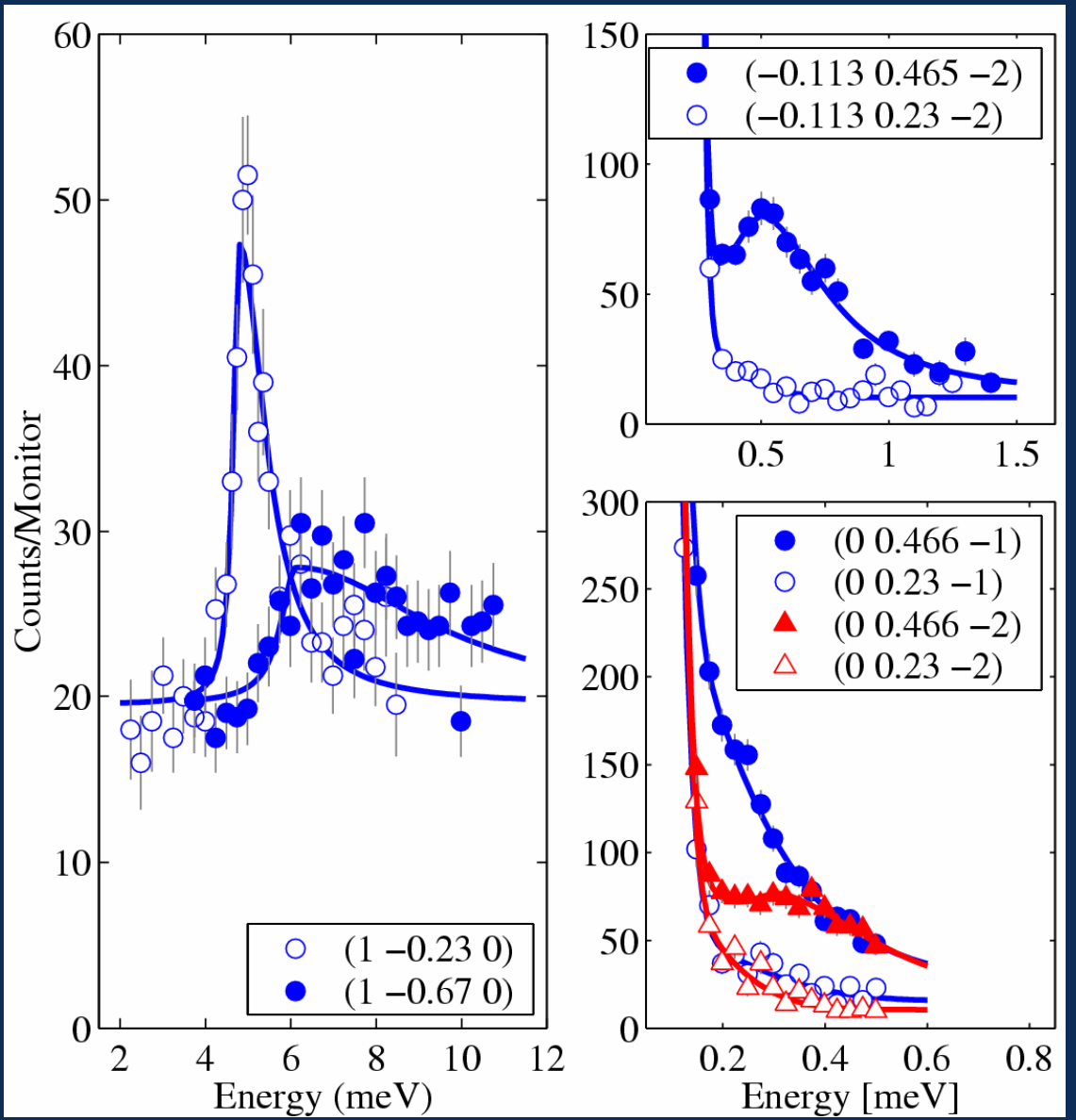

IN12

Dispersion – $LiCuVO_4$

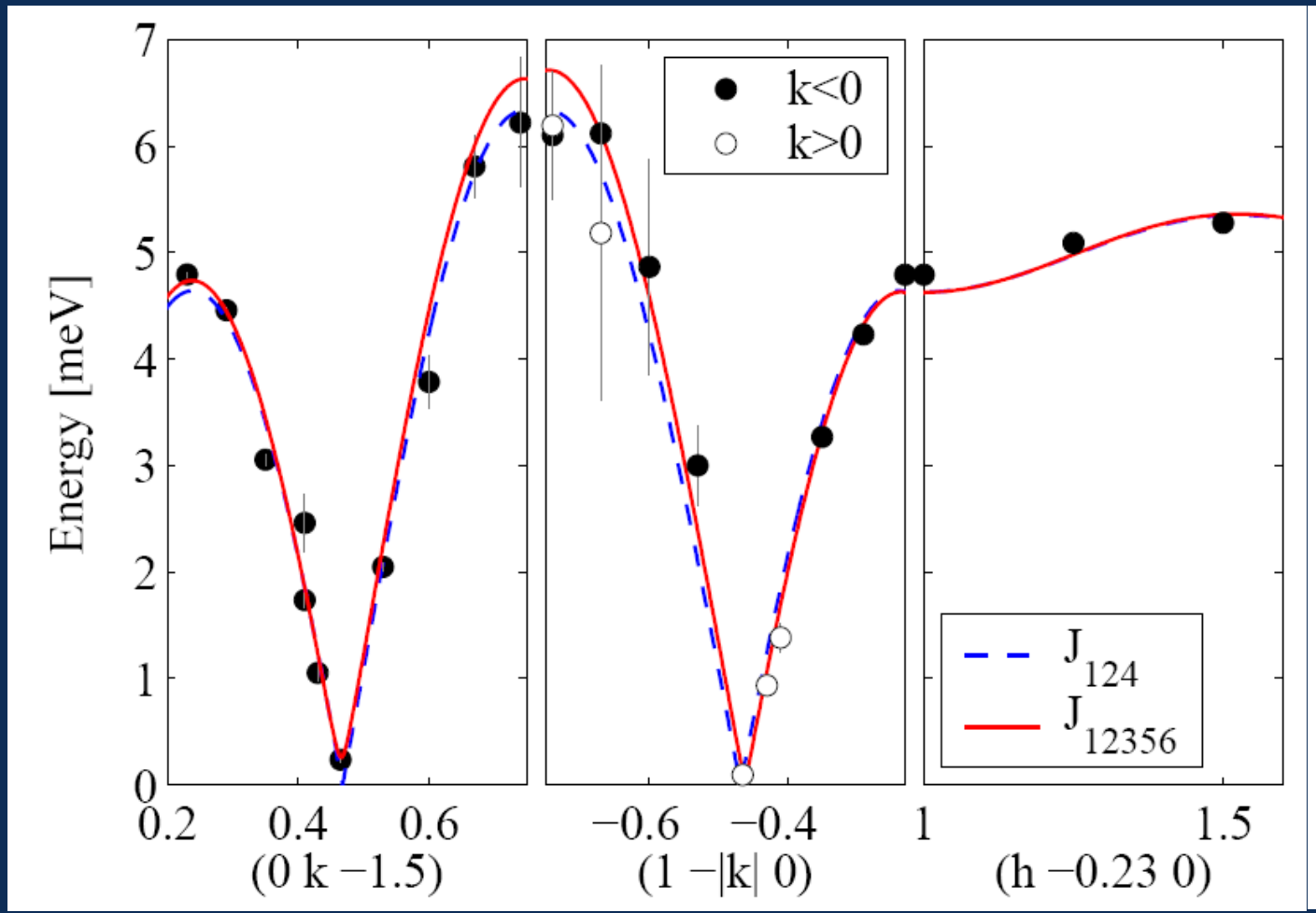

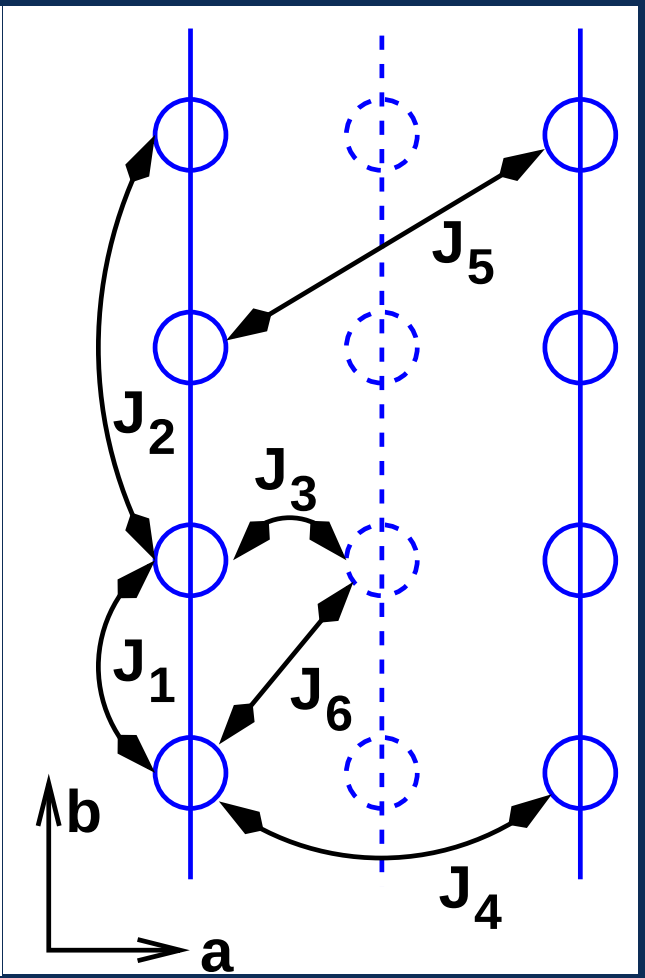

M. E. et al., EPL 2005

Dispersion, low-E, off-symmetry direction

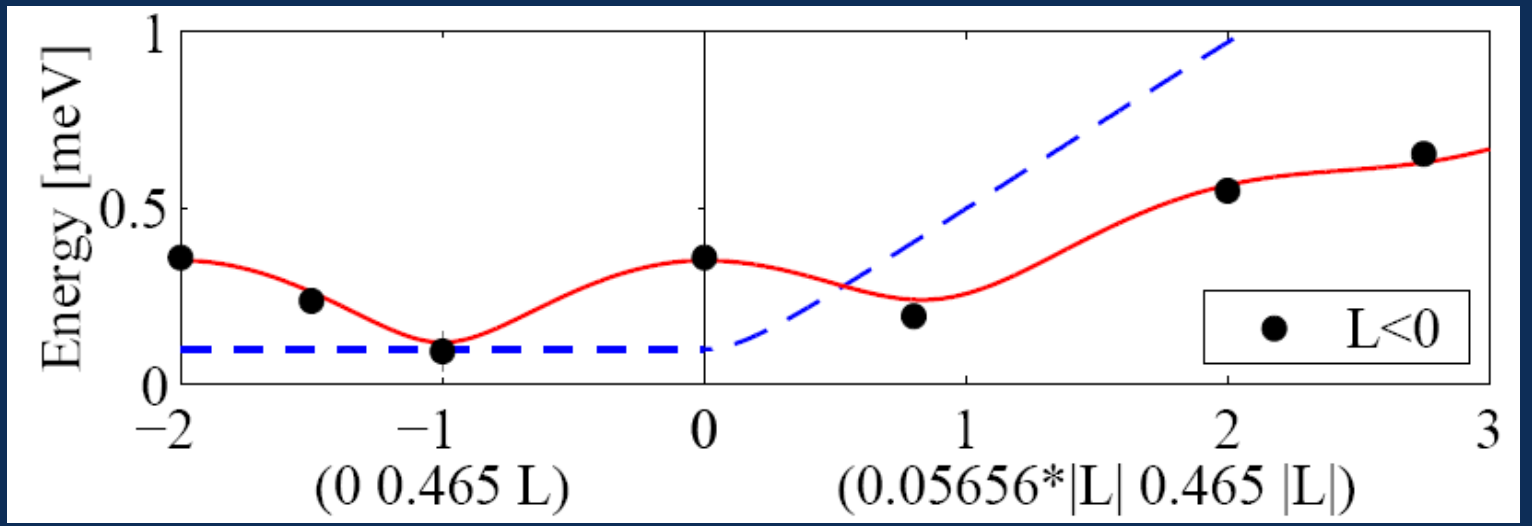

path i	$i=1$	2	3	4	5	6
R_iJ_i (nsc)	-1.6(2)	5.59(8)	-0.014(10)	0.01(3)	-0.40(8)	0.08(4)
	-1.6(2)	5.60(8)	-0.015(9)	-	-0.37(5)	0.08(4)

M. E. et al., EPL 2005

Crystal analyzer spectrometer

Many detectors

k_f constant

$Q_\perp := Q \perp k_i$

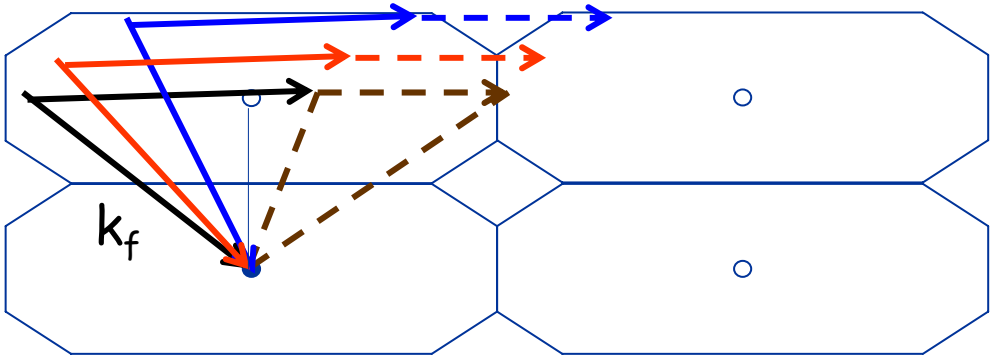

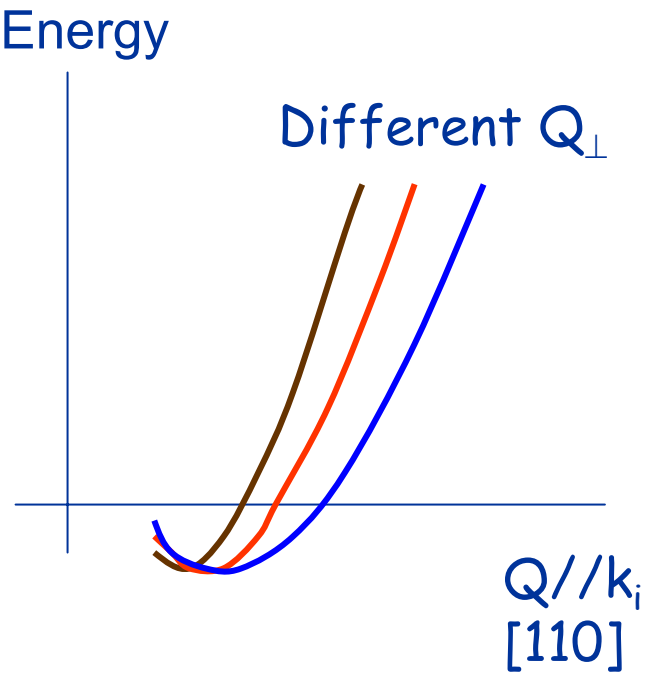

Bjorn Fak

Flat Cone multianalyzer (IN20 / IN14)

• angular coverage	75 deg
• pixel width	1.3 deg
• no. of pixels	31
• SA distance	765 & 1000 mm
• analyzer crystals	Si 111
• cold neutrons	$k_f = 1.5$ Å^{-1}
	$\Delta E = 0 - 10$ meV
• thermal neutrons	$k_f = 3$ Å^{-1}
	$\Delta E = 0 - 40$ meV

R. Currat, B. Detlefs, M. Kempa, J. Kulda

Flatcone

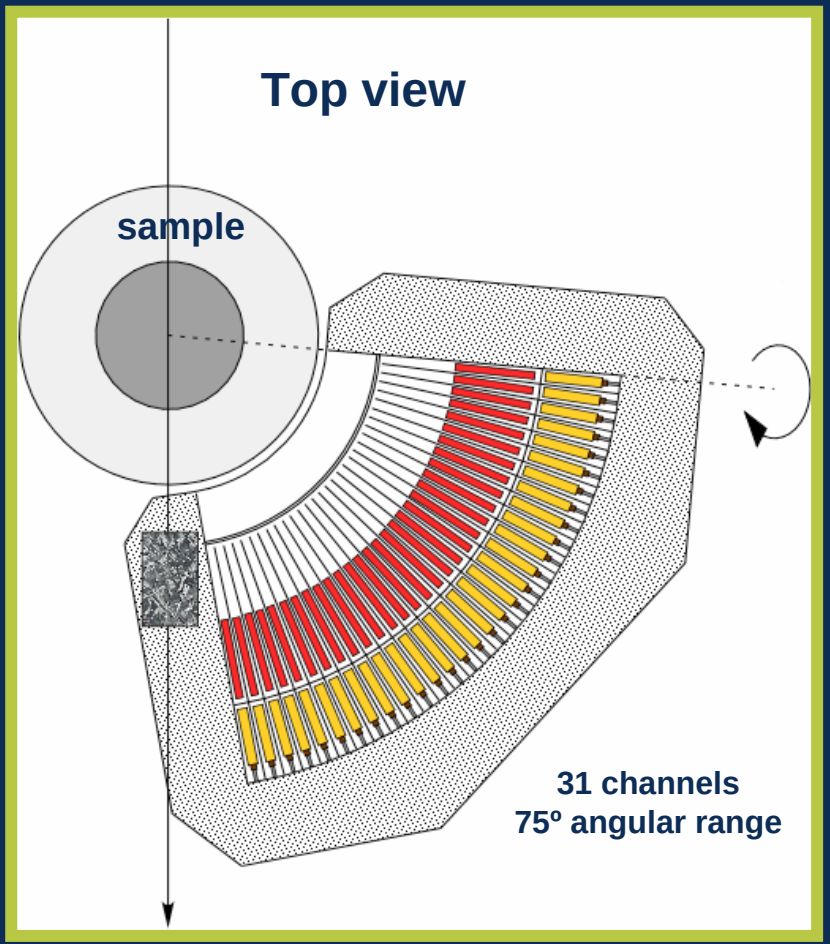
Top view
sample
31 channels
75º angular range

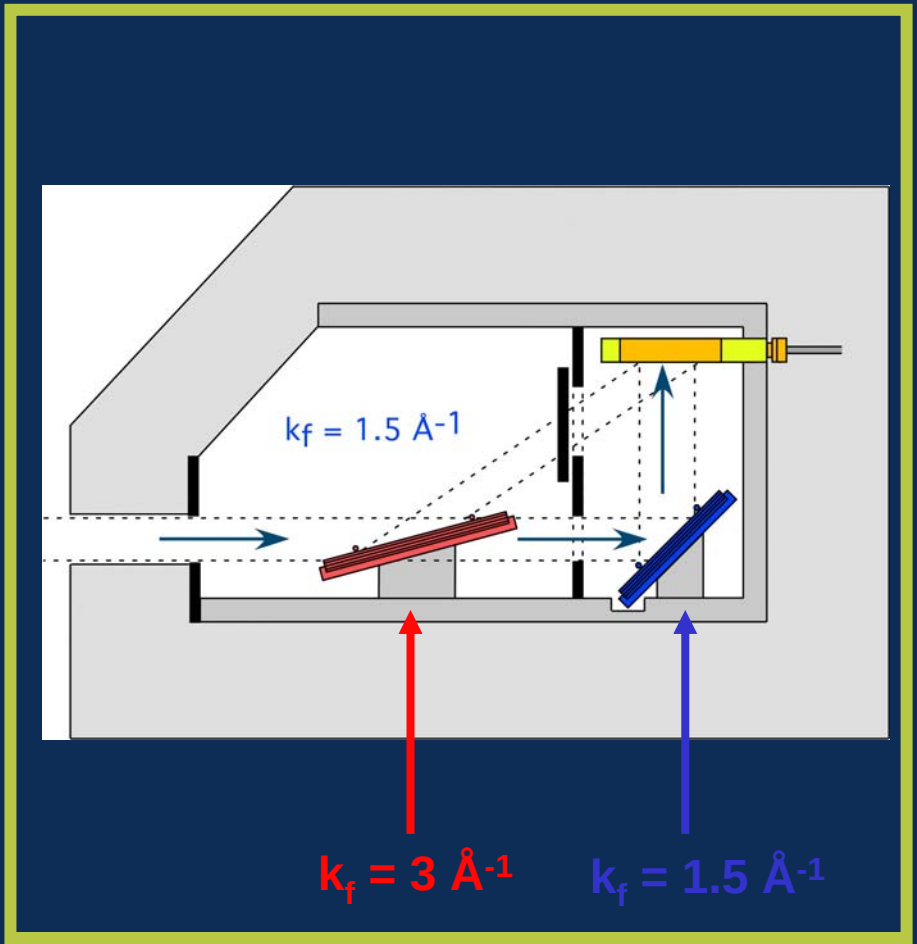
k_f = 1.5 Å^{-1}
k_f = 3 Å^{-1}
k_f = 1.5 Å^{-1}


IN20, July 2005

Multi-Analyser-Detector Box

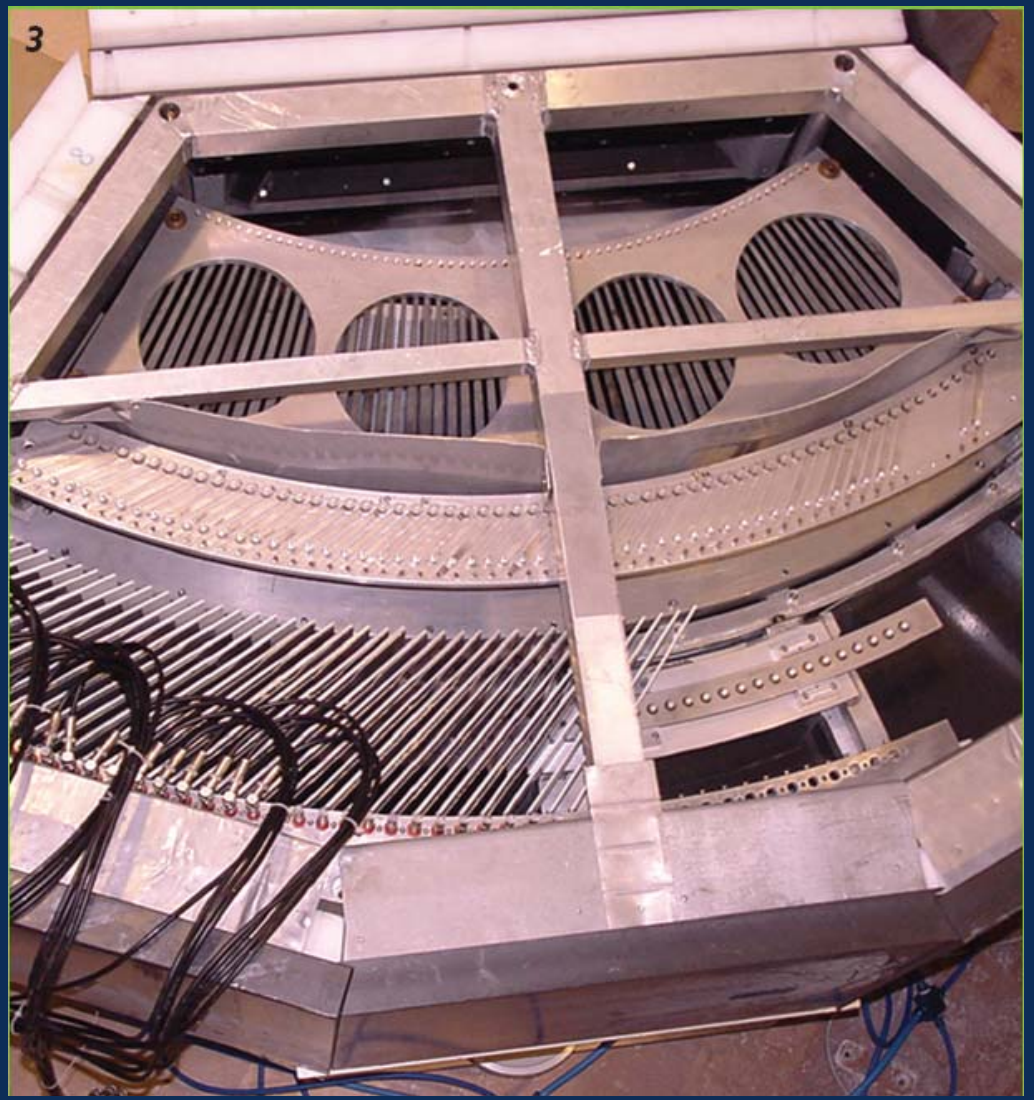

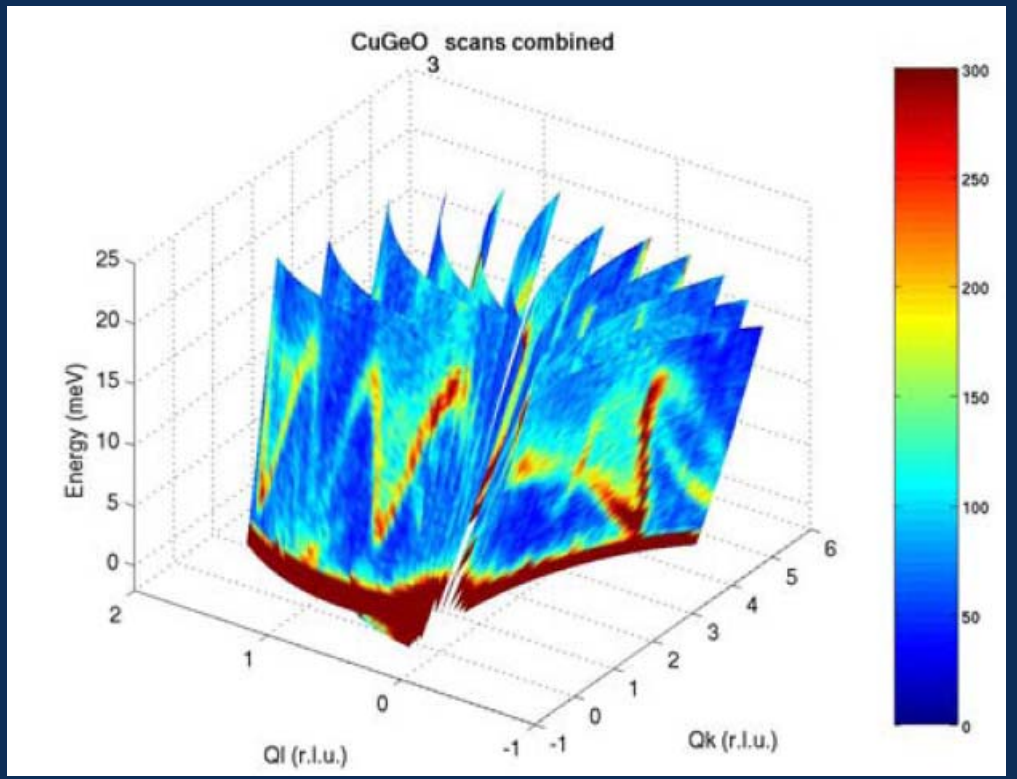

0.7cm^3 single crystal

Data taken on IN8
H.M. Ronnow, F. Demmel

MAD-box on IN8

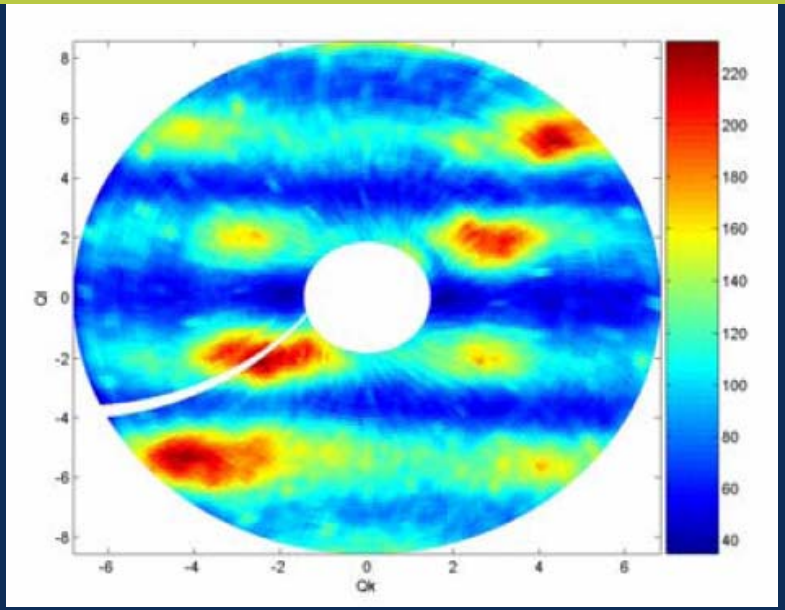

$Ba_2Cu(BO_3)_2$ 1.5cm^3 single crystal, S = $\frac{1}{2}$

dispersionless 8meV band

Intensity (color) at 8meV in (0kl) plane shows dimer structure factor

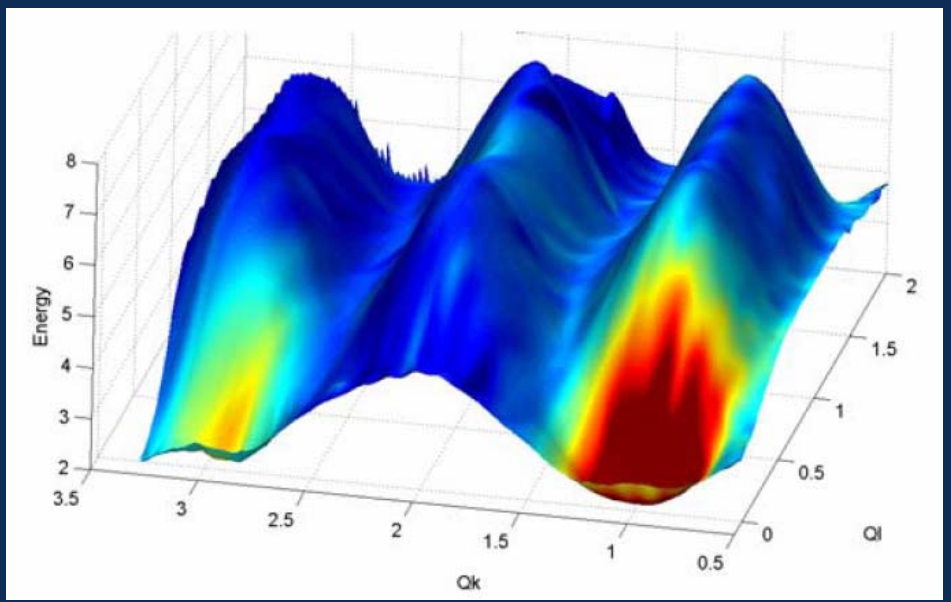

$LiNiPO_4$ 0.2 cm^3 single crystal, S=1

4 h = 20 energy scans with 42 Q
1000 pts on dispersion surface

E(0kl) –surface with
spin wave intensity (color)

H.M. Ronnow, F. Demmel

Constant-$Q_\perp$ spectrometer

Crystal analyser spectrometer with variable k_f

$k_f^j = Q_\perp / \sin\phi^j$

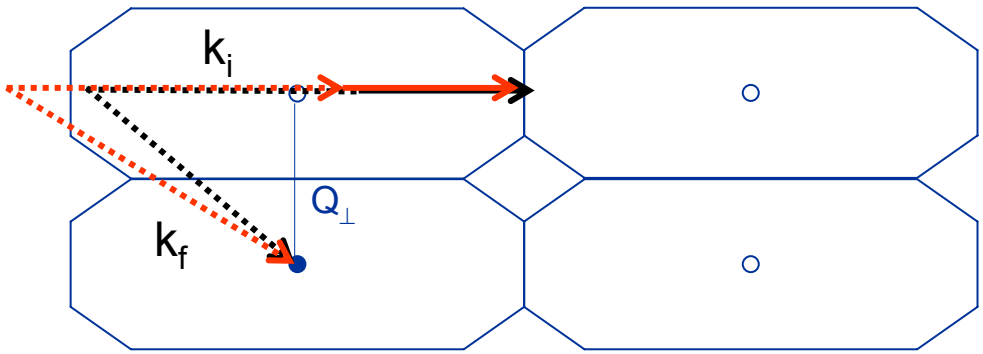

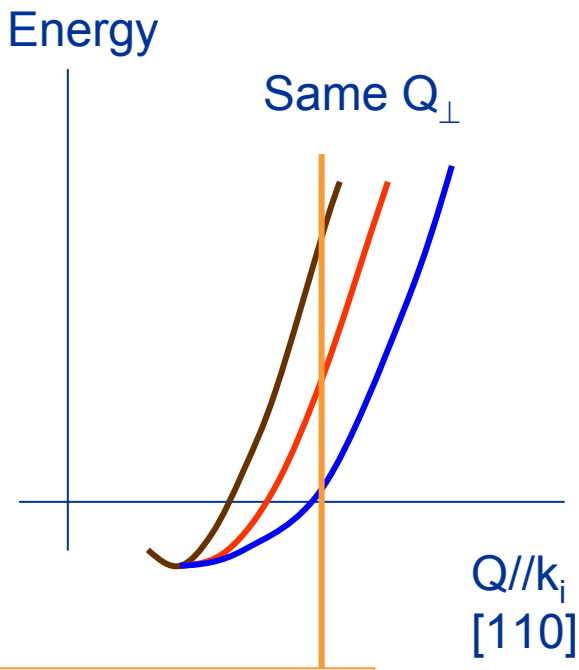

Rebinning gives constant **Q**

Universal Focusing Option on IN12

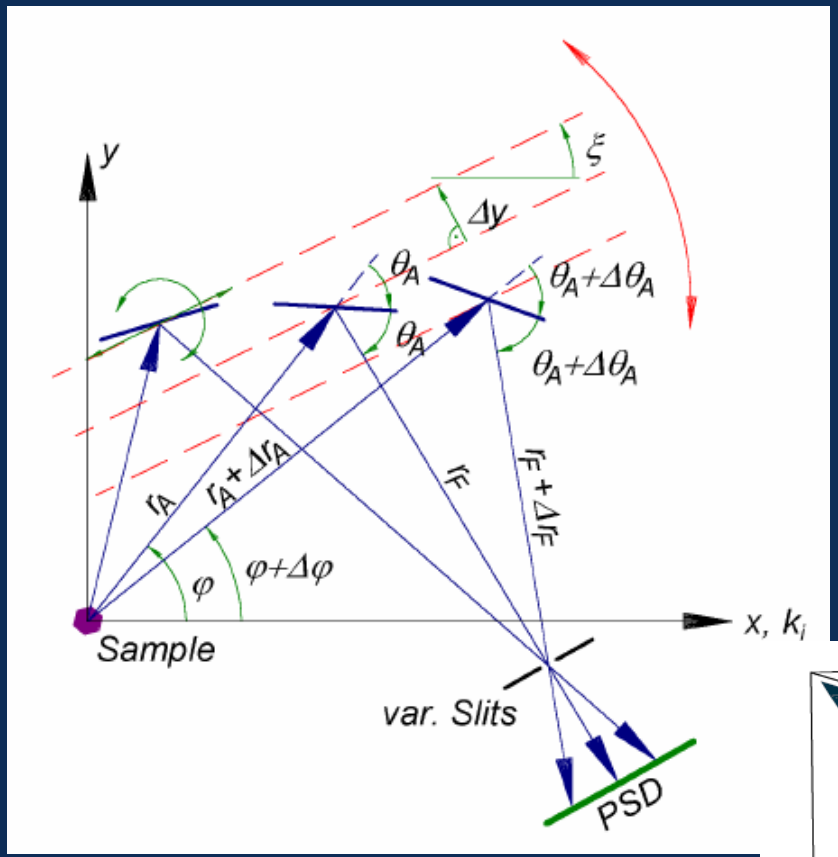

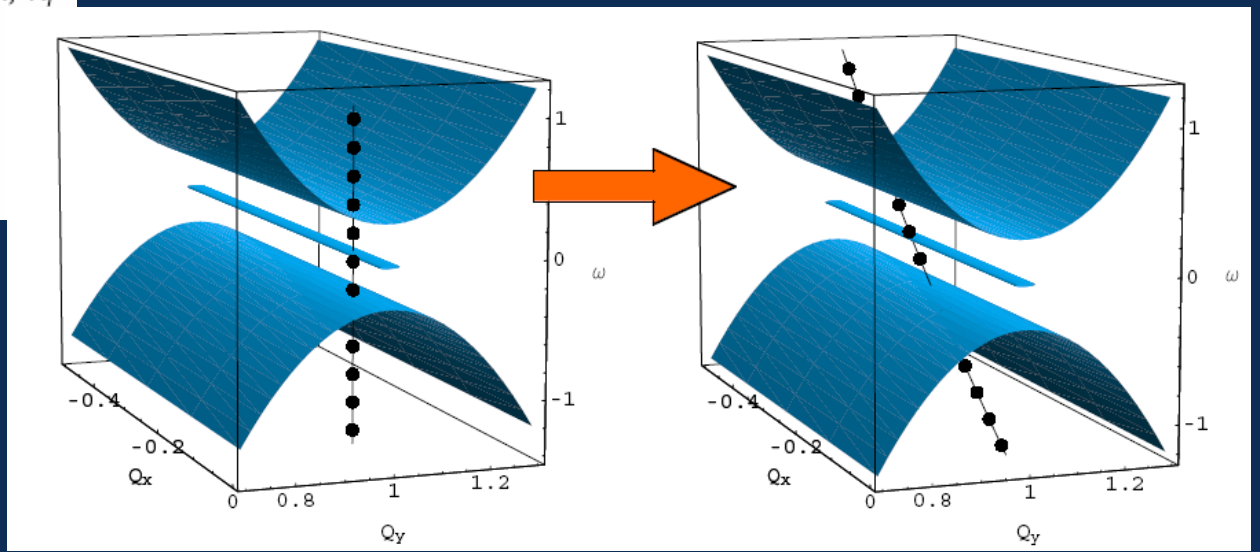

Other variants:
IMPS/IN8
RITAII/PSI

Magnetic excitations

- measured by Triple-Axis Spectroscopy

Part 3: Ground state without long-range order

Macroscopic quantum phenomena

Superfluidity (^{4}He)
Superconductivity (BCS)
} Bose-Einstein condensate

Ground state of
High-Tc-Superconductors ?

Ground state of the FQHE

RSOS-models/
Surface physics

Ground states
of antiferromagnets
} quantum string liquids
with "hidden" order

Macroscopic quantum ground states

Superconductivity	One wave function of all conduction electrons
QHE / FQHE	
AF spin chains	One wave function of all localized spins

S=1/2 Ferro- and Antiferromagnet

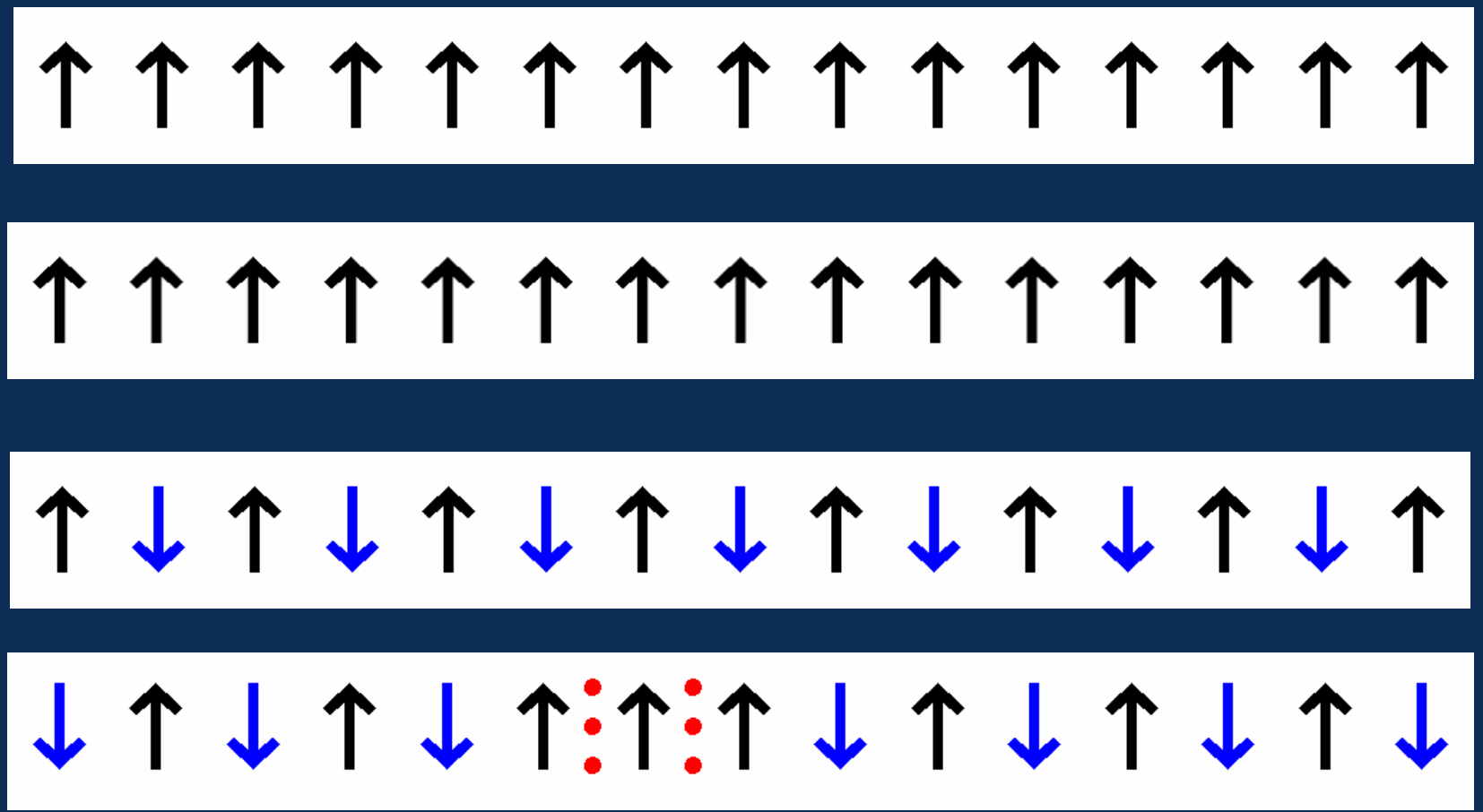

S=1/2 Antiferromagnet

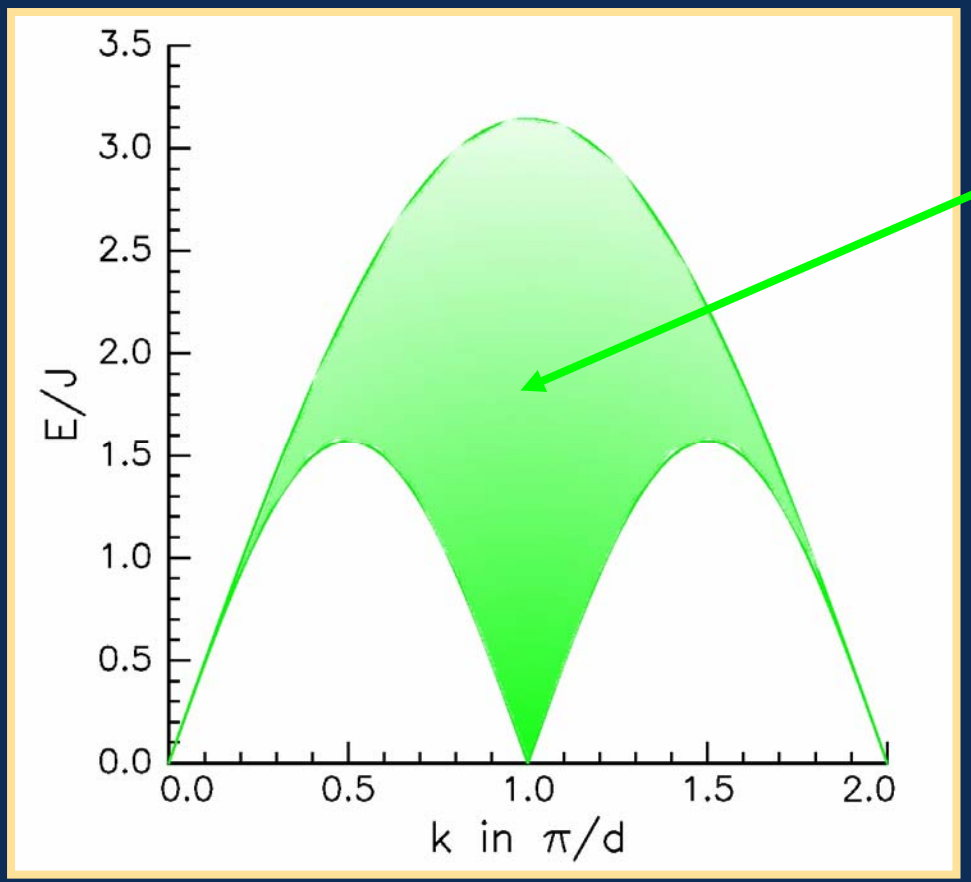

Pairs of two domain walls

Continuum:

$k = k_1 + k_2$

$E(k) = E_1(k_1) + E_2(k_2)$

Magnetization

$S = \infty$

$S = 1/2$

Magnetization

B

$S = \infty$

$S = 1/2$

Magnetization

B

$S = \infty$

$S = 1/2$

Magnetization

B

$S = \infty$

$S = 1/2$

Magnetization

B

$S = \infty$

$S = 1/2$

Magnetization

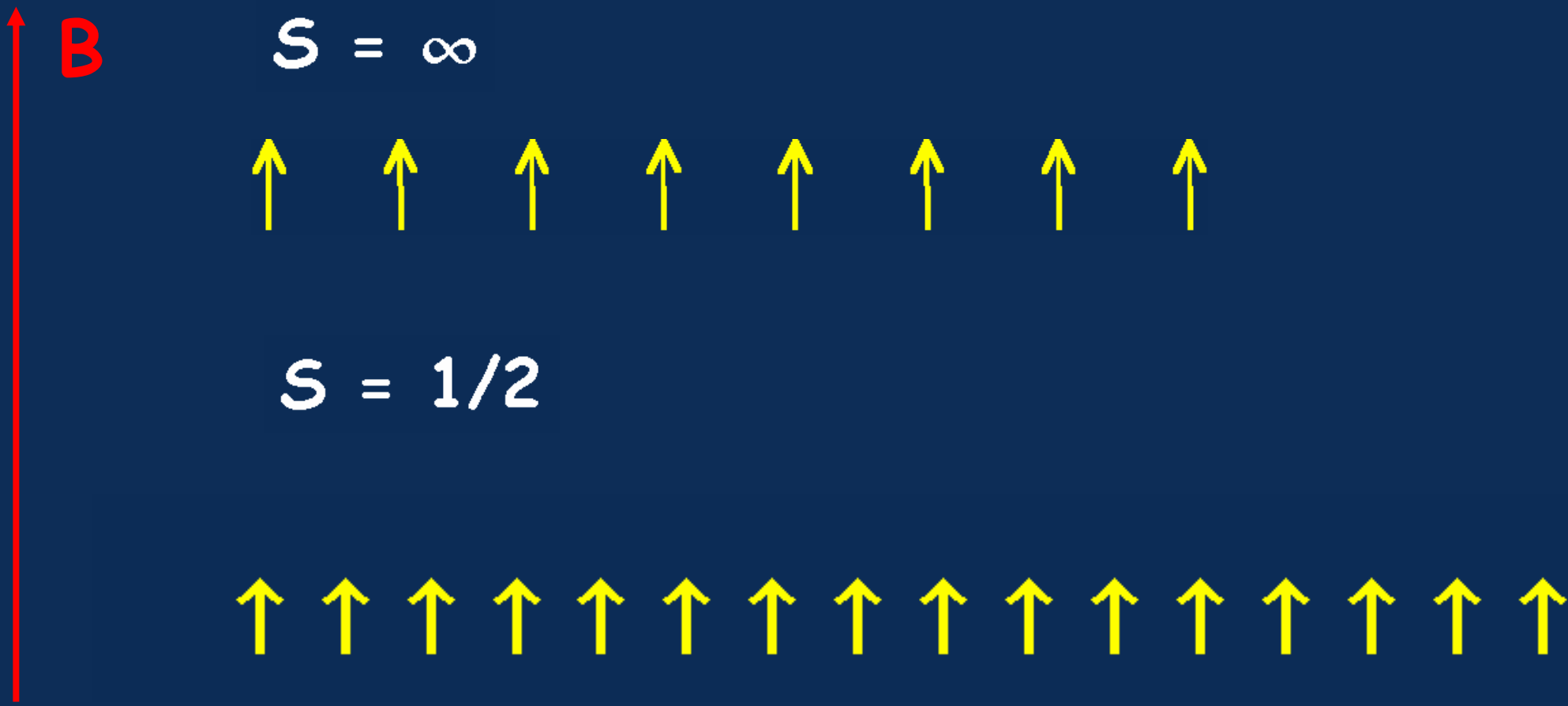

Magnetic Excitations

Classical

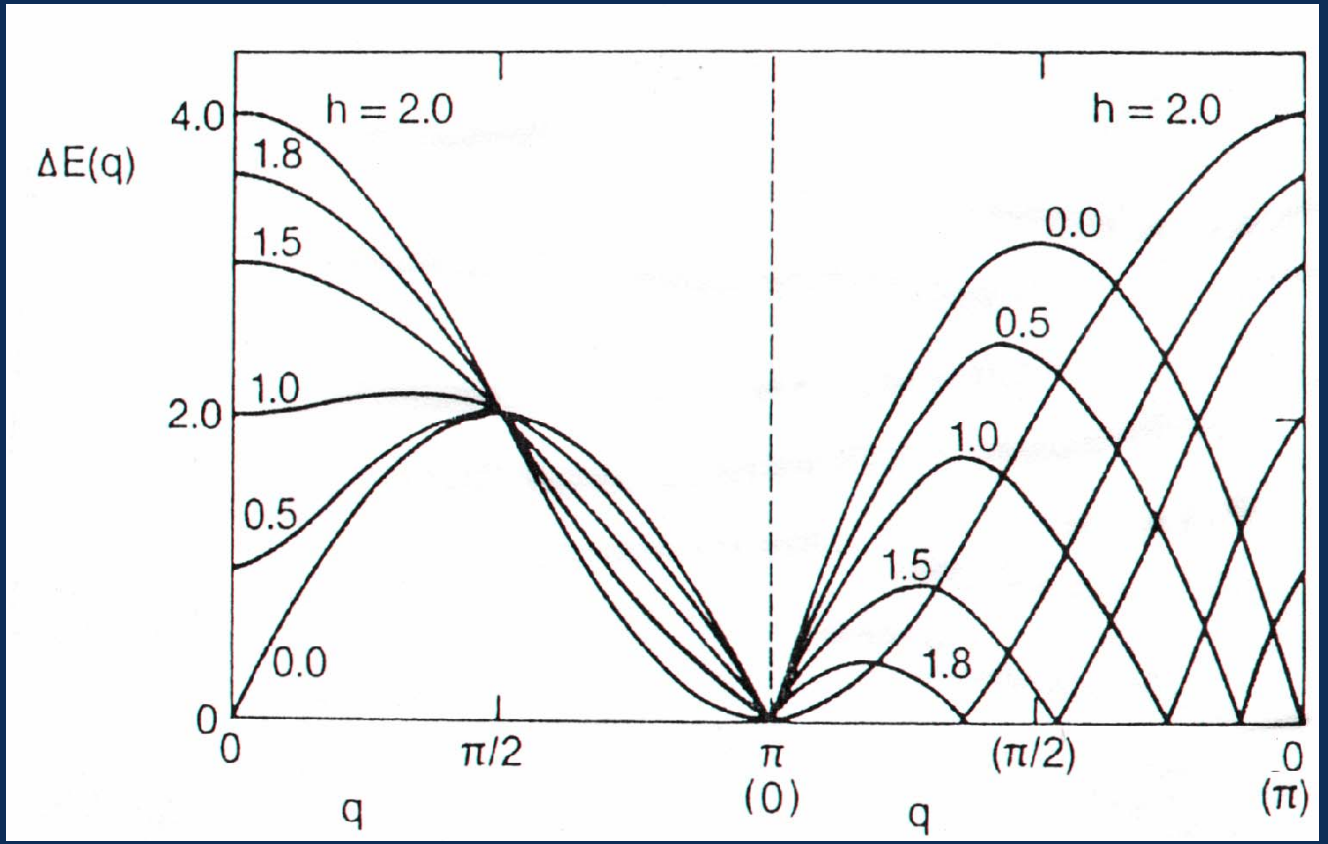

S = 1/2

1D S=1/2 Heisenberg AF

Ground state:

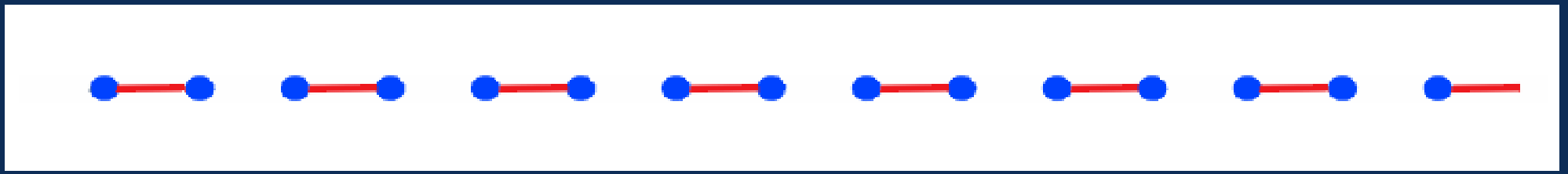

Excitations: spin-1/2 pair continuum

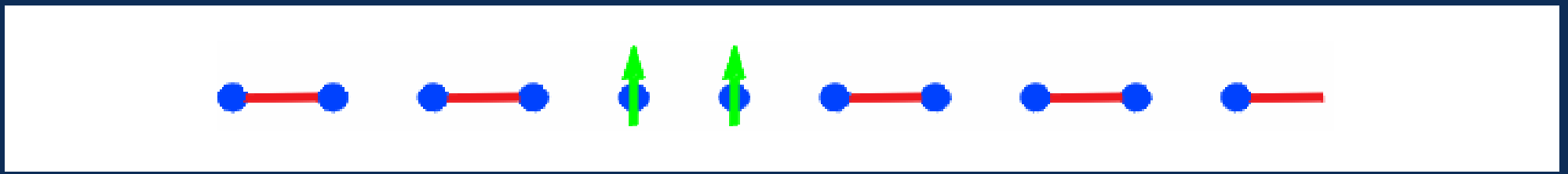

Macroscopic Singlet Ground States

1D S=1/2 HAF Ground state (snapshots)

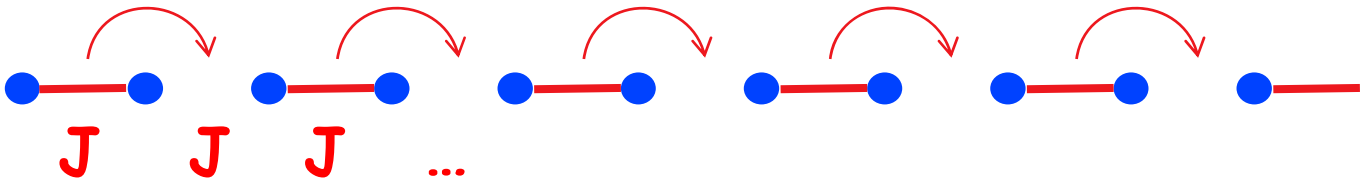

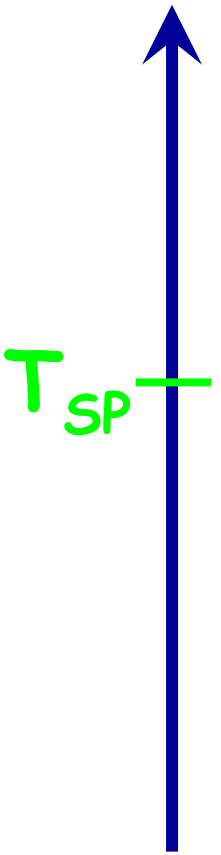

1D S=1/2 Dimer Ground state

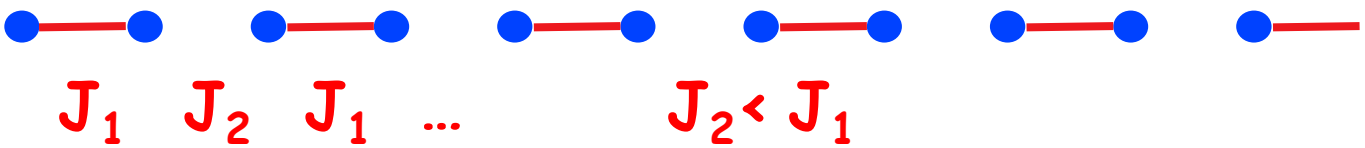

Spin-Peierls material:
1D S=½ HAF coupled to 3D phonons (acoustic or optic)

Break an AF bond: Excitations

1D S=1/2 HAF: continuum, no energy gap

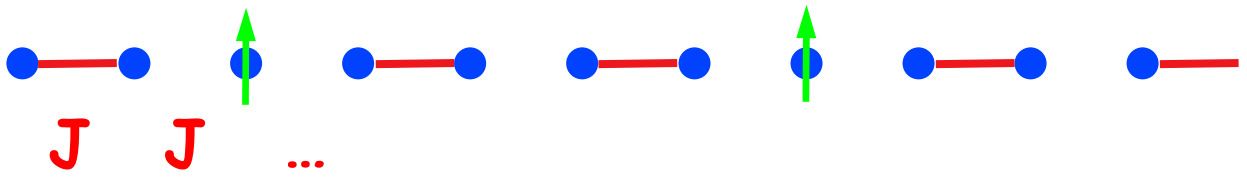

1D S=1/2 Dimer: discrete mode, energy gap(s)

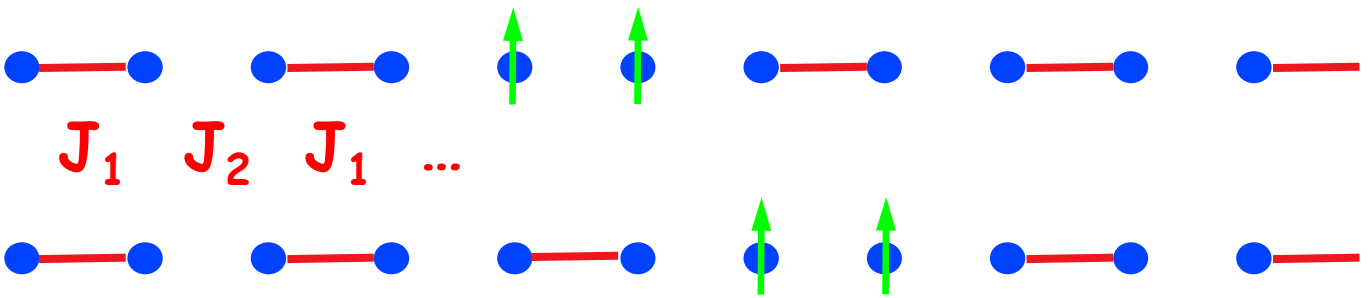

$CuGeO_3$ - Spin-Peierls System

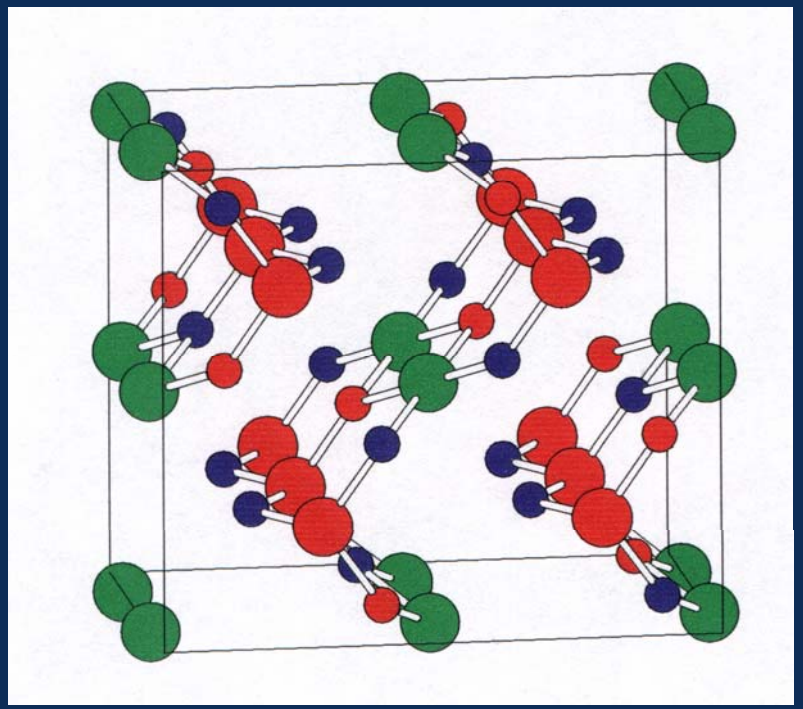

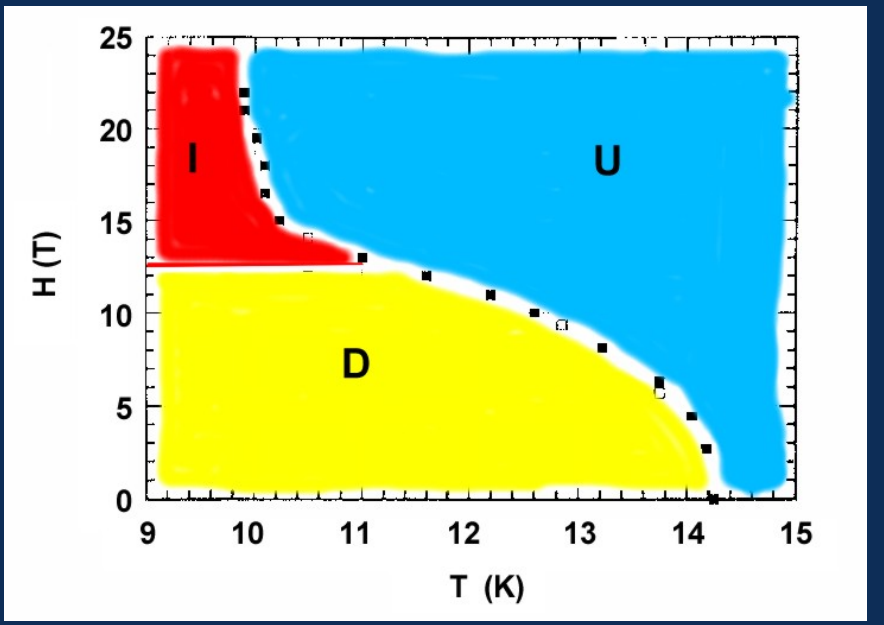

Hegmann et al. 1998

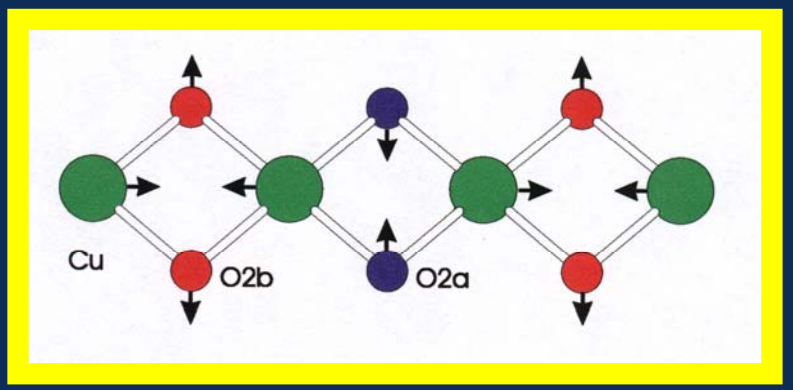

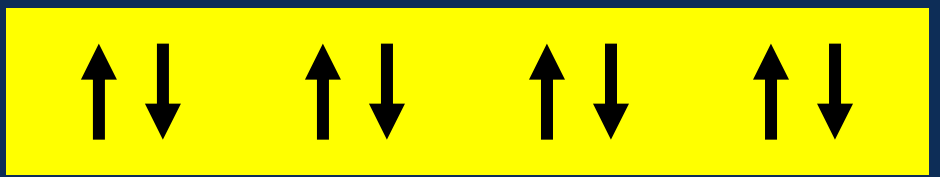

Break an AF bond: Excitations

1D S=1/2 HAF: continuum, no energy gap

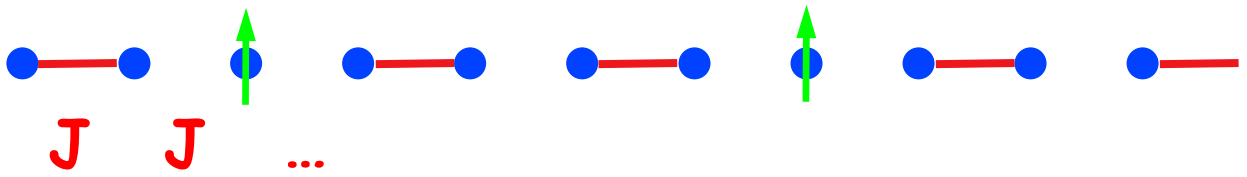

1D S=1/2 Dimer: discrete mode, energy gap(s)

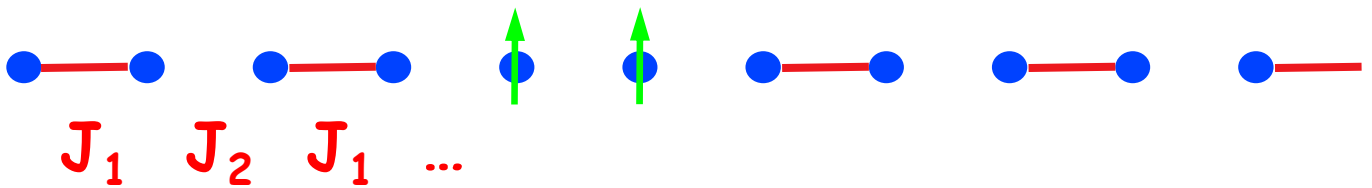

Spin-Peierls: discrete mode, energy gap, continuum

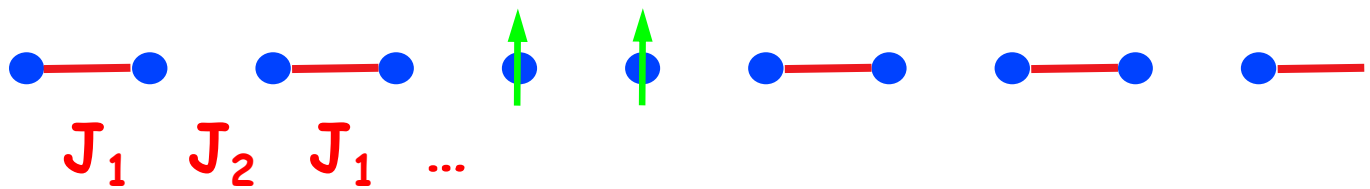

Spin-Peierls: Excitations

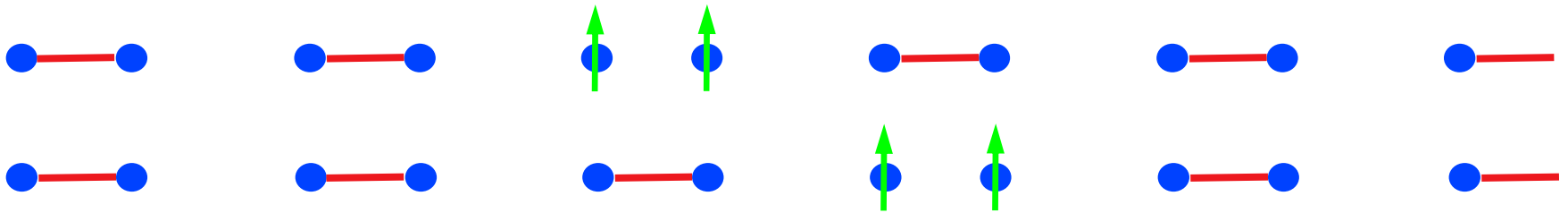

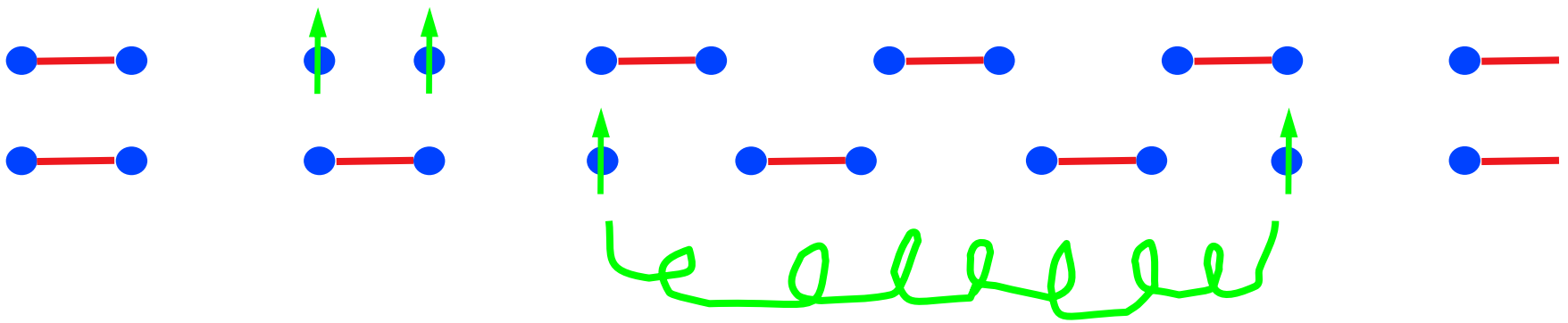

binding energy by 3D elastic coupling

Spin-Peierls System

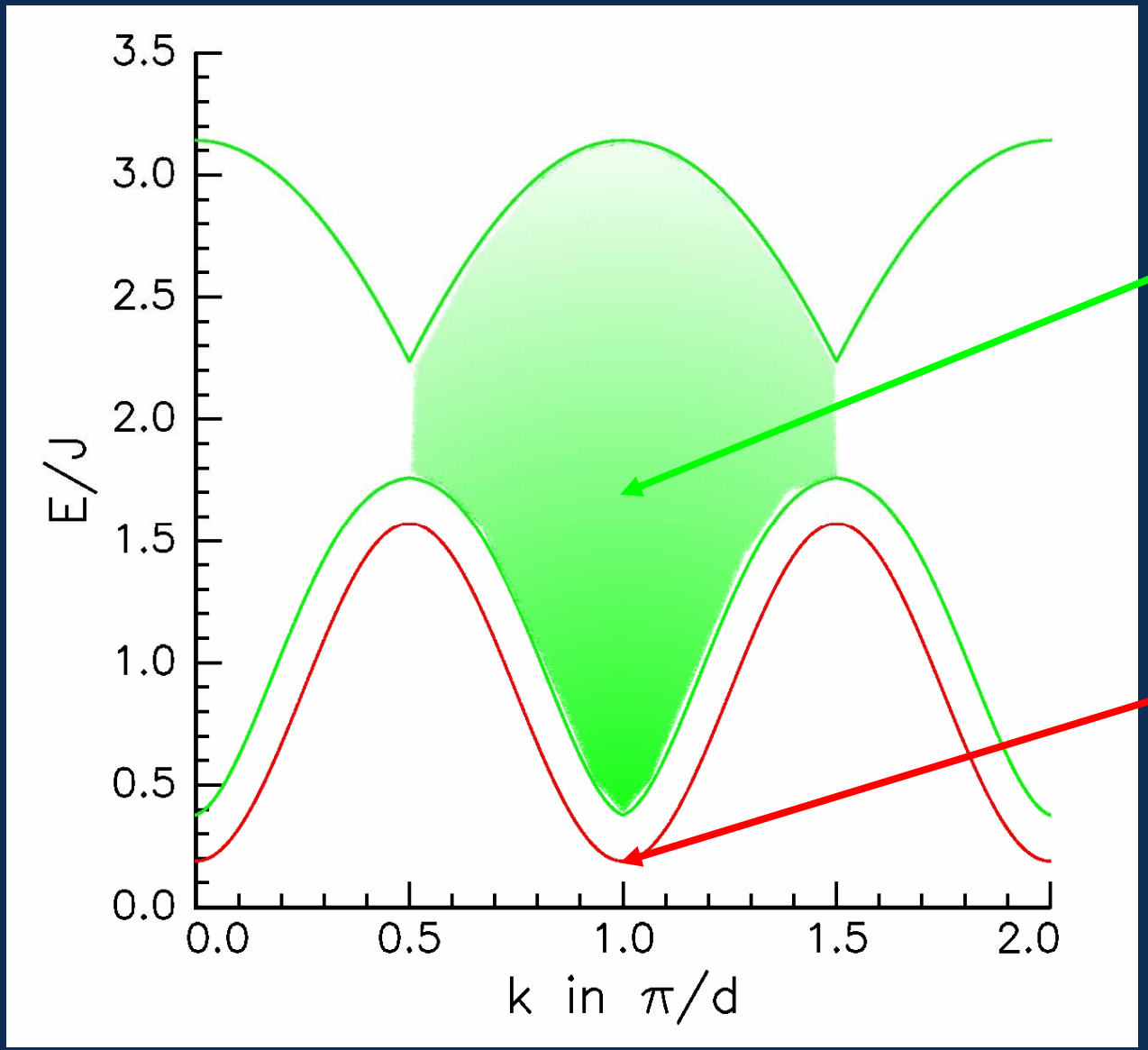

Continuum: two domain wall pairs

Pair of bound domain walls

S=1/2 Spin-Peierls $CuGeO_3$

MARI

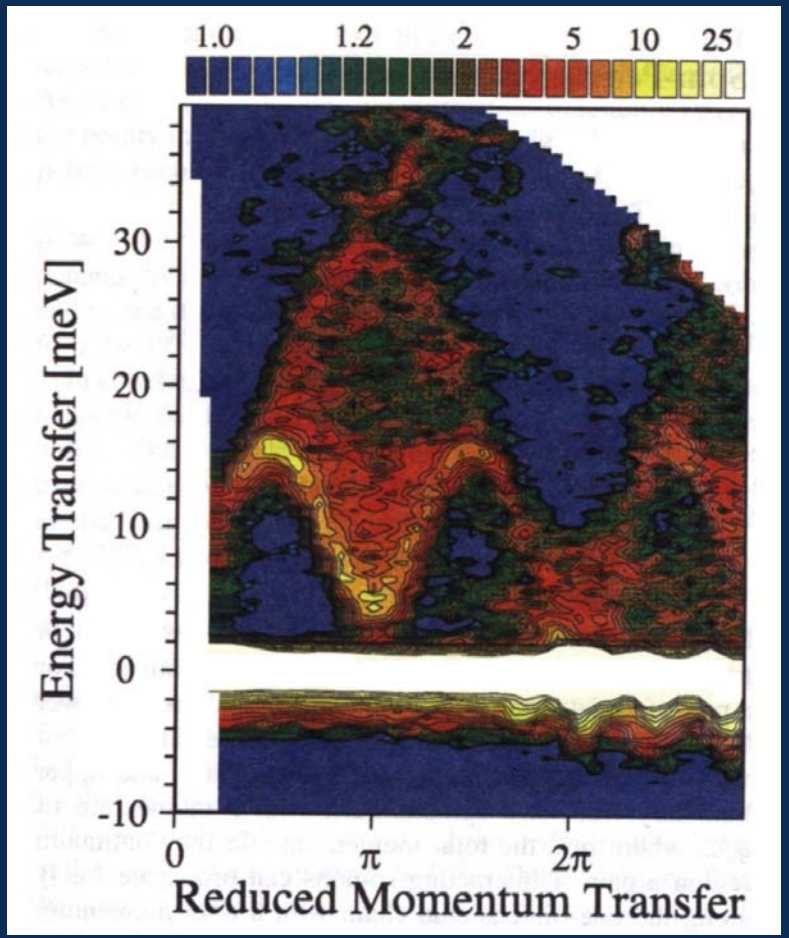

M. Arai et al. 1996

TAS

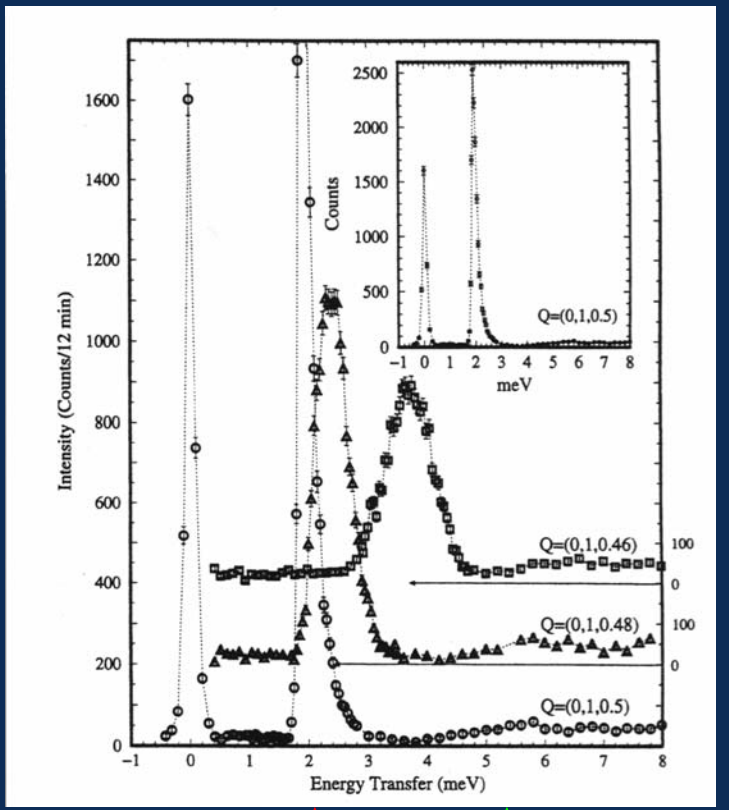

M. Aïn et al. 1997

Continuum

Triplet

$CuGeO_3$ - Triplet Excitation

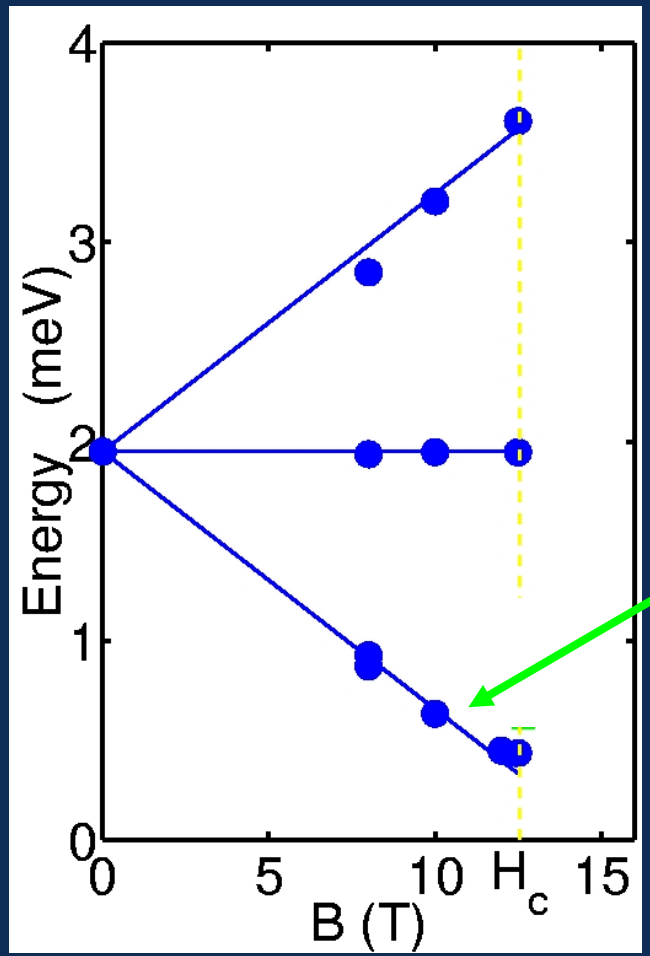

H<Hc

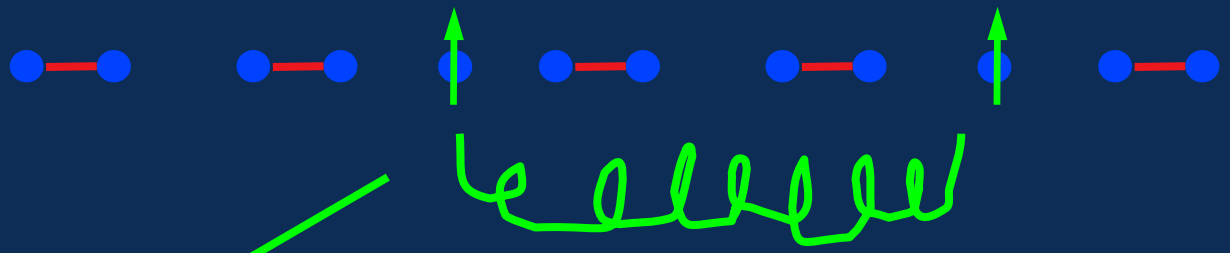

H>Hc

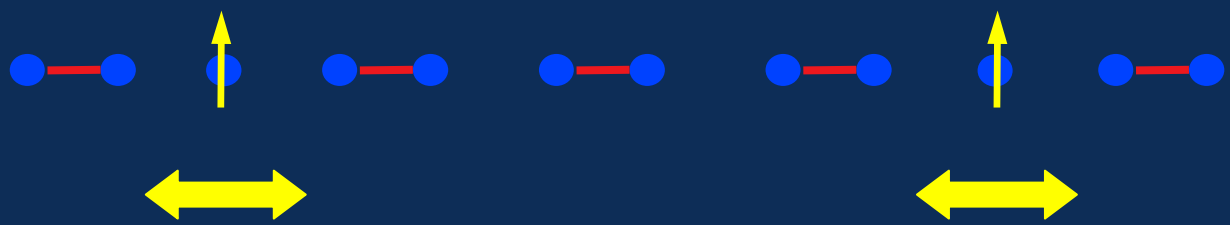

FLEX (HMI)

$CuGeO_3$ - Quantum IC Phase

Bc=12.3T IC Magnetic Soliton Structure

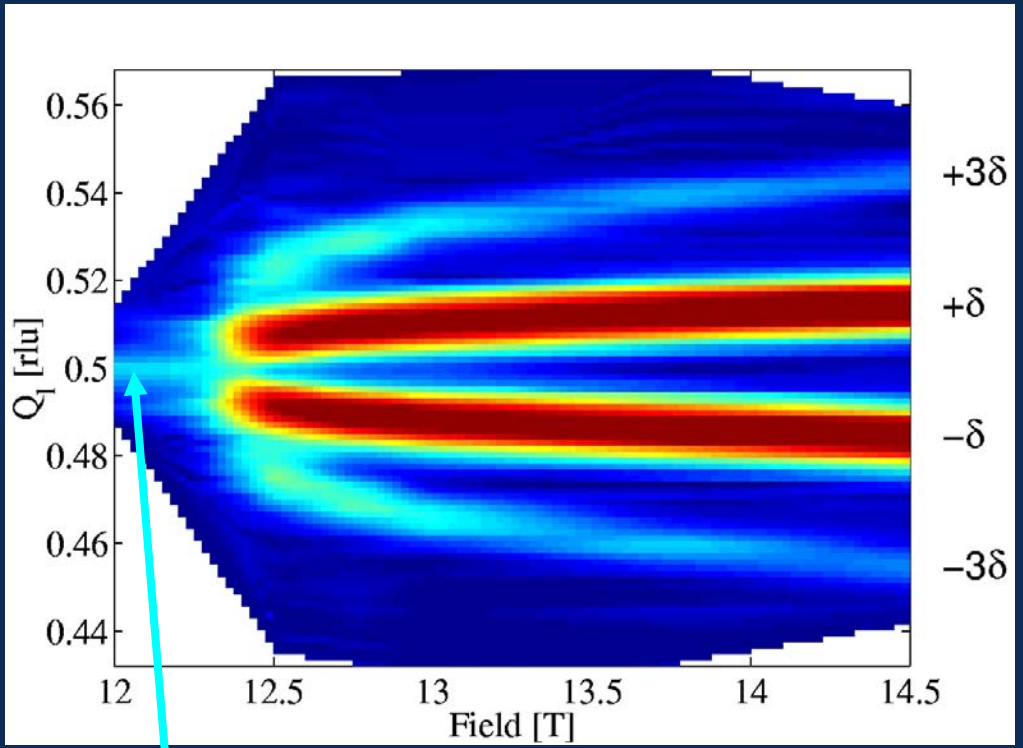

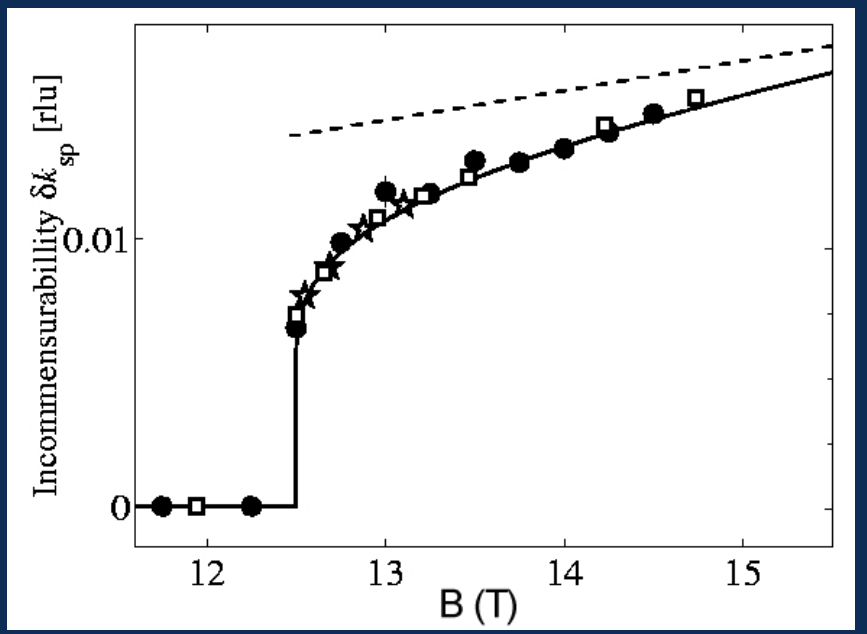

Dimer (lattice) peak
No ordered moment

Quantum IC Phase

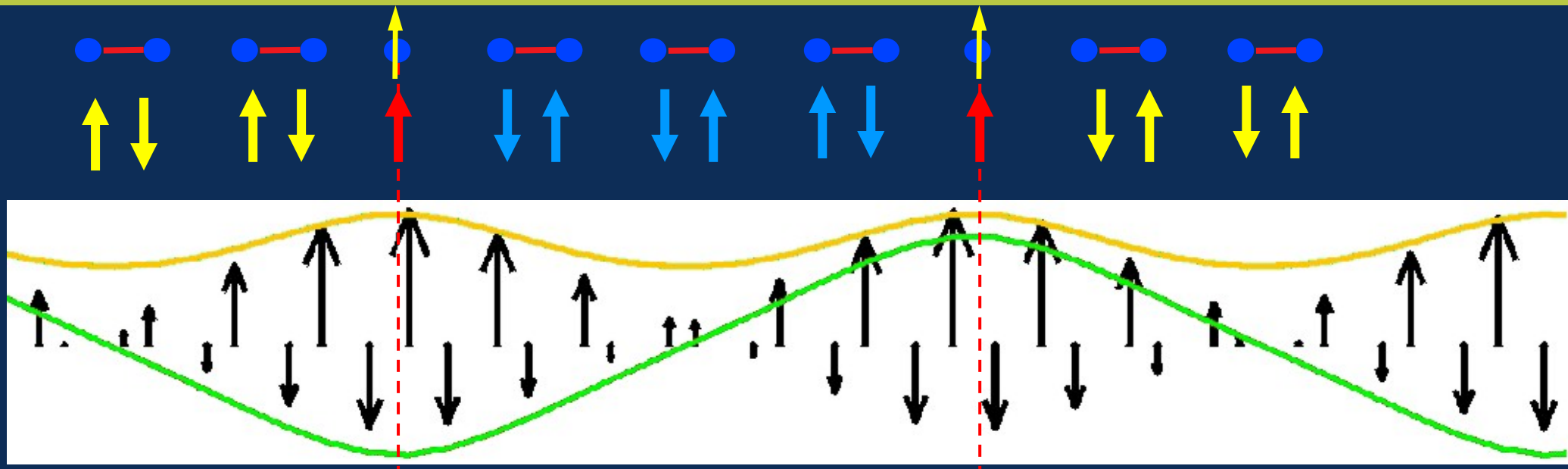

B=14.5T	nsc	NMR	theory
m_s	0.097(3)	0.026	0.11 - 0.14
m_u	0.019(3)	0.023	0.023
m_s/m_u	5.1(8)	1.1	5.4
	Ronnow, Enderle et al.	Horvatic et al.	Uhrig et al.

Quantum IC Phase: Excitations

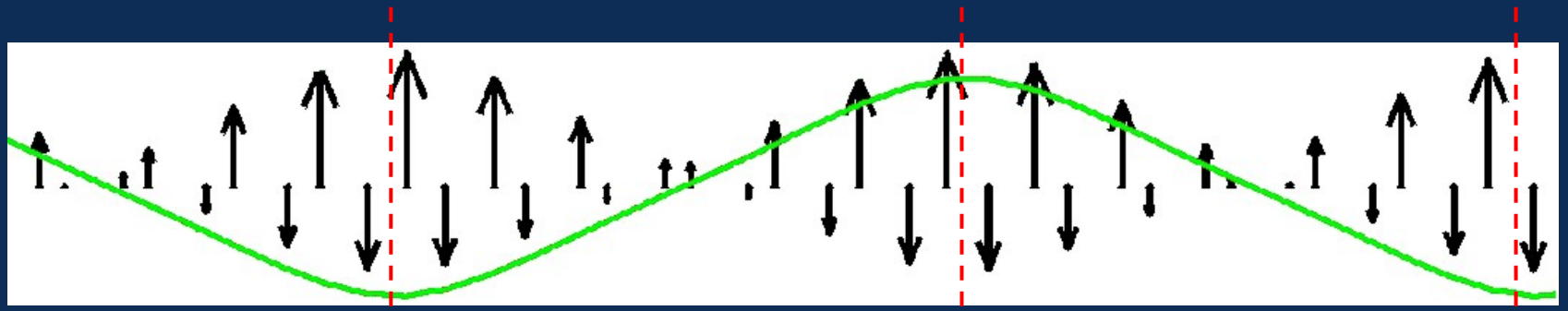

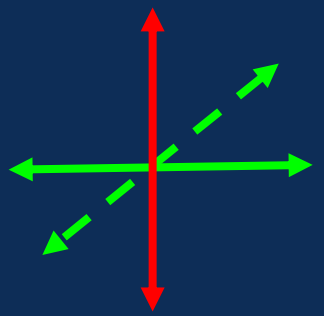

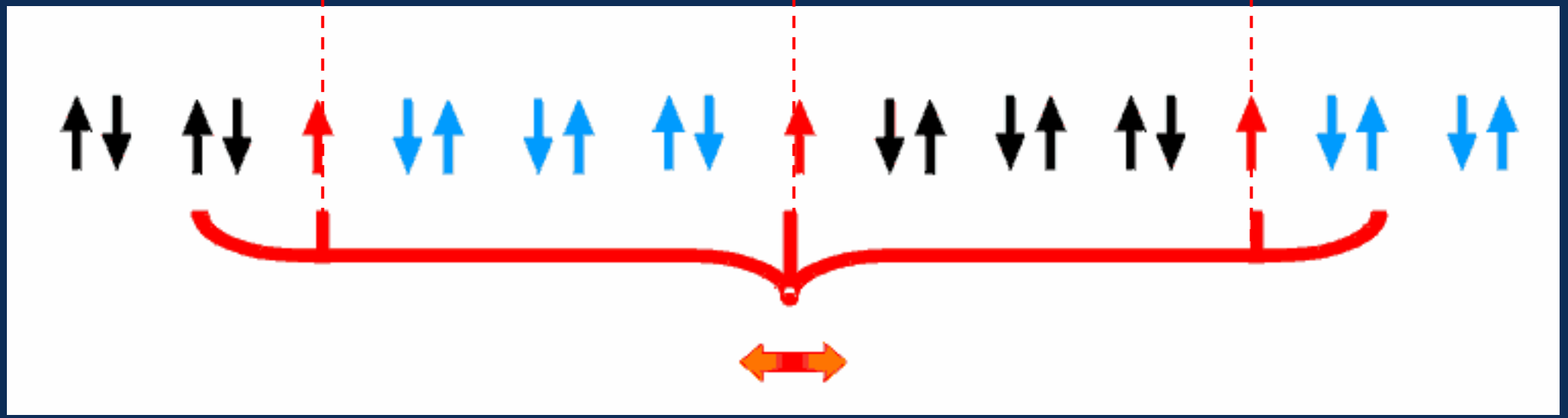

Magnetic excitations, IC-phase

Schönfeld et al. 1998

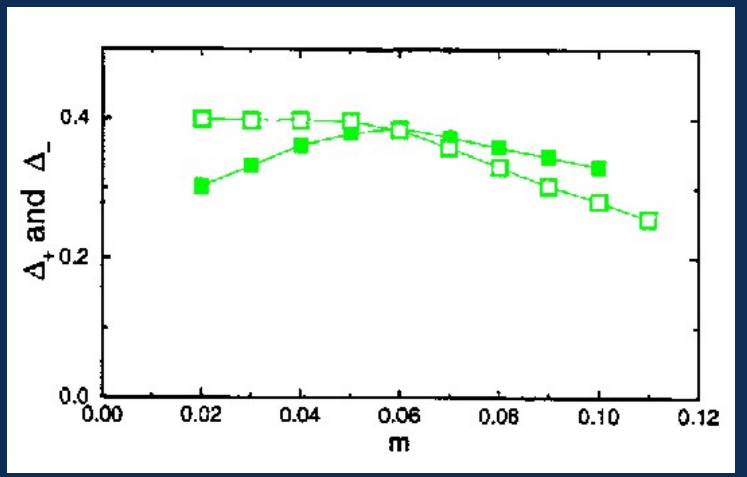

Yu et al. 1999

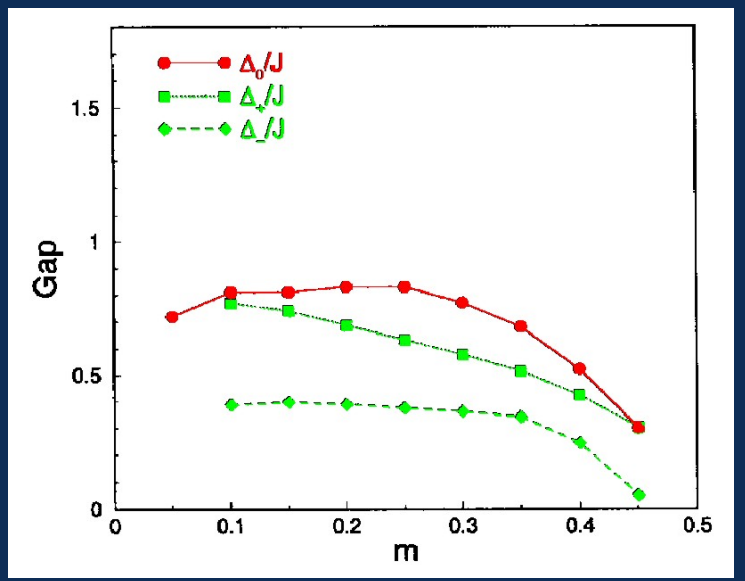

Uhrig et al. 1998

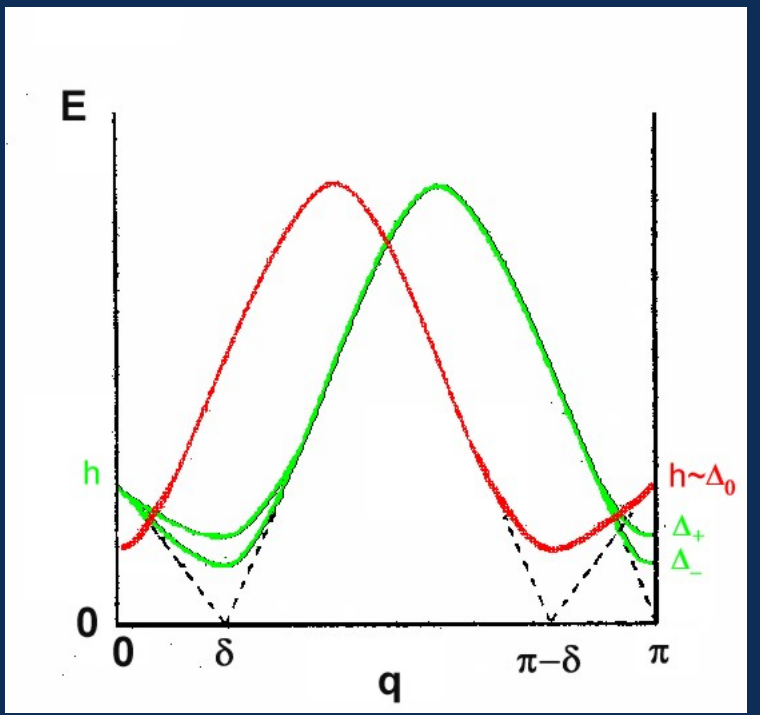

Δ_+, Δ_- : creation / removal of an additional domain wall pair

$CuGeO_3$ Dimerized-Quantum IC Phase

3 magnetic excitations

- and one soft "phason".

Gaps ?

incommensurate
or
commensurate
excitations ?

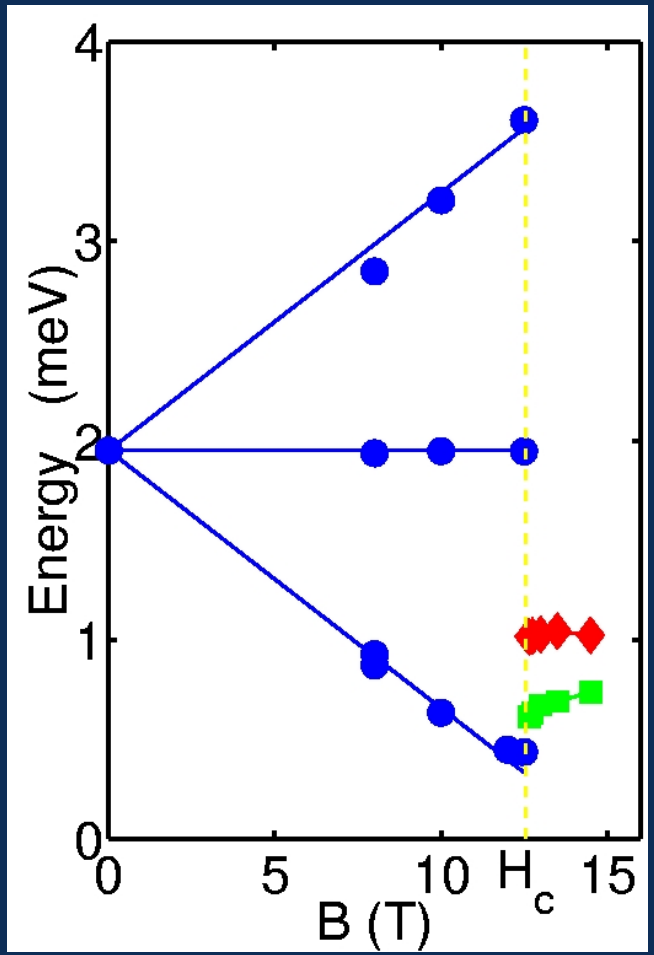

HMI (FLEX with VM-1)

1D quantum phenomena vs. 3D lattice

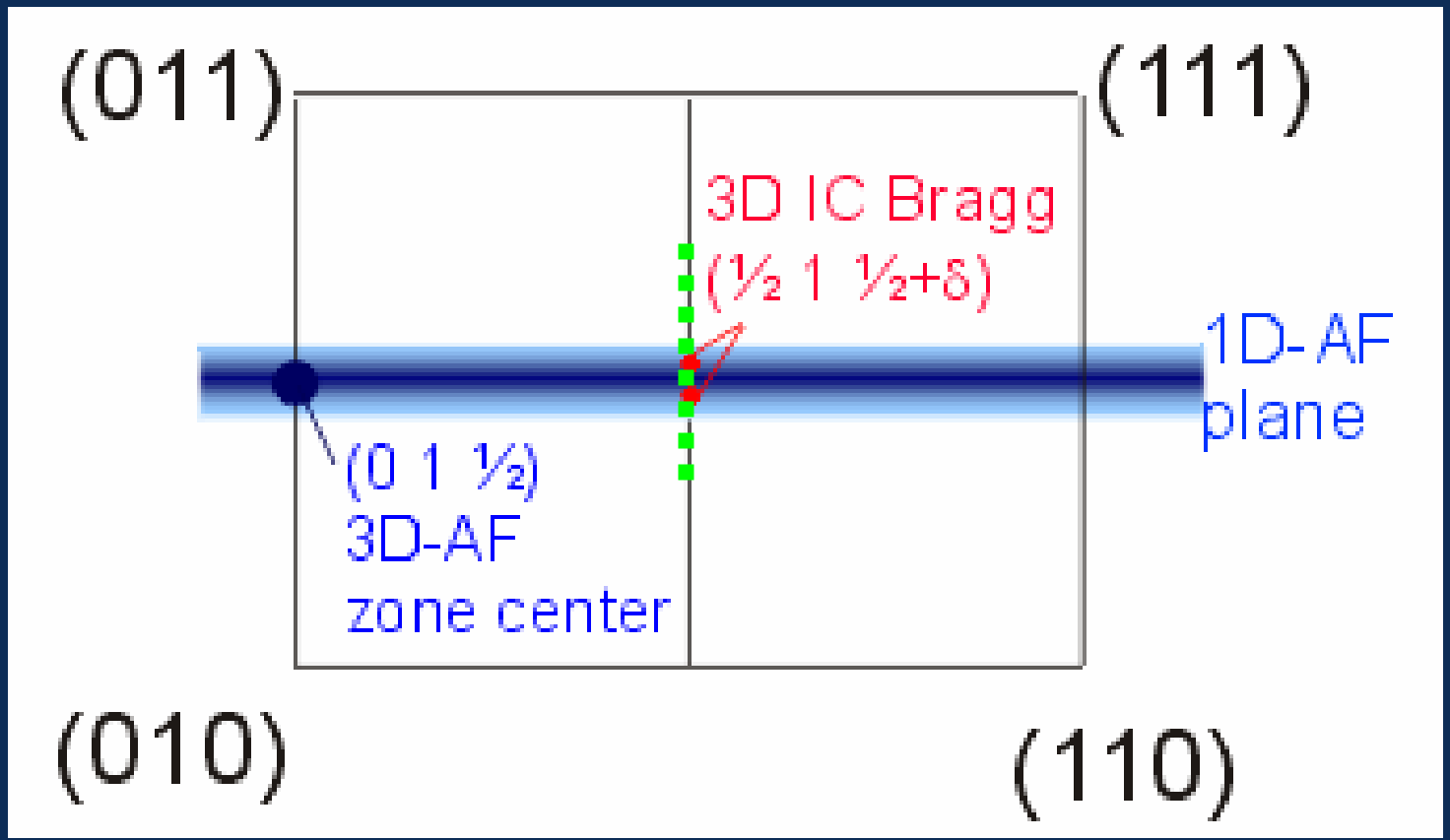

$CuGeO_3$ Quantum IC Phase

14.5 T
1.5 K

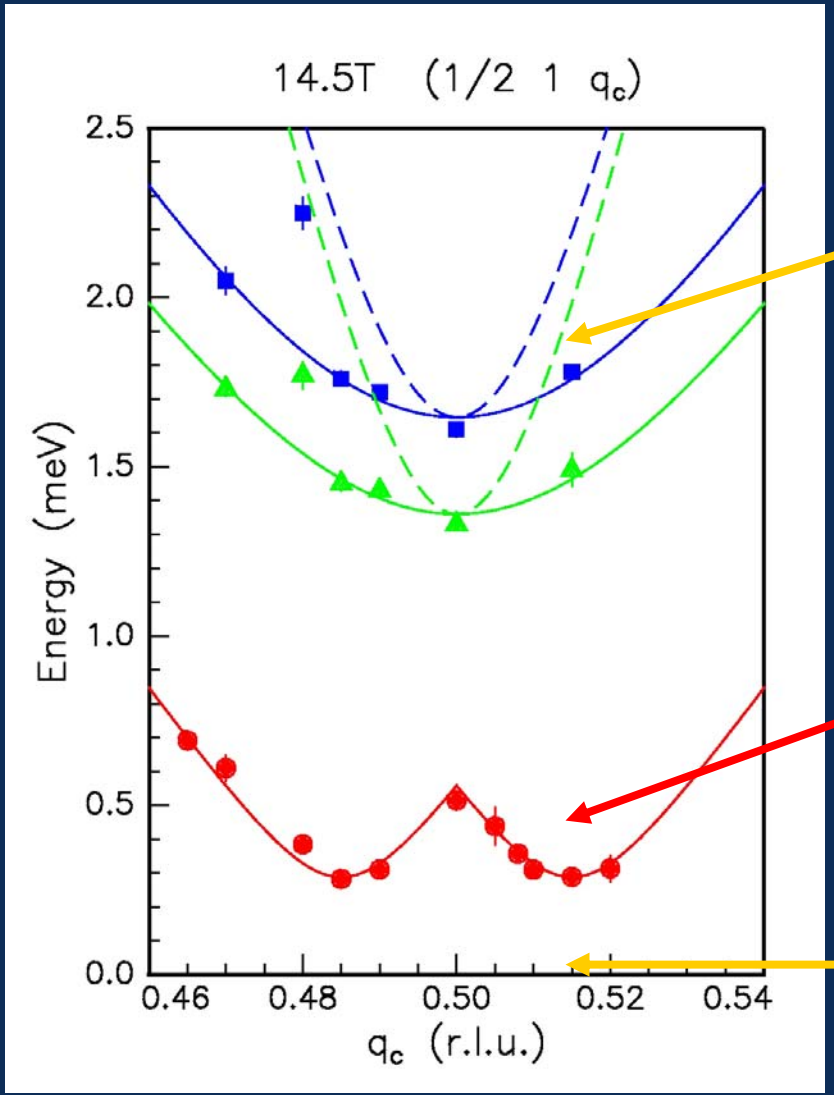

3. magn. mode ?

?

phason ?

HMI
(V2, VM-1)

$$J(h) = 2\,J1\cos(2\pi h) + 2\,J2\cos(4\pi h)$$

$$dJ(h)/dh = -4\pi\,J1\sin(2\pi h) - 8\pi\,J2\sin(4\pi h) = 0$$

use $\sin(4\pi h) = 2\sin(2\pi h)\cos(2\pi h)$

$$-4\pi\,J1\sin(2\pi h) - 16\pi\,J2\sin(2\pi h)\cos(2\pi h) = 0$$

$$\sin(2\pi h)\,(J1 + 4\,J2\cos(2\pi h)) = 0$$

Hence either $\sin(2\pi h) = 0$ ($h=0$ or $h=1/2$)

or $J1 = -4\,J2\cos(2\pi h)$

$\cos(2\pi h) = -J1 / 4J2$ (varying h)

Case 1: h=0:

$J(0)=2J1+2J2 = 2\cos(\text{phi}) + 2\sin(\text{phi}) = 2\cos(\text{phi})\,(1+\tan(\text{phi}))$

Case 2: h=1/2:

$J(1/2)= -2J1+2J2 = -2\cos(\text{phi}) + 2\sin(\text{phi}) = = 2\cos(\text{phi})\,(-1 + \tan(\text{phi}))$

Case 3: h varying, ordering vector $\cos(2\pi H) = -J1 / 4J2$

$J(H) = 2J1 \cos(2\pi H) + 2J2 (\cos(4\pi H))$

$= 2J1 \cos(2\pi H) + 2J2 (\cos(2\pi H)^2 - \sin(2\pi H)^2)$

$= 2J1 \cos(2\pi H) + 2J2 (2 \cos(2\pi H)^2 - 1)$

$= 2J1 (-J1 / 4J2) + 2J2 (2 (-J1 / 4J2)^2 - 1)$

$= -J1^2/4J2 - 2 J2$

Now put in J1=cos(phi), J2=sin(phi)

$= -\cos^2(\text{phi})/4\sin(\text{phi}) + 2 \sin(\text{phi})$

$= -\cos(\text{phi}) (1/(4 \tan(\text{phi})) + 2 \tan(\text{phi}))$

J(0) (means ferromagnet,
angle zero between neighbouring spins)

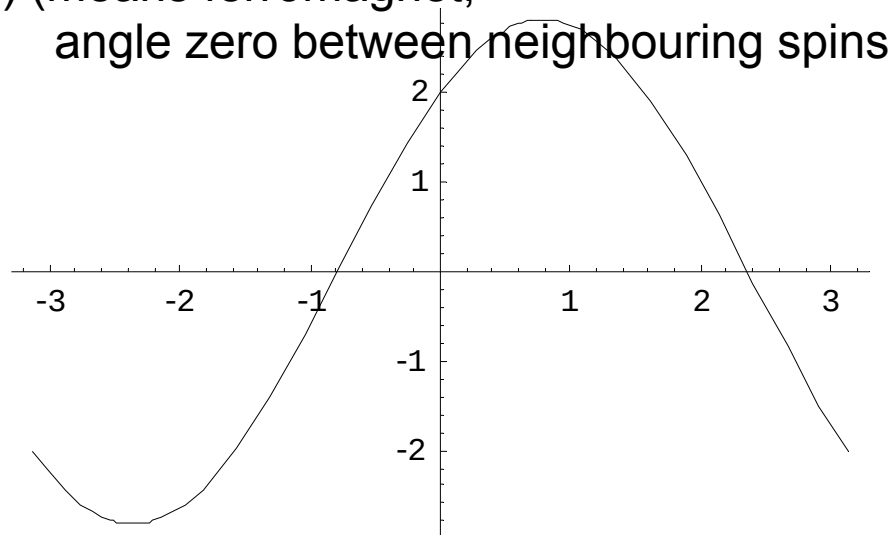

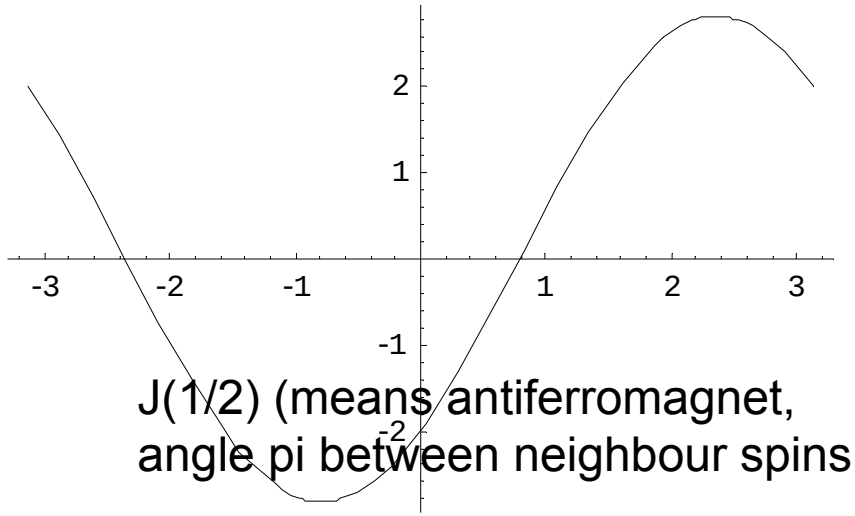

J(1/2) (means antiferromagnet,
angle pi between neighbour spins)

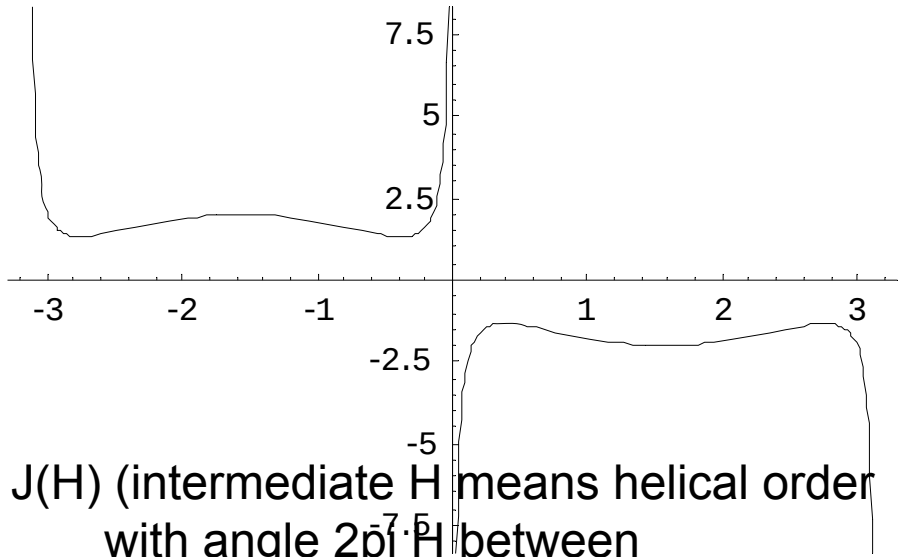

J(H) (intermediate H means helical order
with angle 2pi·H between
neighbouring spins)

Boundaries:
Given by

J(0)=J(1/2) Solution: phi=pi/2
J(0)=J(H) Solution: tan(phi)=-1/4
J(1/2)=J(H) Solution: tan(phi)=1/4

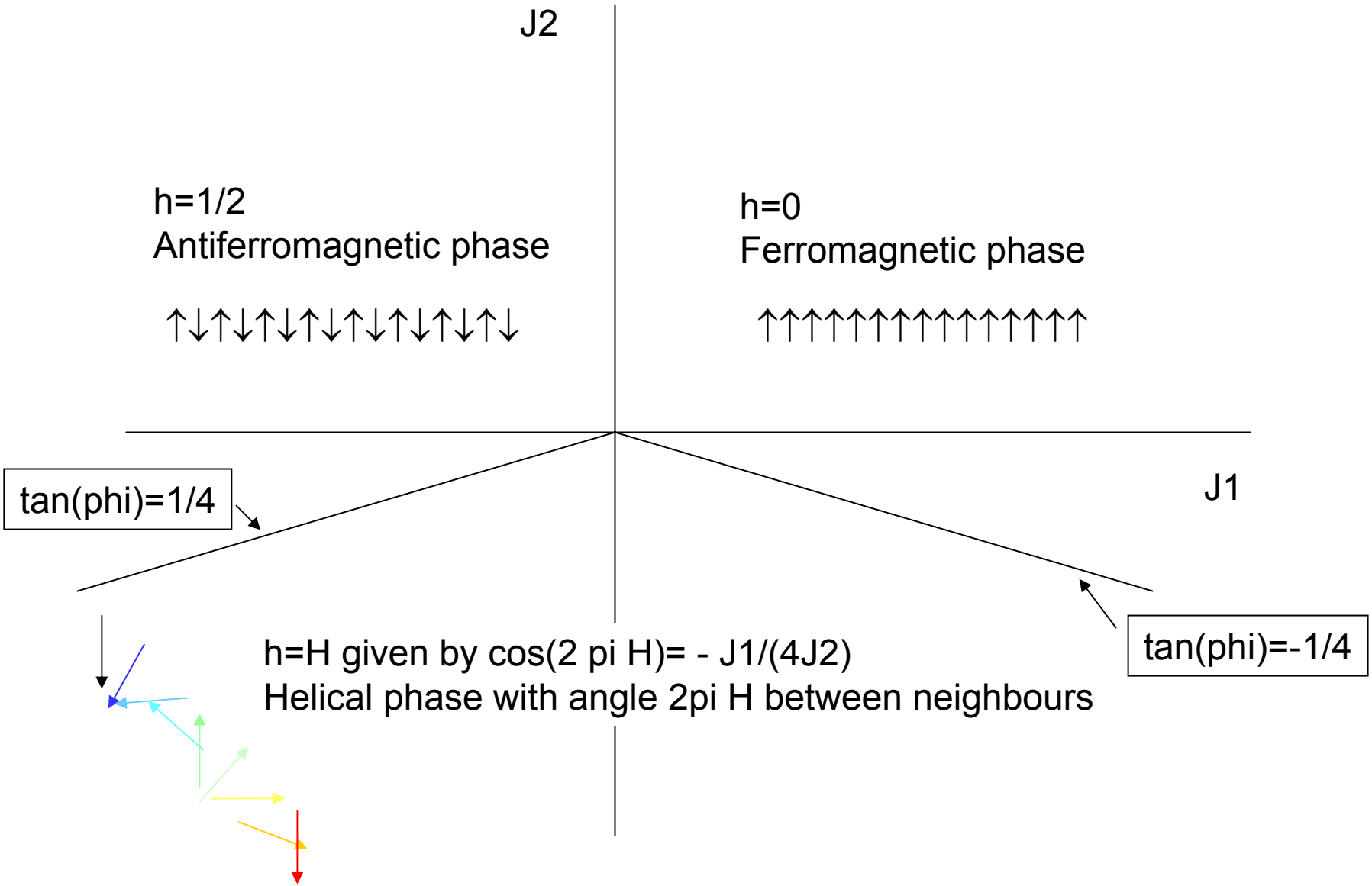
J2
h=1/2
Antiferromagnetic phase
↑↓↑↓↑↓↑↓↑↓↑↓↑↓↑↓
h=0
Ferromagnetic phase
↑↑↑↑↑↑↑↑↑↑↑↑↑↑↑
J1
tan(phi)=1/4
tan(phi)=-1/4
h=H given by cos(2 pi H)= - J1/(4J2)
Helical phase with angle 2pi H between neighbours

Excitations ferromagnetic phase (ordering vector H=0)

$\hbar\omega(h)=4S[J1(1-\cos(2\pi h)) +J2(1-\cos(4\,\pi h))]$

J1=1,J2=-0.24

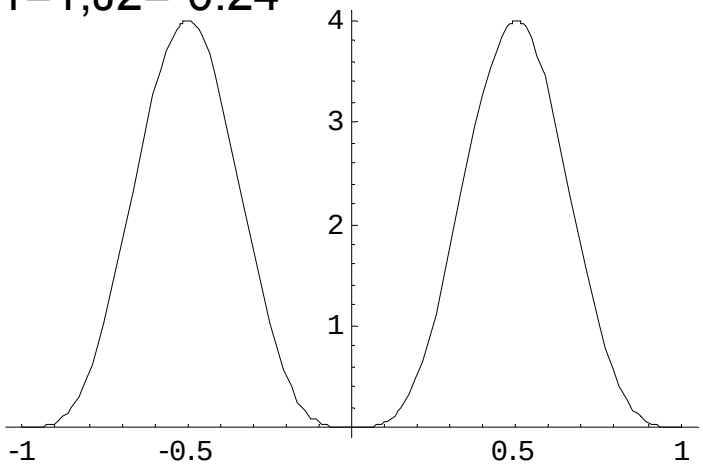

J1=1,J2=0.25

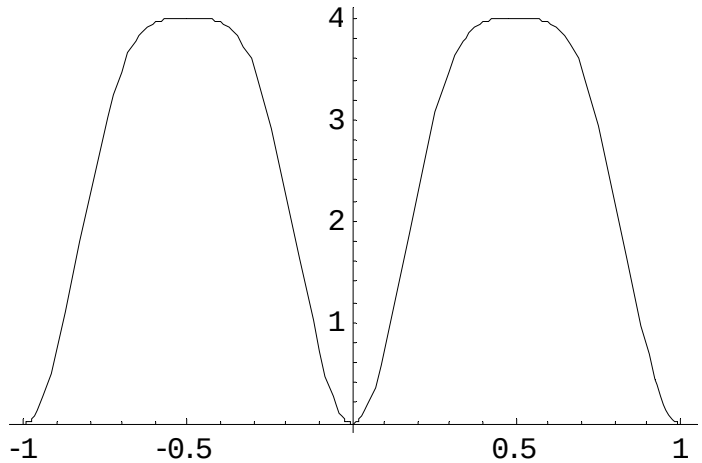

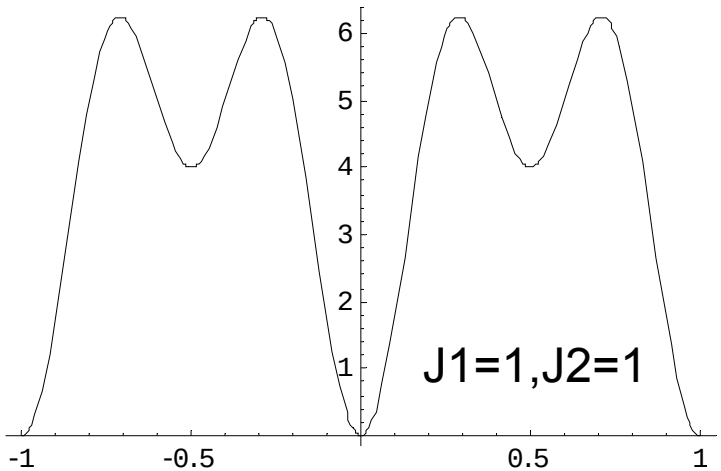

J1=1,J2=1

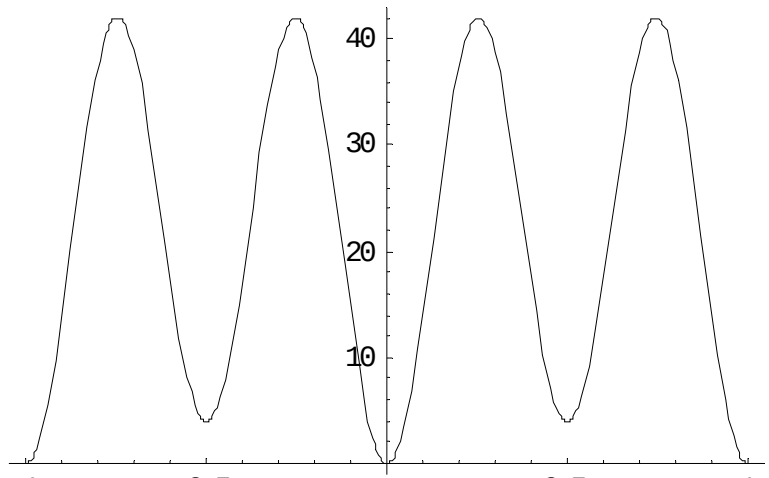

J1=1,J2=10

Excitations antiferromagnetic phase (ordering vector H=1/2)

$$\hbar\omega(h)=4S\ \{\ [-2J1+2J2\ -2J2\ \cos(4\pi h)]^2\ -[2J1\ \cos(2\ \pi h)]^2\}^{1/2}$$

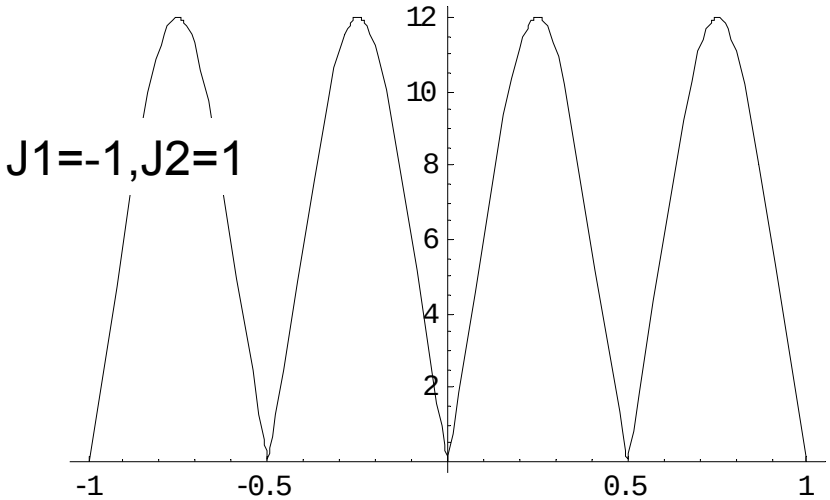

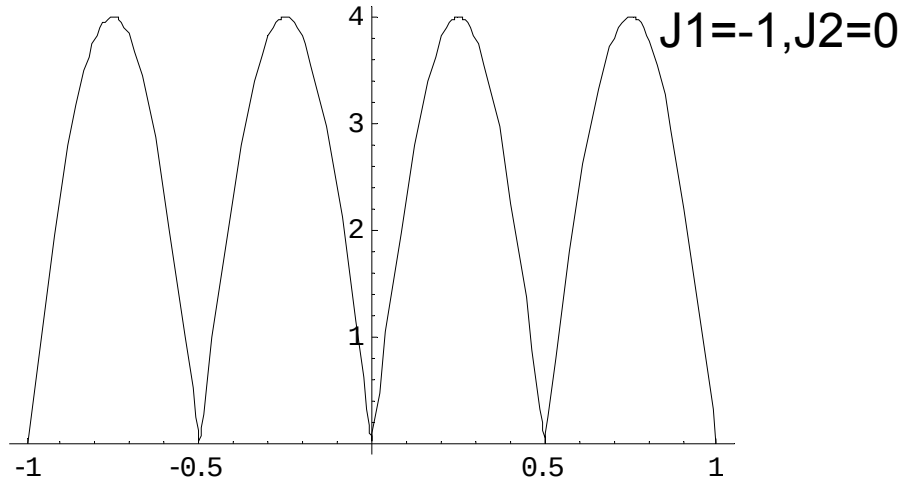

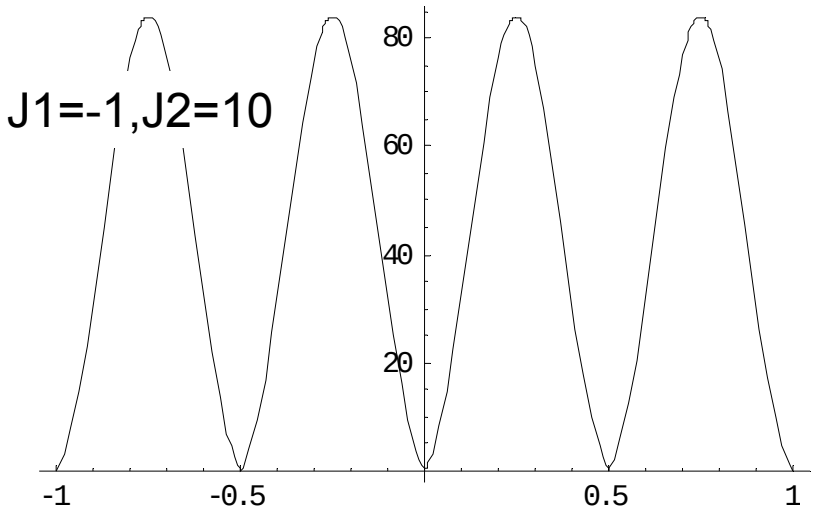

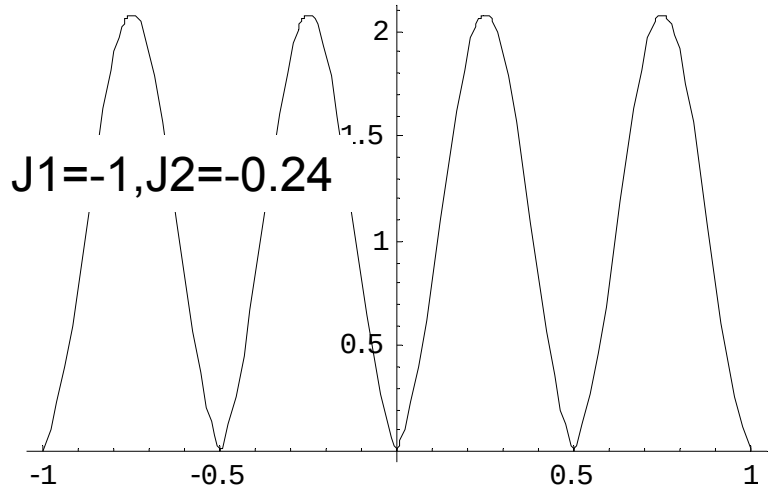

Excitations helically ordered phase

(ordering vector H given by $\cos(2 \pi H) = -J1 / 4J2$

This part will be prepared as a student report in the report session

X 0 Spin fluctuations – the fingerprints of macroscopic quantum ground states

M. Enderle
Institut Laue-Langevin
BP 156, 38042 Grenoble Cédex 9, France

Contents

1 Introduction

The concept of quantum mechanics, developed at the beginning of the last century, is a provocation of the common sense: It principally excludes the simultaneous exact determination of position and momentum of a particle - or other pairs of conjugate variables. Instead the behaviour of a particle is defined by a wave function or probability function which determines exactly the expectation values of observable properties. Macroscopic quantum phenomena, like superconductivity or superfluidity, cannot be described in terms of single-particle properties, but require a wave function of the entire many-particle system. The superfluid as well as the superconducting ground state have wave functions related to the so-called Bose-Einstein condensate. Two other famous phenomena of solid state physics, the integer and fractional quantum Hall effect, and the high-T_c superconductivity have been connected with new types of many-particle wave functions.
It is much less known, that a variety of macroscopic quantum ground states is realized in low-dimensional magnetic materials. The inherent structure of their wave function is closely related to those of the more famous brothers. Again, common sense is challenged by the fact that not all quantities have sharp expectation values simultaneously. Materials with well-localized magnetic moments may have energy eigenstates which cannot be expressed in terms of individual spin states. Nevertheless, characteristic properties of the ground state and the low-lying excitations can be visualized in a series of snap shots of individual spin states, in a similar way as path integrals lead from the classical to the quantum mechanical description of a particle.
Neutron scattering is an indispensable tool in the investigation of macroscopic quantum ground state magnetism. It allows to determine the microscopic interaction parameters essential for classifying the type of the ground state, as well as to take fingerprints of the ground state by measuring the corresponding spin fluctuations, i.e. the wave vector and energy dependent excitation spectrum.

2 Low-dimensional Spin Arrays in Nature

An one-dimensional array of localized interacting spins, a spin chain, is realized by the insulator $KCuF_3$ (Fig. 1). The electron shell of the transition metal ion Cu^{2+} is not entirely filled ($3d^9$), and therefore carries a magnetic moment. The overlap of neighbouring Cu^{2+} $3d$ orbitals is so small that we can consider them as isolated to start with. However, the $3d$ shell is far away from the nucleus, and the Stark effect of the electric field of the neighbouring ions is large compared to the spin-orbit coupling of the electrons. The Cu^{2+} $3d$ electron states are therefore to first approximation eigenstates of the total angular momentum, split by the Stark effect (often called the crystal field). Spin-orbit coupling only enters in the next approximation. Like for many transition metal salts, in $KCuF_3$ the orbital electronic ground state in the crystal electric field is a singlet, i.e. the expectation values of all three components of the electronic total angular momentum vanish ("orbital quenching"). The electron spin is not influenced by the crystal electric field, and given by Hund's rules [1]. Thus $KCuF_3$ displays the behaviour of a pure localized spin $\frac{1}{2}$ system. The small overlap region of the Cu^{2+} $3d$ and the F^- wave functions is governed by the Pauli principle and the Coulomb repulsion in competition with the tiny delocalization of the electrons (insulator !). The energy balance of this so-called superexchange interaction may favour parallel (ferromagnetic) or antiparallel (antiferromagnetic) alignment of neighbouring Cu^{2+} spins, in $KCuF_3$ it is antiferromagnetic. Since the origin of this effective

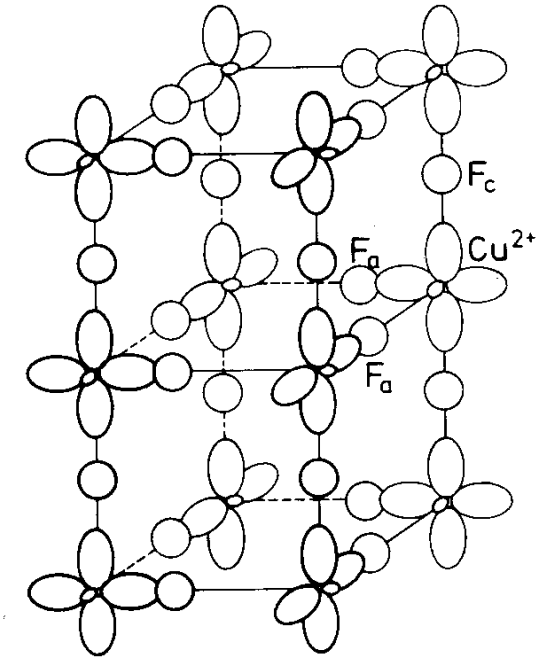

Fig. 1: *Structure of the one-dimensional $S = \frac{1}{2}$ Heisenberg antiferromagnet $KCuF_3$. Only Cu^{2+} and F^- are shown [2].*

magnetic superexchange interaction is the Coulomb interaction, it is many orders of magnitude larger than the magnetic dipole-dipole interaction. Contrary to the latter, the superexchange does not depend on the orientation of the spins with respect to their distance vector or the crystallographic axes. The superexchange depends on the volume of the overlap region. Hence it decreases exponentially fast with increasing distance. It further decreases with increasing ionic character of the bond, and increasing number of non-magnetic ions along the exchange path. To zeroth approximation, the superexchange can be described by a Heisenberg interaction, i.e. an isotropic interaction between neighbouring spins i, j of the form $J_{ij}\vec{S}_i\vec{S}_j$. Here J_{ij} denotes the exchange integral. In $KCuF_3$ the particular orientation of the Cu^{2+} orbitals leads to a 100 times stronger interaction between nearest neighbours along c than between neighbours along a, b [3]. Thus, with respect to magnetic properties, $KCuF_3$ behaves one-dimensional, like a collection of independent chains of spins $\frac{1}{2}$ which interact only within the chain. This magnetic one-dimensionality need not be reflected in the crystal shape.

3 Long Range Order and Quantum Ground States

Why does an antiferromagnetic spin chain not simply establish long-range order ? We consider the Heisenberg Hamiltonian

$$\mathcal{H} \;=\; J \sum_{<ij>} \vec{S}_i\vec{S}_j \;=\; J \sum_{<ij>} S_i^z S_j^z + \frac{1}{2}(S_i^+ S_j^- + S_i^- S_j^+), \tag{1}$$

where J denotes the exchange integral per spin pair. The sum contains each pair of nearest neighbours $< ij >$ once. All operators in the Hamiltonian commute in the classical limit $\hbar \to 0$, $S \to \infty$, $\hbar S$ constant:

$$| < [S_n^\alpha, S_n^\beta] > | \; = \; | < i\hbar\varepsilon^{\alpha\beta\gamma} S_n^\gamma > | \; \leq \; \hbar^2 S \underset{\hbar S = \text{const}}{\overset{S \to \infty}{\longrightarrow}} 0,$$

while the expectation value of the energy is proportional to $(\hbar S)^2$ and remains finite. In the classical limit, the spin becomes a vector with infinitely many possible orientations, while in the quantum limit the expectation values of the projection onto a given axis are discrete. The ground state of a ferro- or antiferromagnetically coupled chain of *vectors* is long-range ordered at $T = 0$. It can be written as a product of eigenstates of the operators S_i^z with eigenvalues $\hbar S_i^z = \pm\hbar S$ (Fig. 2). We choose z parallel to the ordering direction of the spins. The symmetry of the Hamiltonian with respect to arbitrary rotations in spin space is spontaneously broken in the ferromagnetic (FM) as well as the classical antiferromagnetic (AF) ground state, the translation symmetry with respect to translation by one lattice constant d only in the classical AF ground state. In the latter the magnetic unit cell is doubled with respect to the nuclear unit cell. The classical *ferromagnetic* ground state in Fig. 2 is an eigenstate of $\mathcal{H}$ even for small

FM: $\cdots \uparrow \uparrow \uparrow \uparrow \uparrow \uparrow \uparrow \cdots$

AF: $\cdots \uparrow \downarrow \uparrow \downarrow \uparrow \downarrow \uparrow \cdots$

Fig. 2: *Ground states of the classical ferromagnetic (FM) and antiferromagnetic (AF) Heisenberg-chain.* $\uparrow$ *and* $\downarrow$ *denote localized spin states* $S_i^z = +S$ *and* $S_i^z = -S$*. The order of the AF is described by two "sublattices" with opposite magnetization, or more general, by the ordering amplitude* m_0 *and wave vector* $k = \pi/d$ *in* $m(r) = m_0 \cos(kr)$*.* d *is the distance between two spins.*

spin values S, because it is an eigenstate of all individual operators $S_i^z S_j^z$ (with eigenvalues $(\hbar S)^2$) as well as of all operators $S_i^- S_j^+$ and $S_i^+ S_j^-$ (with eigenvalues 0). However, the classical *antiferromagnetic* ground state (Néel state) is *no* eigenstate of $\mathcal{H}$. It changes under the raising and lowering operators S_i^+ and S_i^-, cf. Fig. 3. In this sense the antiferromagnetic spin chain

					i	j			
	$\cdots$	S	$-S$	S	$-S$	S	$-S$	S	$-S$ $\cdots$
$S_i^+ S_j^-$ $\longrightarrow$	$\cdots$	S	$-S$	S	$(-S+1)$	$(S-1)$	$-S$	S	$-S$ $\cdots$

Fig. 3: $S_i^+ S_j^-$ *operating on the classical antiferromagnetic ground state. The local spin states are given in the basis of eigenstates/values of* S_i^z*,* $S_i^z = S, -S$*.*

behaves more "quantum mechanical" than a ferromagnetic chain [4, 5].

Obviously the transverse operators $S_i^+ S_j^-$ destroy the long-range order, and the ground state of the Ising-Hamiltonian,

$$\mathcal{H} \;=\; J \sum_{<ij>} S_i^z S_j^z,$$

is the classical antiferromagnetic ground state of Fig. 2, even for $S = \frac{1}{2}$. Therefore we will focus on the Heisenberg antiferromagnet (HAF).

To get an idea which role the *dimensionality* of the spin array (the interaction) plays we consider domain walls in the Néel ground state (Fig. 4). At these domain walls the sublattice magnetization changes sign. The energy of such a domain wall in a three-, two-, and one-dimensional (3D, 2D, 1D) spin system with N^3, N^2, N spins is proportional to $2JS^2N^2$, $2JS^2N$, and $2JS^2$, respectively. The degeneracy of the Néel state with one domain wall is $3N$, $2N$, and N for 3D, 2D, and 1D. Hence, at any finite temperature T, the the free energy of the 1D system is dominated by the entropy term $-k_BT \ln N$ which diverges in the thermodynamic limit, because the energy of the domain wall in 1D does not depend on the size of the system.

$$\Delta F \;=\; 2JS^2 - k_BT \ln N \;\rightarrow\; -\infty, \quad N \rightarrow \infty.$$

Therefore, at any finite temperature, the 1D Néel state is instable with respect to the formation of domain walls and long-range order is not established [5]. A Heisenberg system can delocalize the domain wall over its whole extension and reduce the energy of the domain wall by another factor N. Neighbouring spins then include an angle of $\frac{\pi}{N}$. In the classical limit ($S \rightarrow \infty$) domain walls are introduced into the Néel state by thermal fluctuations, in the quantum limit (for small values of S), the terms $S_i^+ S_j^-$ in the Hamiltonian create domain walls even at $T = 0$. These "zero point fluctuations" destroy the long-range order of the Heisenberg antiferromagnetic chain (1D HAF) even at $T = 0$ [5]. For the 1D HAF with spins $\frac{1}{2}$ at each site we visualize this in Fig. 4 by applying the operators $S_i^+ S_j^-$ successively to the Néel state: We

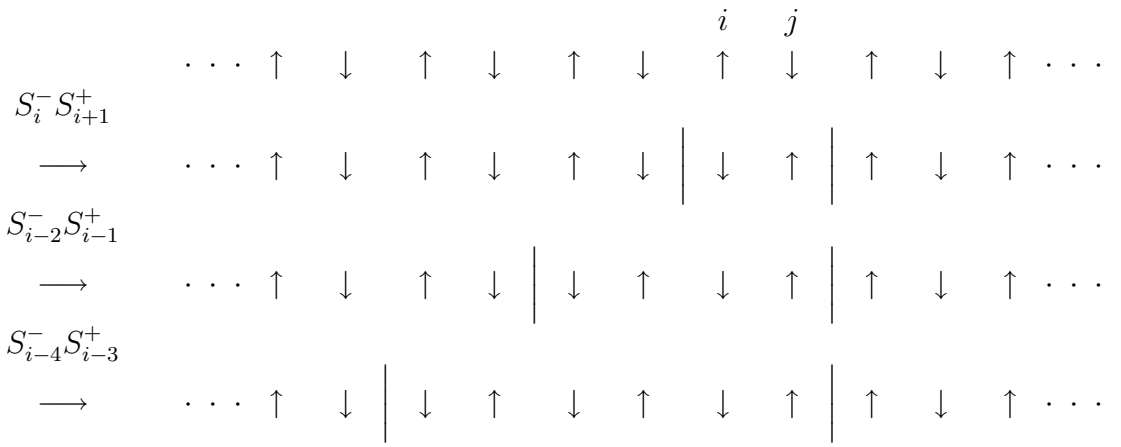

Fig. 4: *Successive application of $S_i^- S_j^+$ to a long-range ordered Néel state of the 1D $S = \frac{1}{2}$ Heisenberg antiferromagnet. The first operation generates two domain walls (marked by |), the following "move" an individual domain wall, i.e. delocalize it. The delocalization creates a region with inverted sublattice magnetisations between the two domain walls, compared to the rest of the spin chain.*

realize that successive application of the operators $S_i^- S_j^+$ to the Néel state generates domain

wall pairs, but also moves (delocalizes) single domain walls, and separates a pair of walls. In an Ising system, the Néel state is the correct ground state. If we smoothly introduce an operator $\lambda \sum S_i^+ S_j^- + S_i^- S_j^+$ by increasing λ from zero, the successive application of $S_i^- S_j^+$ to the Néel state simulates the increasing relative strength λ of the term $S_i^- S_j^+$. The resulting ground state can be imagined as a superposition of the Néel state with all the new states created by the perturbation. With growing λ, it contains more and more domain walls which are better and better delocalized [5]. The delocalization of the domain walls lowers their energy, and at $\lambda = \frac{1}{2}$ (HAF) the long-range order is completely destroyed at $T = 0$.
Obviously non-frustrating *further-than-nearest neighbour* interactions lead to an increase of the domain wall energy and hence favour longe-range order. In contrast, *frustrating* interactions lead to a higher degeneracy of the classical ground state, increase the ground state energy and reduce the domain wall energy. Therefore frustrating interactions support the creation of domain walls by thermal fluctuations as well as by quantum operators and thus promote macroscopic quantum ground states against long-range order.

We return to the pure Heisenberg chain, but now with spins 1 at each site. Here the transverse operators create another type of domain wall as in the spin $\frac{1}{2}$ chain, but again a domain wall pair is generated by a single application of $S_i^+ S_j^-$ to the classical Néel state, and a second application moves the domain wall (Fig. 5). Already for $S = \frac{3}{2}$ the situation is different: Unique application

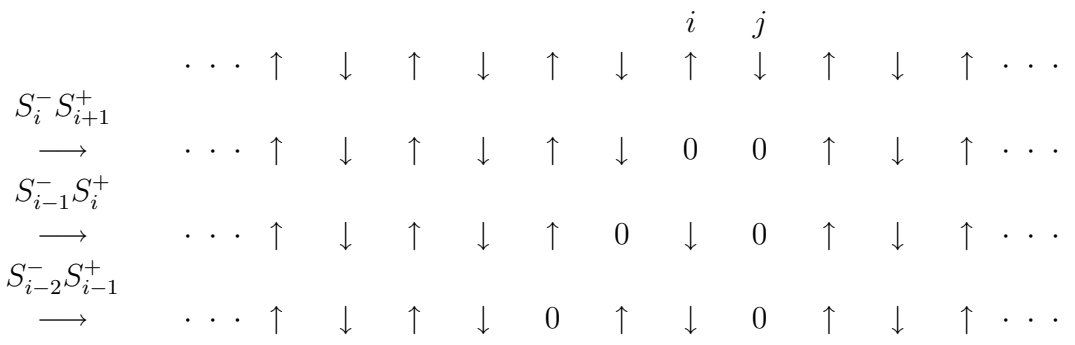

Fig. 5: *Successive application of operators $S_i^- S_j^+$ to a long-range ordered state of a 1D $S = 1$ Heisenberg antiferromagnet. The quantization axis is chosen parallel to z, $\uparrow, 0, \downarrow$ denote local spin states with $S_i^z = +1, 0, -1$. The first application of $S_i^- S_j^+$ creates a domain wall pair in the center of which we find two sites $S_i^z i = 0$. The following applications "move" a single domain wall/$S_i^z = 0$ state, i.e. delocalize it. These domain walls destroy the long-range order, but preserve the "hidden" antiferromagnetic order described in the text.*

of $S_i^+ S_j^-$ decreases the sublattice magnetization, but does not yet create a domain wall pair. These simple pictures visualize correctly that the classical limit is reached very fast. Indeed, the classical ground state is a good starting point to understand antiferromagnetic spin $\frac{3}{2}$ Heisenberg chains (for the experts: higher order spin-wave expansions work well.)
Now we consider the ground states of the spin $\frac{1}{2}$ and spin 1 chains in more detail. Both are described by a macroscopic wave function which is translation invariant, i.e. has the same period d as the lattice (d is the distance between two spins). It is characterized by the wave vector $k = 0$ (identical to $\frac{2\pi}{d}$) like in the ferromagnetic case, while the wave vector of the Néel state is $k_{AF} = \frac{\pi}{d}$. The 1D spin $\frac{1}{2}$ and spin 1 HAF have no long-range order, neither with period

$2d$ nor with any other. The Heisenberg Hamiltonian commutes with the total spin operator S^2_{tot} ($\vec{S}_{tot} = \sum_i \vec{S}_i$). The energy eigenstates are therefore eigenstates of the total spin operator. The ground state of the HAF is an eigenstate with $S_{tot} = 0$, i.e. a singlet with respect to the total spin. The classical Néel state is neither an eigenstate of the Heisenberg Hamiltonian nor of the total spin S^2_{tot}, but only of S^z_{tot}. Nevertheless a snapshot of the macroscopic quantum ground state of the spin $\frac{1}{2}$ and spin 1 HAF-chains will resemble a the Néel state on short chain pieces. This short-range order is described by the spin correlation function $g(\ell) =< \vec{S}_i \vec{S}_{i+\ell} >$. In a long-range ordered state, $g(\ell)$ remains finite for $\ell \to \infty$. The spin correlation function of the spin $\frac{1}{2}$ chain decays to zero with $1/\ell$, that of the spin 1 chain even exponentially fast ($\propto \exp(-\ell/\xi)/\sqrt{\ell}$) with a correlation length of $\xi \approx 6d$. The power law of the spin $\frac{1}{2}$ chain correlation can be interpreted as an infinitely long correlation length. Hence, surprisingly, the short range order is much better developed in the case of spin $\frac{1}{2}$ than that of spin 1. The finite correlation length ξ of the spin 1 chain translates to an energy gap between ground state and excited states in the spectrum of magnetic excitations, $\Delta E = 0.41J$, while the excitation spectrum of the spin $\frac{1}{2}$ chain is gapless like that of the classical chain. This surprising difference between spin $\frac{1}{2}$ and spin 1 HAF chains was first postulated as a hypothesis by Haldane [6], later confirmed by numerous analytical, numerical and experimental studies (for a review see [4]). The difference between the two ground states originates in the different type of domain walls: starting from the Ising limit and the Néel state, the spin 1 chain experiences a quantum phase transition, a Bose-Einstein condensation of domain walls, already before the isotropic Heisenberg case is reached. The spin $\frac{1}{2}$ chain just reaches the critical point at the isotropic limit. The domain walls in the Heisenberg ground state of the spin 1 chain are free, those in the ground state of the spin $\frac{1}{2}$ chain still form pairs but the distance between the pair spins may be infinite. An excitation gap in a spin $\frac{1}{2}$ chain is generated e.g. by infinitesimally small *alternating* exchange in addition to the Heisenberg exchange

$$\mathcal{H} = J \sum_n (1 + (-1)^n \epsilon) \vec{S}_n \vec{S}_{n+1}. \tag{2}$$

In a real material alternating exchange can be produced by the crystal structure, e.g. alternating larger and smaller distances between the spins. This alternating exchange breaks translation symmetry, the ground state is now described by the wave vector $k = \frac{\pi}{d}$ but still $S_{tot} = 0$. The extreme limit of the alternating chain is $\epsilon = 1$, the isolated dimer limit. In this limit the ground state consists of isolated spin pairs, forming $S_{pair} = 0$ pair states (perfect dimer ground state). For $0 < \epsilon < 1$ the dimerised ground state can be imagined as a dimer ground state, where quantum fluctuations lead to some singlet formation on the weak bond as well. In a virtual series of snapshots of this ground state, "from time to time" the antisymmetric pair state is formed across the weak exchange connection, i.e. the dimer bond "sometimes" flips from the strong to the weak connection. In the Heisenberg limit $\epsilon = 0$ the dimer bond flips forth and back and leads to singlet formation on each connection with equal probability.

A similar picture correctly describes the wave function of the $S = 1$ HAF chain (Haldane ground state): The spins 1 at each site are imagined as two spins $\frac{1}{2}$, strongly (ferromagnetically) bound to a symmetric state at each site, but at the same time, each spin $\frac{1}{2}$ forms an antisymmetric pair state with a spin $\frac{1}{2}$ at the neighbouring site. This does not require a flipping forth and back of the singlet bond, the ground state is a "valence bond solid", and the translation invariance of this ground state (period d, wave vector $k = 0$) is immediately obvious. This Haldane ground state is characterized by a "hidden" antiferromagnetic order: A local state $S^z = -1$ is followed by arbitrarily many states $S^z = 0$ which then have to be followed by a state $S^z = +1$ [7, 8].

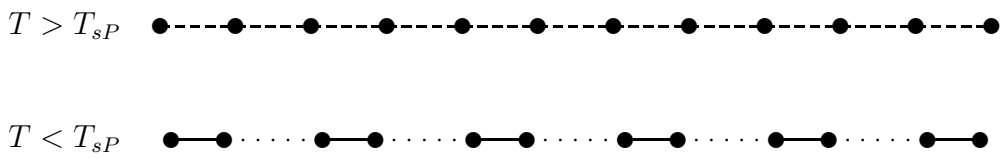

Fig. 6: *Spin-Peierls system, schematic: antiferromagnetic short range order ("formation of singlets with probability $\frac{1}{2}$ on all bonds") and translation invariant spin distances above T_{sP}, structural and magnetic dimerization below T_{sP}. The magnetic dimerisation (formation of singlet-pairs) is indicated by solid lines. The structural dimerisation is exaggerated. The magnetic dimerisation is not fully developed, "every now and then" one should imagine a singlet on the weak bond, indicated by dotted lines.*

Antiferromagnetic next-nearest neighbour (nnn) interaction in the $S = \frac{1}{2}$ chain leads to a dimerised ground state with an excitation gap above a critical strength of the nnn-interaction:

$$\mathcal{H} = J \sum_n \left(\vec{S}_n \vec{S}_{n+1} + \alpha \vec{S}_n \vec{S}_{n+2} \right). \tag{3}$$

Nearest- and next-nearest neighbour antiferromagnetic exchange compete and lead to frustration. The nnn-interaction connects the spin $\frac{1}{2}$ chain to so-called *spin ladders* (see e.g. [9, 10, 11]). In a spin-ladder, the spins are sitting at the connection point of the rung to the leg, and the rungs and the leg-pieces symbolize the exchange bonds. Exchange between different ladders in the crystal is negligible. The nnn-frustrated chain is equivalent to a two-leg spin ladder with equal antiferromagnetic exchange J on the rungs and one diagonal, and αJ along the legs.
Spin ladders have been regarded as an entirely academic toy, until a series of Sr-cuprates was found to be described by this model. The isotropic spin ladder with zero exchange on the diagonals and equal exchange on rungs and legs has a valence bond solid ground state, as the Haldane ground state. Furthermore, isotropic spin ladders with an even number of legs have a valence bond solid ground state with an excitation gap as the Haldane chain while those with an odd number are gapless and similar to the $S = \frac{1}{2}$ HAF chain. Experimental examples of two- and three-leg ladders are $SrCu_2O_3$ and $Sr_2Cu_3O_5$. Hence spin ladders connect the macroscopic quantum ground states of one-dimensional antiferromagnets smoothly to those on two-dimensional lattices.
In contrast to the examples considered so far, where the coupling of the magnetic moments to the lattice can be neglected or regarded as entirely static (alternating chain), magnetoelastic spin-phonon coupling is an essential requirement for the *spin-Peierls* ground state. The spin-Peierls chain is a Heisenberg antiferromagnetic chain of spins $\frac{1}{2}$ on an elastic three-dimensional lattice. The coupling to the three-dimensional lattice leads to a phase transition at finite temperatures, into a magnetically and structurally dimerised phase (Fig. 6). The elastic energy required for the distortion is provided by the spin system. For the magnetic subsystem, the dimerised ground state with an energy gap to the first excitations is energetically favorable to the uniform ground state. In the latter, zero point fluctuations increase the ground state energy with respect to a long-range ordered ground state.
At $T = 0$ (and zero magnetic field), the spin-Peierls ground state is equivalent to that of an alternating chain. Under certain conditions, the spin-phonon coupling can act as an effective an-

tiferromagnetic next-nearest neighbour intrachain exchange. Moreover, above the spin-Peierls transition temperature, the behaviour is expected to resemble that of a uniform $S = \frac{1}{2}$ Heisenberg chain, with or without next-nearest neighbour intrachain interaction.
All these macroscopic quantum ground states have in common to be macroscopic singlet states, $S_{tot} = 0$, while S_{tot} is not a "good" quantum number, i.e. is not defined or "sharp", for the classical long-range ordered Néel state.
Presence or absence of an excitation gap between the ground state and the lowest-lying excitations, however, is not sufficient to characterize a quantum ground state. Excitation gaps appear as well in "classical" antiferromagnets, due to anisotropic interactions or crystal-field anisotropies. The anisotropy of the underlying lattice is transferred to the magnetic moment by the spin-orbit coupling and makes the spins prefer a specific direction or plane with respect to the crystallographic axes. Next, the determination of the relevant superexchange couplings in a real material is highly non-trivial. Although calculations of the nearest neighbour exchange appear to become more reliable, they are still extremely expensive and only performed in special cases. Even then one is far away from a prediction of next-nearest neighbour couplings or weaker disturbances which nevertheless may be essential for the character of the ground state. The experimental determination is not less trivial. It requires the consideration of different physical quantities, the comparison with different calculations, and is usually achieved in a kind of consistency check. Before theories can be tested, interactions and anisotropies must be known.
The requirement of good one-dimensionality and low anisotropy is met by very few materials. This is the main reason why there is not a flood of good and established model systems, but usually only very few for each class of macroscopic ground state and why a detailed characterization of these model systems is indispensable.

4 Spin Fluctuations

The excitation gap is a characteristic feature of some quantum ground states, but not of all. Moreover, there are also classical ground states with an excitation gap due to anisotropies. Which aspects distinguish macroscopic quantum ground states from classical ground states ? An essential feature, comparable to a fingerprint, is the wave vector dependent entire spectrum of the magnetic excitations of the respective ground state, and its dependence on the magnetic field. The entire energy-momentum relation of the magnetic excitation spectrum can (only) be investigated by inelastic neutron scattering. At special wave vectors ($k = 0$), ESR and light scattering are possible, eventually one can derive a density of states using light scattering.
In a *classical* antiferromagnet, the excitations can be imagined as precessions of the magnetic moments (which now can be regarded as vectors) about their ordering direction. Acoustic spin waves at the antiferromagnetic Bragg peak $k_{AF} = \frac{\pi}{d}$ correspond to precessions of both sublattices in such a way, that the 180° angle between neighbouring magnetic moments is unchanged. In a classical Heisenberg antiferromagnet, this does not cost any energy, and the excitation is gapless. The acoustic spin waves with wave vectors $k \neq k_{AF}$ imply a phase difference between neighbouring spins, and consequently an angle different from 180°. The energy $\hbar\omega(k)$ of the spin wave increases with the phase difference kd, $\hbar\omega(k) = 2JS|\sin(kd)|$. There are two degenerate branches, corresponding to the two precession directions. With the wave vector k changing from the antiferromagnetic zone center $\frac{\pi}{d}$ to the zone boundary $\frac{\pi}{2d}$, the ratio of the transverse amplitudes of the two sublattices changes as well (the transverse amplitude defines

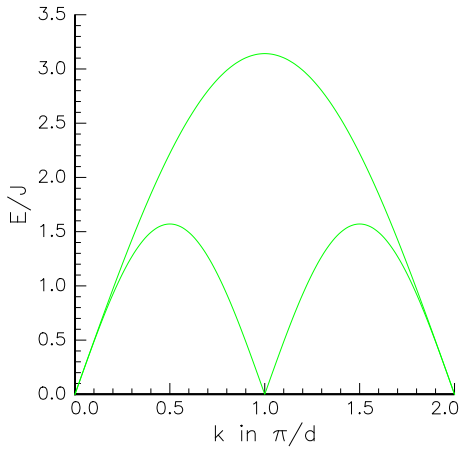

Fig. 7: *Excitation spectrum $E(k)$ of the $S = \frac{1}{2}$ HAF chain. The lines indicate the lower and upper boundary of the continuum of magnetic excitations, which are pairs of free solitons with respect to an antiferromagnetic arrangement. The pair has $S_{tot} = 0, 1$. J denotes the intrachain exchange, d the spin distance. A classical HAF chain has two degenerate branches with $E(k) = 2J|\sin(kd)|$, polarized transverse to the ordering direction. Hence the lower boundary of the excitation spectrum of the spin $\frac{1}{2}$ HAF chain appears "classical", apart from a different maximum value at $k = \frac{\pi}{2d}, \frac{3\pi}{2d}$.*

the cone angle of the precession in the respective sublattice). At the antiferromagnetic zone center the ratio of the transverse amplitudes is -1, at the zone boundary 0 [1]. Classical spin-waves in antiferromagnets are treated in [12, 13, 14].

In a *quantum* antiferromagnetic chain, i.e. in a one-dimensional antiferromagnet with small spins, $S = \frac{1}{2}$ ($S = 1$), such a precession is not possible because there are only two (three) possible states S^z with respect to the ordering direction z which defines the quantization axis. Quantum excitations therefore are of an entirely different nature. The elementary excitation in the uniform $S = \frac{1}{2}$ HAF chain is a delocalized antiferromagnetic domain wall (soliton), which creates a 180° phase change of the ground state wave function between left and right half of the chain, i.e. corresponds to breaking one "bond". The dispersion relation of the soliton is $\hbar\omega = \frac{\pi}{2}J|\sin(kd)|$. The excitation spectrum consists of pairs of free (non-interacting) solitons. Two solitons with arbitrary momenta k_1, k_2 can be combined ($k = k_1 + k_2$, $E(k) = E_1(k_1) + E_2(k_2)$), hence the spectrum is a continuum reaching from $E(k) = \frac{\pi}{2}J|\sin(kd)|$ to $E(k) = \pi J|\sin(\frac{kd}{2})|$ (Fig.7) [15]. The domain wall pairs carry spin 0 or 1. The lower edge of the excitation spectrum corresponds to the classical spin wave dispersion relation, multiplied by the renormalisation factor $\frac{\pi}{2}$. Indeed there is a certain similarity between domain wall *pairs* and classical spin waves, both are only weak perturbations of the antiferromagnetic order. Sloppy speaking, the excitation of a domain wall pair corresponds to breaking a singlet bond which is "already flipping back and forth between two positions" in the ground state. Therefore there is no threshold energy for the excitations, the spectrum begins at zero energy. The domain wall continuum was found experimentally by inelastic neutron scattering on $KCuF_3$ [3]. The left side of Fig. 8 displays the dispersion of the ideal one-dimensional $S = \frac{1}{2}$ Heisenberg antiferromagnet together with a curve in the energy-momentum space. The right hand side shows the number of scattered neutrons measured by the time-of-flight technique, which have

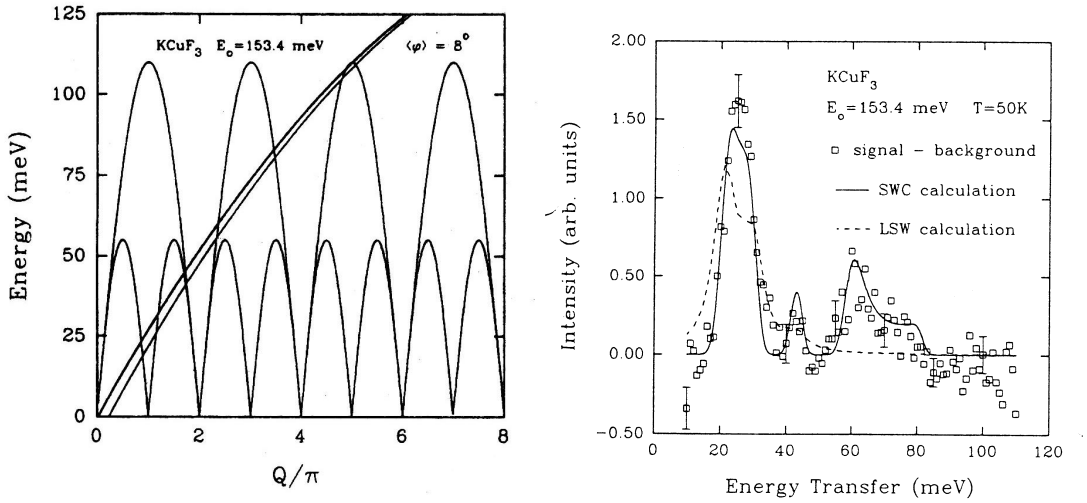

Fig. 8: *Excitation spectrum of the antiferromagnetic $S = \frac{1}{2}$ Heisenberg chain $KCuF_3$ [3], cf. text.*

experienced an energy and momentum transfer along this curve. The solid line is the expected intensity of an ideal one-dimensional $S = \frac{1}{2}$-Heisenberg antiferromagnet. The intensity of the continuum is clearly visible and proves the quantum character of the excitations.

The excitations of the strongly *nnn-frustrated chain* are pairs of free domain walls with respect to the dimer order. A domain wall pair corresponds to breaking one singlet (dimer) bond into a triplet state $S_{tot} = 1$. There is no flipping of dimer bonds in the ground state, and breaking the singlet costs energy. Therefore the continuous excitation spectrum is gapped. Otherwise it looks very similar to that of the pure $S = \frac{1}{2}$ Heisenberg antiferromagnet.

The excitations of the *alternating chain* are bound pairs of mutually attractive domain walls: If the domain walls move apart, the singlet bonds in between are formed on the weak exchange bond instead of the strong one. This increases the energy of the excited pair state, hence corresponds to a binding energy of the two domain walls. The excitation continuum is formed of pairs of such bound domain wall pairs. It is separated from the elementary bound domain wall pair by a second energy gap, Fig. 9.

In the *spin 1 Heisenberg antiferromagnetic chain* the elementary excitation again corresponds to breaking one of the "valence bonds". This creates *one* soliton with respect to the "hidden" antiferromagnetic order. The dispersion has the period $\frac{2\pi}{d}$, corresponding to the wave vector of the ground state wave function (cf. the alternating spin $\frac{1}{2}$ chain with the period $\frac{\pi}{d}$ of the dispersion and ground state wave function). The continuum is formed by states formed of two, three etc. of the elementary solitons, leading to a spectrum as schematically shown in Fig. 10. Close to $k_{AF} = \frac{\pi}{d}$, the elementary excitation is isolated from the continua, and the three-soliton excitation has a lower energy than two-soliton excitations. Fig. 11 displays the dispersion of the elementary soliton of the spin 1 Heisenberg antiferromagnet NENP ($Ni(C_2D_8N_2)_2NO_2(ClO_4)$), measured by inelastic neutron scattering on a triple axis spectrometer [16]. So far, none of the continua has been found experimentally.

Like in the alternating spin $\frac{1}{2}$ chain, a magnetic excitation of the *spin-Peierls* chain breaks a dimer bond. This threshold energy needs to be overcome, thus the excitation spectrum displays a gap. Breaking a dimer bond creates two domain walls which attract each other. In the spin-

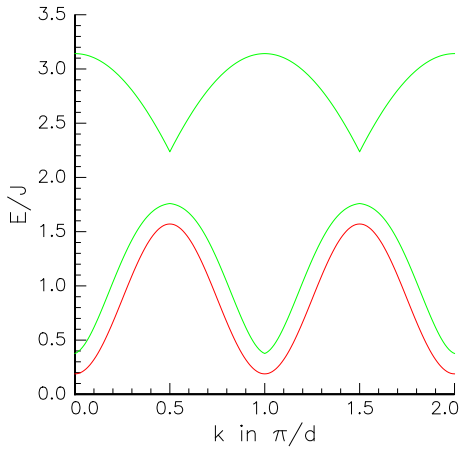

Fig. 9: *Excitation spectrum $E(k)$ of the alternating and the spin-Peierls chain. The green lines indicate the lower and upper boundary of the continuum. The elementary triplet branch is shown as a red line. J denotes the average intrachain exchange, d the spin distance. The size of the excitation gap depends on the alternation parameter (alternating chain) and the spin-phonon coupling (spin-Peierls systems), respectively.*

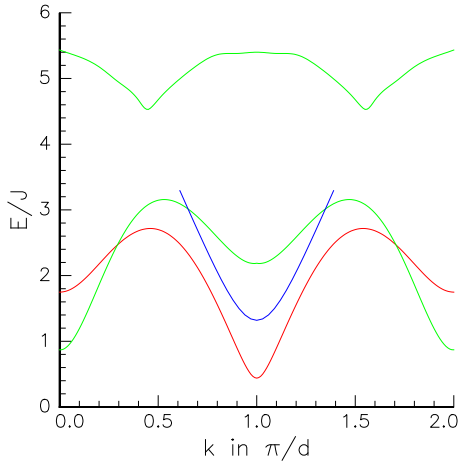

Fig. 10: *Scheme of the magnetic excitation spectrum of the $S = 1$ Heisenberg antiferromagnetic chain. The red line indicates the isolated elementary triplet excitations, which are domain walls (solitons) with respect to the hidden antiferromagnetic order. The green lines display the lower and upper edge of the continuum of pair excitations of the elementary soliton. The blue line shows the lower edge of the three-soliton excitation continuum. The energies are given in units of the superexchange J. $k_{AF} = \frac{\pi}{d}$ denotes the antiferromagnetic zone center. The elementary soliton branch has vanishing spectral weight for $k < \frac{\pi}{2d}$.*

Peierls chain, the attractive potential is created by the three-dimensional elastic energy and the alternating exchange on the dimerised lattice: The separation of two domain walls belonging to one pair leads to a mismatch of the dimerisation with respect to the neighbouring chains. Keeping the separation distance short limits the mismatch and lowers the energy of the excitation.

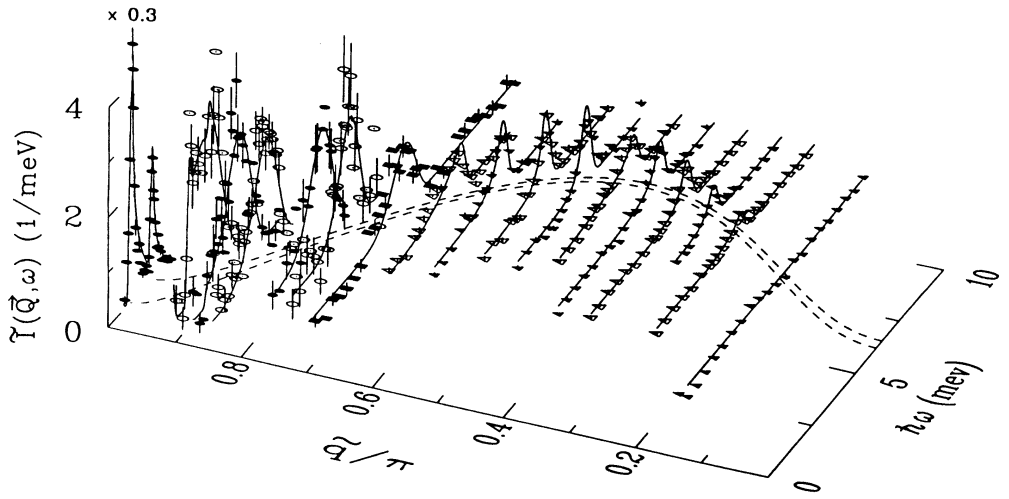

Fig. 11: *Dispersion of the elementary soliton triplet of the $S = 1$ Heisenberg antiferromagnetic chain NENP. The picture displays the number of scattered neutrons in dependence of energy at different momentum transfers along the chain direction [16].*

The elementary excitation of the spin-Peierls chain is therefore a bound domain wall pair with $(S_{tot} = 1)$ which corresponds to a bound soliton–anti-soliton pair. The continuum is formed by pairs of the elementary triplet (fig.9), i.e. by free pairs of bound domain wall pairs.

The left hand side of Fig. 12 displays the triplet dispersion and the lower boundary of the continuum of the spin-Peierls system $CuGeO_3$, measured by inelastic neutron scattering on a triple axis spectrometer [17]. The triplet has a considerably lower energy than the lower continuum boundary. The right hand side of Fig. 12 displays the entire excitation spectrum of $CuGeO_3$, measured by neutron time-of-flight spectroscopy [18]. The triplet branch and the lower boundary of the continuum are not resolved in this measurement.

A common feature of all *quantum* excitation spectra is the existence of a continuum and the isotropic polarization of the excitations, arising from the three components of the $S_{tot} = 1$ state. Classical spin waves are only twofold degenerate, with a polarization transverse to the ordering direction. These properties can be used to distinguish quantum gaps from anisotropy gaps: In a magnetic field, a quantum gap state with $S_{tot} = 1$ will display the threefold splitting according to $g\mu_B H S^z_{tot}$ and independent of J, while the energy of a classical spin-wave is barely influenced by magnetic fields $g\mu_B H << J$. Fig. 13 displays the field dependent triplet splitting at $k = k_{AF}$ of the spin-Peierls system $CuGeO_3$ (left) [19] and the spin 1 Heisenberg antiferromagnetic chain NENP (right) [20, 21], measured by inelastic neutron scattering with triple axis spectrometers. In the right panel the open circles denote the data obtained by neutron scattering ($S(k,\omega)$), the other symbols indicate gap-energies that were derived from different physical quantities. The triplet of NENP is already split at $H = 0$ by a crystal field anisotropy. The observation of *three* and not just two excited states, and the strong field dependence of the excited states, which correspond to an anisotropy-split triplet, evidence the quantum character of the excitations.

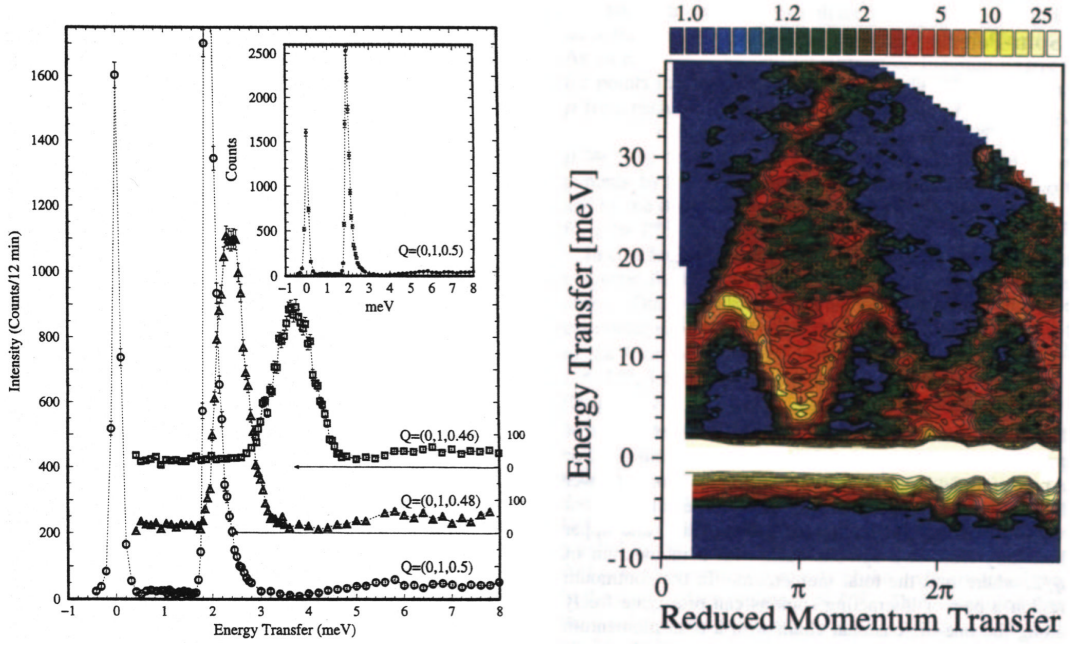

Fig. 12: *Dispersion of the triplet and continuum of the magnetic excitations of the spin-Peierls systems $CuGeO_3$ in its dimerised phase. Left: separation of the triplet (intense excitation at 2-4meV) and the continuum (weak hill above 5meV), measured by neutron scattering with a triple axis spectrometer, in energy scans with fixed momentum transfer [17]. Right panel: entire excitation spectrum, measured by neutron time-of-flight spectroscopy (here the triplet is not resolved from the lower boundary of the continuum). The neutron intensity is color coded over energy (ordinate) and momentum (abscissa) [18].*

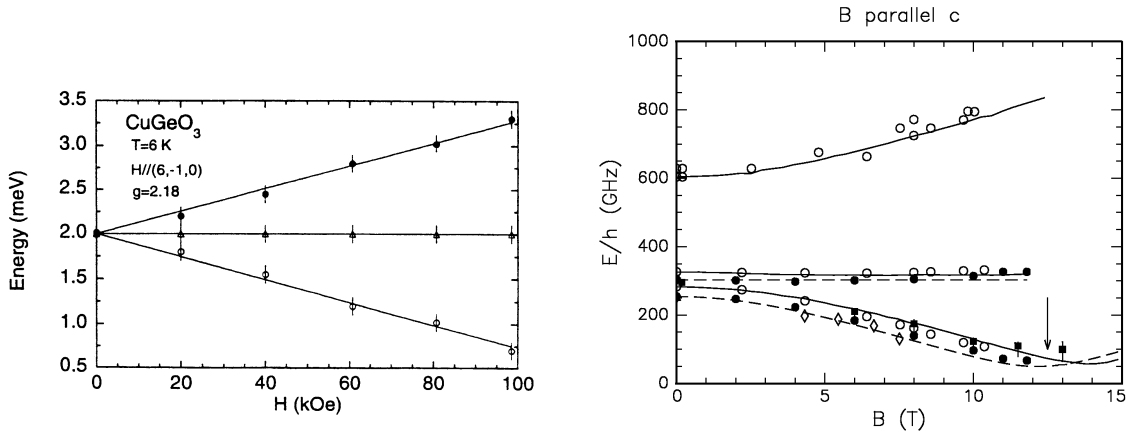

Fig. 13: *Field dependent splitting of the excited triplets at k_{AF}. Left panel: spin-Peierls system $CuGeO_3$ [19], right panel: $S = 1$ Heisenberg antiferromagnetic chain NENP [20, 21].*

5 Spin Fluctuations in a Magnetic Field

The threefold splitting of the excitation gap of a quantum spin chain imposes the question what happens at the field strength where the lowest excitation branch hits the ground state. Above

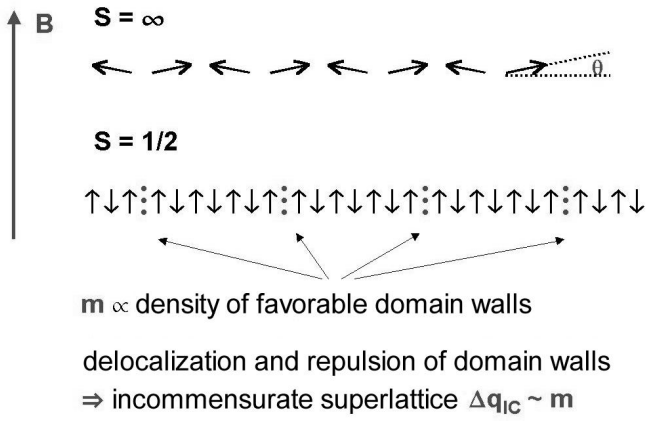

Fig. 14: *Magnetization of the classical and the quantum $S = \frac{1}{2}$ Heisenberg antiferromagnetic chain. The $S = \frac{1}{2}$-case is shown as a "caricature" with infinitely sharp domain walls (dotted).*

this critical field the ground state is magnetized, but how does the magnetized ground state look like and how its excitation spectrum ? We start again with the classical antiferromagnetic chain in comparison with the uniform $S = \frac{1}{2}$ Heisenberg antiferromagnetic chain (Fig. 14).

Magnetization in a classical Heisenberg antiferromagnetic chain is generated in the following way [22]: At infinitesimally small magnetic field, all magnetic moments flop into the plane perpendicular to the magnetic field and then are continuously tilted towards the field. This allows the moments to keep an almost antiparallel arrangement as long as possible. The wave vector $k = \frac{\pi}{d}$ which describes the periodicity of the ground state does not change until the saturation field is reached, where it drops to $k = 0$ discontinuously. The saturated $k = 0$ state has all moments parallel to the field.

Such a continuous tilting is not possible in an antiferromagnetic spin chain of small spin values. Once more the domain walls or solitons are the essential elements which help to understand the magnetization process. In the spin $\frac{1}{2}$ HAF chain, a soliton constitutes a delocalized "broken bond" between two adjacent spins. For a moment we picture the soliton in the localized caricature, where it leads to two parallel spins to the left and right of the center of the domain wall. If these spins are parallel to the magnetic field, the magnetization of the entire spin chain is increased from $g\mu_B S^z_{tot} = 0$ to $\frac{1}{2}g\mu_B$. This holds also for a delocalised domain wall. Creating more and more of these solitons with favourable orientation with respect to the magnetic field increases the magnetization, until all spins are in the same S^z-state (saturation). Our domain wall picture explains why the antiferromagnetic polarisation (the staggered magnetization) of a quantum antiferromagnet in a magnetic field is parallel to the field direction and not perpendicular as in the classical case. Next we must take into account that the soliton is not an infinitely sharp domain wall but delocalized. The delocalization is produced by the transverse parts $S^+_n S^-_{n+1}$ of the Hamiltonian (z is chosen along the field direction). The $S^z_n S^z_{n+1}$ parts then lead to a repulsion of the domain wall centers and the final arrangement displays equal spaces between the soliton centers. This arrangement is not static, but must be imagined as a

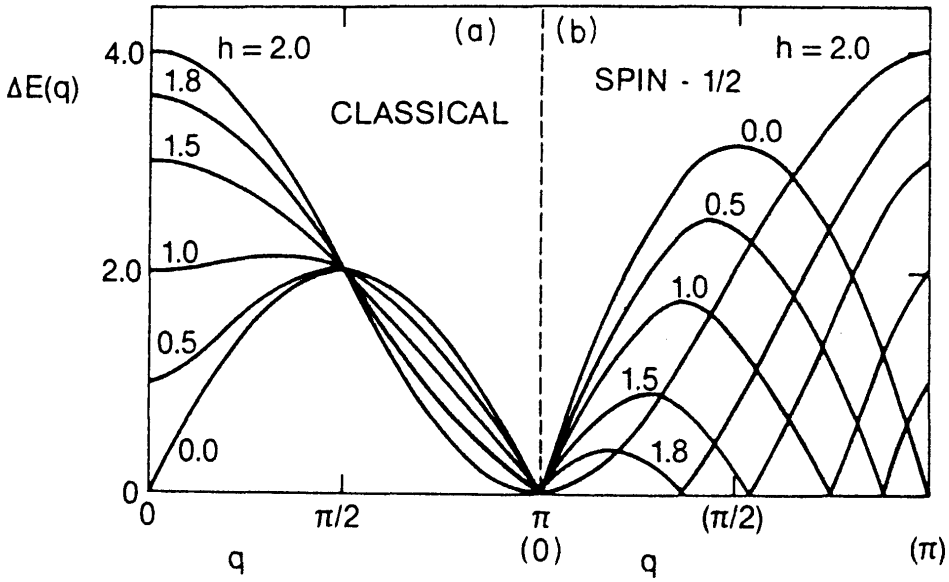

Fig. 15: *Excitation spectrum of the $S = \frac{1}{2}$ HAF chain in a magnetic field in comparison to that of a classical spin chain [23]. $q = 0$ corresponds to the antiferromagnetic zone center $k = \frac{\pi}{d}$, $q = \pi$ to the lattice Brillouin zone center $k = 0$. The curves in the right hand panel correspond to excitations polarized parallel to the magnetic field if $q = (\pi)$ is identified with the antiferromagnetic zone center $k = \frac{\pi}{d}$, and to polarization perpendicular to the field if $q = (\pi)$ is identified with $k = 0$. Only the lower boundary of the continuum is shown in the $S = \frac{1}{2}$ case. h denotes the magnetic field in reduced units, $h = 2$ is the saturation field. The energies are normalized to the intrachain interaction J per bond.*

floating pattern, with fixed distance between the soliton centers. The distance depends on the magnetization and vice versa, and in general is incommensurate. This incommensurate floating superstructure corresponds to gapless excitations at field dependent incommensurate wave vectors $k \propto m$ [23]. There are no Bragg peaks, because the arrangement is not static. But at those wave vectors where the Bragg peaks would appear, if the arrangement were static, the excitation spectrum becomes gapless. Figure 15 illustrates the magnetic field dependence of the classical Heisenberg antiferromagnetic chain and the $S = \frac{1}{2}$ chain. Details concerning the excitation spectrum of the uniform $S = \frac{1}{2}$ Heisenberg antiferromagnetic chain in a magnetic field can be found in [15, 24, 23, 25]. These incommensurate soft modes are a characteristic quantum feature of the $S = \frac{1}{2}$ HAF chain. Another characteristic difference can be observed at the antiferromagnetic zone boundary ($q = \frac{\pi}{2}$ in figure 15): At this wave vector the classical spin wave energy does not change at all, while in the quantum case, the lower boundary of the continuum splits. One of the two branches is shown in Figure 15, the second branch is given by the mirror image of the displayed dispersion at the axis $q = \frac{\pi}{2}$.

Figure 16 displays energy scans at the antiferromagnetic zone center $k = \frac{\pi}{2d}$ ($q = \frac{\pi}{2}$) of Cs_2CuCl_4, measured by inelastic neutron scattering on a triple axis spectrometer [26]. Cs_2CuCl_4 is a $S = \frac{1}{2}$ Heisenberg antiferromagnet with considerably smaller superexchange than $KCuF_3$. The magnetic fields available in combination with neutron scattering allow to create a significant magnetization and a measurable splitting of the lower continuum boundary. The splitting

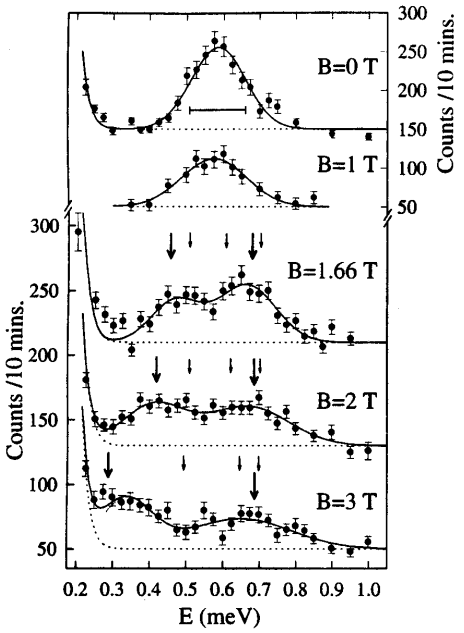

Fig. 16: *Energy scans at the antiferromagnetic zone boundary of Cs_2CuCl_4, at different magnetic fields. The data were taken using inelastic neutron scattering with a triple axis spectrometer. A classical spin chain would show no visible change below the saturation field [26].*

of the lower continuum boundary is clearly visible in the figure. A classical spin chain would show no change below the saturation field.

Figure 17 shows field dependent incommensurate soft-modes of the $S = \frac{1}{2}$-Heisenberg antiferromagnetic chain Cu-benzoate, measured by inelastic neutron scattering on a triple axis spectrometer [27]. The figure displays k-scans along the chain direction at fixed energy transfer. The left panel indicates the scan in the energy-momentum space (dotted line close to $\tilde{q}/\pi = 1$), the right panel shows the number of scattered neutrons for this scan versus wave vector. Ideally one should see two maxima which shift away from $\tilde{q}/\pi = 1$ with increasing magnetic field, plus a central peak at all fields. The additional splitting observed at intermediate fields is due to an anisotropy of the g-tensor which changes orientation from one site to the next within the spin chain. However, a classical chain would not show visible changes at these small magnetic fields.

One might expect that a similar soliton picture will lead to incommensurate gapless excitations in the high-field phases of the spin-Peierls system, the Haldane chain and other gapped quantum ground states. However, it is still under discussion, which ground states evolve gapless incommensurate excitations in the high-field phase, and whether there will be at least excitation minima at incommensurate wave vectors if the excitation spectrum remains gapped. As an example we consider the spin-Peierls system $CuGeO_3$ in its high-field phase. The coupling to the three-dimensional lattice and a sizable magnetic interchain interaction ($CuGeO_3$ is not very one-dimensional but has superexchange interactions with a ratio of 1:10:100 along the crystallographic directions a, b, c [28]) lead to static long-range order of the magnetic domain wall pattern. Since the magnetic domain walls are simultaneously structural domain walls in the spin-Peierls system, both magnetic and structural superlattice peaks can be observed, and have been detected by neutron and synchrotron diffraction [29, 30, 31]. Figure 18 displays a

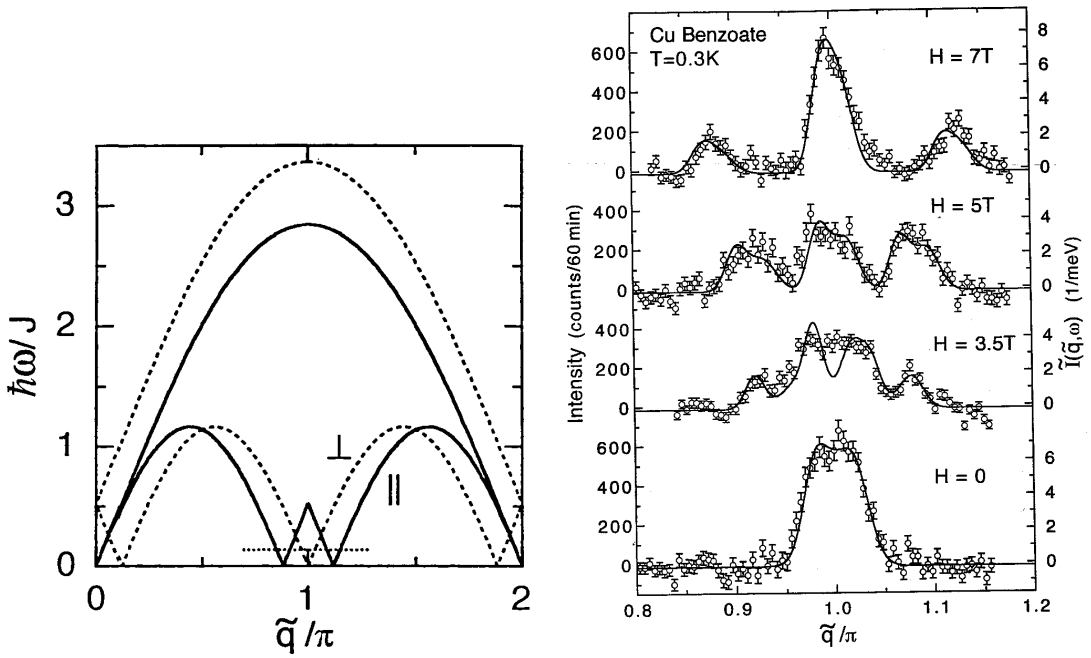

Fig. 17: *Field dependent incommensurate magnetic excitations of the $S = \frac{1}{2}$-Heisenberg antiferromagnetic chain Cu-benzoate. k-scans at small fixed energy transfer and different magnetic fields measured with a triple axis neutron spectrometer [27].*

sketch of the magnetic and structural modulation of an individual spin chain in the high-field phase.

Next we consider magnetic excitations in the high-field phase of a spin-Peierls system. Cre-

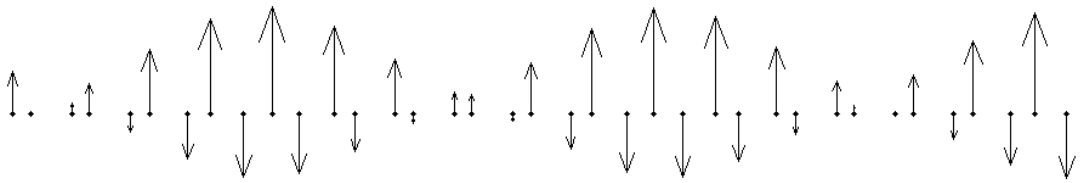

Fig. 18: *Sketch of the magnetic and structural domain wall pattern in the high-field phase of spin-Peierls systems. The structural dimerisation is largely exaggerated.*

ation and annihilation of a favourably oriented domain wall pair increases and lowers the magnetization by $\Delta S_{tot} = 1$, respectively. In the infinitely long chain, the magnetization change is infinitely small, and changes the distance of the domain walls by an infinitesimal amount, thus $\Delta k \propto m = \Delta S_{tot}/N$. Such an excited domain wall pair resembles a transverse spin wave. If this excitation happened on a immobile lattice (as eg. in case of the alternating chain), we would expect a dispersion with vanishing energy at the field dependent incommensurate $k \propto m$: At the critical field one branch of the excited triplet $S_{tot} = 1$ really crosses the ground state level, and at each higher field a dispersion branch with higher S_{tot} crosses the ground state. In $CuGeO_3$ the spins couple to hard (i.e. fast) phonons. The lattice "immediately" reacts to a magnetic exci-

tation and adapts to the new domain wall number [32, 33]. This "giving in" of the elastic lattice corresponds to matrix elements between ground and excited state which lead to a repulsion of the levels, an "anti-crossing". Therefore the energy gap never closes, neither at the critical field nor above.
Figure 19 displays the magnetic field dependence of the lowest magnetic excitation with wave vector k_{AF} [21]. The two branches at $H > H_c \approx 12.5$T correspond to excitations with $\Delta S = \pm 1$. The number of scattered neutrons is represented by a colour scale.

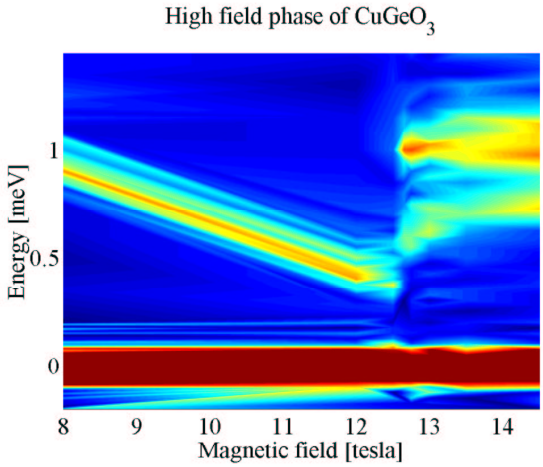

Fig. 19: *Lowest magnetic excitations at k_{AF} of the spin-Peierls system $CuGeO_3$ in dependence of the magnetic field, measured with a triple axis neutron spectrometer. The colour indicates the number of scattered neutrons in dependence of the magnetic field (abscissa) and energy transfer (ordinate) [21].*

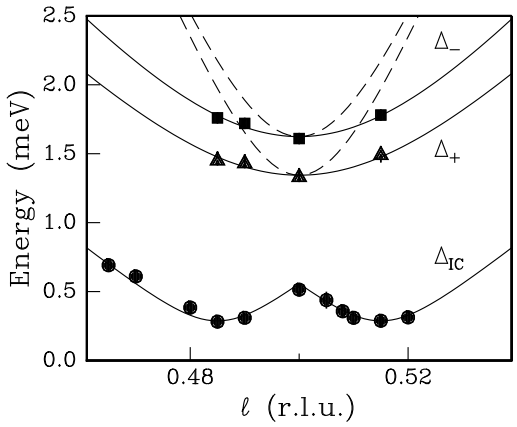

Fig. 20: *Magnetic excitations at $B = 14.5$ T in the high-field phase of $CuGeO_3$, close to the incommensurate magnetic superlattice peaks. The dispersion is measured along $(1\frac{1}{2}\ell)$ with a triple axis neutron spectrometer. $\Delta_\pm$ indicate the transverse, Δ_{IC} the phason excitation. The solid and broken lines indicate a dispersion with adapted spin wave velocities and $B = 0$ spin wave velocities, respectively [34].*

In addition to the transverse excitations above (sometimes called "amplitudons"), the phase

of the incommensurate magneto-elastic superlattice can oscillate, i.e. the domain wall centers oscillate collectively around their equilibrium position [35, 36, 37, 38]. This excitation is called phason. It involves a longitudinal amplitude of the sublattice magnetization near the domain wall center. The theory expects a dispersive phason, with zero energy at the incommensurate wave vector (for the experts: the phason energy is expected to vanish for non-elastic lattices, for elastic lattices with spin-phonon coupling to slow phonons and for elastic lattices with frequency-independent spin-phonon coupling to Einstein-phonons). Experimentally, the phason energy is known to be finite [34]. The finite energy may be related to a dispersive spin-phonon coupling, and/or pinning of the soliton lattice to crystal imperfections. Figure 20 shows the dispersion of all three high-field excitations of $CuGeO_3$ close to the incommensurate magnetic superlattice peaks, $(1\frac{1}{2}\frac{1}{2} \pm \delta)$ ($\delta \approx 0.015$ at 14.5 T).

The spin 1 Heisenberg antiferromagnetic chain NENP undergoes a phase transition into a high-field phase as well. Although theory expects incommensurate minima of the dispersion or incommensurate soft modes in the high-field phase, no signs of incommensurability were found [21], neither in NENP, nor in any other spin 1 chain. Regarding the materials investigated so far, it is not clear, whether the incommensurability is suppressed by crystal field anisotropies or alternating orientation of the g-tensor, or whether the lack of incommensurate modes is a fundamental property of spin 1 Heisenberg antiferromagnetic chains in the field region directly above the critical field.

References

[1] K. H. Hellwege, *Einführung in die Festkörperphysik*, (Springer-Verlag, Berlin, 1981).

[2] M. Steiner, J. Villain, and C. G. Windsor, *Adv. Phys.* **25**, 87 (1976).

[3] S. E. Nagler, D. A. Tennant, R. A. Cowley, T. G. Perring, and S. K. Satija, *Phys. Rev. B* **44**, 12361 (1991).

[4] I. Affleck, *J. Phys.: Condens. Matter* **1**, 3047 (1989).

[5] H. J. Mikeska and M. Steiner, *Adv. Phys.* **40**, 191 (1991).

[6] F. D. M. Haldane, *Phys. Lett.* **93A**, 464 (1983).

[7] Y. Hatsugai and M. Kohmoto, *Phys. Rev. B* **44**, 11789 (1991).

[8] T. Kennedy and H. Tasaki, *Phys. Rev. B* **45**, 304 (1992).

[9] E. Dagotto and T. M. Rice, *Science* **271**, 618 (1996).

[10] S. Brehmer, H. J. Mikeska, and U. Neugebauer, *J. Phys.: Condens. Matter* **8**, 7161 (1996).

[11] S. Brehmer, A. K. Kolezhuk, and H. J. Mikeska, *J. Phys.: Condens. Matter* **10**, 1103 (1998).

[12] R. Kubo, *Phys. Rev.* **87**, 568 (1952).

[13] J. Kanamori and K. Yoshida, *Progr. Theor. Phys.* **14**, 423 (1955).

[14] T. Oguchi, *Phys. Rev.* **117**, 117 (1960).

[15] G. Müller, H. Thomas, H. Beck, and J. C. Bonner, *Phys. Rev. B* **24**, 1429 (1981).

[16] S. Ma, C. Broholm, D. H. Reich, B. J. Sternlieb, and R. W. Erwin, *Phys. Rev. Lett.* **69**, 3571 (1992).

[17] M. A”in, J. E. Lorenzo, L. P. Regnault, G. Dhalenne, A. Revcolevschi, B. Hennion, and T. Jolicœur, *Phys. Rev. Lett.* **78**, 1560 (1997).

[18] M. Arai, M. Fujita, M. Motokawa, J. Akimitsu, and S. M. Bennington, *Phys. Rev. Lett.* **77**, 3649 (1996).

[19] L. P. Regnault, M. Aïn, B. Hennion, G. Dhalenne, and A. Revcolevschi, *Phys. Rev. B* **53**, 5579 (1996).

[20] L. P. Regnault and J. P. Renard, *Physica B* **234-236**, 541 (1997).

[21] M. Enderle, *Habilitationsschrift*, Universität des Saarlandes, Saarbrücken, Germany (1999).

[22] C. Kittel. *Introduction to Solid State Physics*. (John Wiley & Sons Inc., New York, 1986).

[23] J. B. Parkinson and J. C. Bonner, *Phys. Rev. B* **32**, 4703 (1985).

[24] G. Müller, H. Thomas, H. Beck, and J. C. Bonner, *Sol. State Commun.* **38**, 1 (1981).

[25] K. Lefmann and C. Rischel, *Phys. Rev. B* **54**, 6340 (1996).

[26] R. Coldea, D. A. Tennant, R. A. Cowley, D. F. McMorrow, Z. Tylczynski, and B. Dorner, *Phys. Rev. Lett.* **79**, 151 (1997).

[27] D. C. Dender, P. R. Hammar, D. H. Reich, C. Broholm, and G. Aeppli, *Phys. Rev. Lett.* **79**, 1750 (1997).

[28] J.P. Boucher and L.P. Regnault, *J. Phys. I* **6**, 1939 (1996).

[29] V. Kiryukhin, B. Keimer, J.P. Hill, and A. Vigliante, *Phys. Rev. Lett.* **76**, 4608 (1996).

[30] V. Kiryukhin, B. Keimer, J. P. Hill, S. M. Coad, and D. McK. Paul, *Phys. Rev. B* **54**, 7269 (1996).

[31] H.M. Rønnow, M. Enderle, D.F. McMorrow, L.P. Regnault, G. Dhalenne, A. Revcolevschi, A. Hoser, K. Prokes, P. Vorderwisch, and H. Schneider, *Phys. Rev. Lett.* **84**, 4469 (2000).

[32] F. Schönfeld, G. Bouzerar, G.S. Uhrig, and E. Müller-Hartmann, *Eur. Phys. J. B* **5**, 521 (1998).

[33] G.S. Uhrig, F. Schönfeld, and J.P. Boucher, *Europhys. Lett.* **41**, 431 (1998).

[34] M. Enderle, H.M. Rønnow, D.F. McMorrow, L.P. Regnault, G. Dhalenne, A. Revcholevschi, P. Vorderwisch, H. Schneider, P. Smeibidl, and M. Meißner, *Phys. Rev. Lett.* **87**, 177203 (2001).

[35] A.I. Buzdin, M.L. Kulic, and V.V. Tugushev, *Sol. State Commun.* **48**, 483 (1983).

[36] S. Bhattacharjee, T. Nattermann, and C. Ronnewinkel, *Phys. Rev. B* **58**, 2658 (1998).

[37] R.A. Cowley and A.D. Bruce, *J. Phys. C* **11**, 3577 (1978).

[38] A.D. Bruce, R.A. Cowley, and A.F. Murray, *J. Phys. C* **11**, 3591 (1978).